A Study of Interdiffusion in β + γ/γ + γ' Ni-Cr-Al Alloys at 1200 °C

Lawrence A. Carol

Michigan Technological University
Houghton, Michigan

February 1985

TABLE OF CONTENTS

TABLE OF CONTENTS (Continued)

Introduction

When a metal or alloy is exposed to high temperatures, relative to its melting point, it will generally undergo some type of reaction with the surrounding environment. In many instances this reaction has a detrimental effect; the end result being surface degradation, loss of critical alloying elements, and an overall reduction in the performance of the alloy. It is important in these instances to provide some means of stopping or reducing this reaction, in order to improve the quality, performance, and life of the alloy. Many times the decision to provide protection is not a matter of choice, but rather of necessity. Such is the case for modern superalloys used as turbine blades and vanes in aircraft gas turbine engines (1). The need to operate at higher engine temperatures has led to new alloy developments with greatly improved mechanical properties, but usually this occurs at the expense of oxidation resistance (2). Therefore in order to achieve practical component lives in high-temperature, oxidizing environments, superalloys require protective surface coatings.

Protective coatings are generally of two types, aluminide diffusion coatings and overlay coatings. (Ni, Co) CrAl overlay coatings are being developed for use in gas turbine applications (3-6) because they offer specific advantages

over aluminide coatings (1,7). One of the main advantages of overlay coatings is the ability to design the coating composition for maximum oxidation and hot corrosion resistance, and minimum coating - substrate interaction (1,7). In addition, overlay coatings offer better oxidation, hot corrosion, and thermal fatigue protection (7). Typically, overlay coatings are about twice as thick as diffusional aluminide coatings (8), thus allowing longer protective coating life.

Coating Degradation Mechanisms

The major purpose of a coating is to protect the underlying substrate from undergoing high temperature corrosion processes, thereby increasing the life of the substrate alloy. Coatings are typically made to contain high amounts of the element(s) necessary to slow or inhibit the corrosion processes. Because high temperature corrosion processes are predominantly ones of oxidation (9), coating degradation involves the selective oxidation of the less noble elemental species in the coating. Coating life, therefore, is dictated by the rate of consumption of the less noble elemental species in the coating. In the case of $\beta+\gamma$ Ni-or Co-base overlay coatings, the coating life is dictated by the rate of consumption of Al. High temperature oxidation results in the selective oxidation of Al

to form an adherent Al_2O_3 scale (7, 10). This scale provides a satisfactory kinetic barrier for continued reaction of the coating with the oxidizing environment (9, 11-13). The barrier is not maintained, however, because thermal cycling results in oxide spallation. This spallation can expose fresh metal to the oxidizing environment, and the oxide must be reformed to afford protection. Al must, therefore, be continually supplied to the oxide/metal interface in proper concentration to allow selective Al_2O_3 formation. Thus, one mechanism responsible for reduced overlay coating life is loss of Al to the Al_2O_3 scale (2, 3).

Another mechanism responsible for coating degradation is loss of corrosion resisting elements through interdiffusion with the substrate alloy. Coatings are typically made to contain higher amounts of corrosion resisting elements than the substrate alloy. This creates a chemical potential gradient which drives the diffusion process. The most advanced of the (Ni, Co) Cr Al Y overlay coatings contain nominally 22.5 at.% Al (8, 14), while typical cast Ni-base superalloys contain between 7-12.6 at.% Al (15-16). This substantial difference in bulk Al content causes Al to diffuse from the coating into the substrate. As Al diffuses into the substrate it depletes the coating of Al, thereby reducing the amount of Al available to supply oxidation resistance. Thus, a second mechanism responsible for reduced overlay coating life is loss of Al by interdiffusion

with the substrate (2, 3, 14).

Both types of coating degradation - i.e., loss of Al to the Al_2O_3 scale, and loss of Al by coating/substrate interdiffusion - involve diffusional transport of Al (2, 3, 8, 13). Because the processes are diffusion controlled, the loss of Al from each mechanism increases with increasing temperature (8, 12). Loss of oxide by spallation due to thermal cycling significantly accelerates the loss of Al due to oxidation (7, 11, 13). Similarily, increasing the bulk Al difference between coating and substrate increases the driving force for interdiffusion, and hence loss of Al to the substrate (8). Both types of degradation simultaneously reduce the Al content in the coating. This in turn reduces the time in which the coating can supply the necessary Al to the oxide/metal interface to form an Al_2O_3 scale. Once the Al content is depleted to the point where continued growth of an Al_2O_3 scale cannot occur, less protective oxides of Ni and Cr form (10). This point is referred to as breakaway oxidation (17), and results in accelerated failure of the coating/alloy system.

Previous Coating Studies

In order to improve the quality, performance, and life of overlay coatings, it is fundamental to study and understand both forms of coating degradation. By reducing the rate of consumption of Al - either by improvements in oxida-

4

tion resistance or reductions in coating/substrate interdiffusion - the life of the coating will be increased, and also, the life of the underlying substrate alloy (14). The first form of coating degradation - i.e., loss of Al to the oxide scale - has been addressed in a study of the cyclic oxidation behavior of as-cast $\beta+\gamma$, Ni-Cr-Al (with small amounts of Zr) alloys (11,18). These studies correlated the cyclic-oxidation weight change as a function of time with the type of oxide formed, the microstructure, and the concentration-distance profiles of Ni, Cr, and Al near the forming/spalling oxide layer. In these studies it was found that Al is supplied to the coating/oxide interface via dissolution of the Al-rich β phase. As the β phase dissolved, a γ layer formed adjacent to the oxide. The γ layer thickened by diffusion of Al from the $\gamma/\gamma+\beta$ interface to the γ/oxide interface. As the loss of Al progressed with time, the Al concentration at the $\gamma/\beta+\gamma$ interface increased, while the Al concentration at the γ/oxide interface decreased. These changes in Al concentration resulted in a time independent Al gradient at the γ/oxide interface. This time-independent gradient resulted in a constant Al flux at the γ/oxide interface. This was in accord with the almost constant rate of weight loss of the sample due to oxide spallation.

It was also found that breakaway oxidation occurred when the Al concentration at the γ/oxide interface neared zero (11,18). A numerical model was developed to predict $\gamma/\gamma+\beta$ interface positions as well as Al concentration-distance pro-

5

files in the γ phase. The model identified three critical system parameters for coating life as the Al content in the coating, the diffusion coefficient in the γ phase, and the relative amounts of β and γ in the coating.

The second form of coating degradation - i.e., loss of Al by coating/substrate interdiffusion - has been addressed in a study of overlay coating degradation by simultaneous oxidation and coating/substrate interdiffusion (19). Four γ phase (Ni solid solution) Ni-Cr, Ni-Al, and Ni-Cr-Al alloys were used as substrates. The overlay was a low-pressure plasma sprayed β + γ Ni-Cr-Al-Zr coating. Results of this work showed that extensive interdiffusion occurred at times as short as 10 hours. Coatings on all substrates underwent complete loss of the β phase within 5 to 15 hours of oxidation (approximately 5-10% of the failure time of the coating). Although complete loss of β occurred at short times, the Al that diffused into the substrate was found to diffuse back out at longer times and provide oxidation protection. Another result of this study (19) was that as the Al content in the substrate increased, the amount of Al interdiffusion decreased. This result was expected since a reduction in the bulk Al gradient between coating and substrate would be expected to reduce the chemical potential gradient driving the diffusion process. Other results (19) showed that as the rate of Al consumption (due to oxide formation/spallation) increased, the loss of Al due to coating/substrate interdiffusion also

increased. As the rate of Al consumption decreases, the amount of coating/substrate interdiffusion increases, but a larger fraction of the Al is able to diffuse back out of the substrate before coating failure.

A numerical model was developed (19) to predict the effective life of a coating undergoing simultaneous coating/substrate interdiffusion and oxide spallation associated with cyclic oxidation. This model was utilized to identify the critical system parameters affecting coating life as being the rate of Al consumption (from oxidation/spallation and/or coating/substrate interdiffusion) and the Al content in the substrate. It was found that the Al content in the coating had a lesser impact on coating life. Likewise, the Cr content in either the coating or the substrate had little impact on coating life.

Philosophy and Approach

Superalloys are designed with compositions and structures to withstand stress conditions at high temperature (20-21). Because these alloys must operate at high temperature in severely corrosive environments, precipitation-alloys based on the Ni-Cr system have been developed (22). While the composition of these alloys is very complex (15, 20), the structure is quite simple, consisting of a matrix of Ni-base solid solution (γ) dispersed with ordered γ' particles up to 60 vol. percent (20). The γ' is an ordered fcc structure based on the composition (Ni, Co)$_3$ (Al, Ti) (15, 22). These alloys derive their

high temperature strength and microstructural stability from the γ' precipitates (15,20-27). In studying the effect of coating degradation by coating/substrate interdiffusion, a first choice substrate would be an actual $\gamma+\gamma'$ superalloy. Real superalloys, however, are compositionally complex, and can easily contain 3-14 elements (15,28,29). Ternary or higher order diffusional interactions can complicate and hinder a complete understanding of coating degradation by coating/substrate interdiffusion (19). To this end, simplifications must be made in order to first understand the basic mechanisms responsible for coating degradation by coating/substrate interdiffusion.

In considering the compositional complexity of Ni-base superalloys, it becomes apparent that they are basically Ni-Cr alloys (15,16,22) with major additions of Co (8.6-13.8 at.%) and Al (7.1-12.6 at.%) (15,16). Minor additions of not more than 5 at.% include Ti, W, Mo, Mn, Si, Fe, as well as trace additions of Ta, Hf, Nb, and C (15-16). To simplify the system, a first choice would be to consider the Ni-Cr-Co-Al system. However, because Co and Ni are very similar in atomic number, weight, and size (30), and are completely miscible at the compositions of interest (31), they can be substituted interchangeably. Thus, the Ni-Cr-Al system is by far the simplest to consider for substrates representing superalloys. This was the approach taken in previous studies of coating degradation (11, 18,19). Although superalloys are basically two phase $\gamma+\gamma'$ alloys, the compositions of Ni, Cr, and Al found in them trans-

8

late to one phase γ(Ni solid solution) alloys in the Ni-Cr-Al
system. This is why γ substrates were considered in a previous
study of coating degradation by coating/substrate interdiffu-
sion (19).

To understand coating degradation by coating/substrate in-
terdiffusion in real coating/superalloy systems, choices of
simplified model systems which represent the real system must
be made. The β+γ NiCrAl coating can easily be modeled with
β+γ Ni-Cr-Al alloys of similar composition. In modeling super-
alloy substrates, however, both composition and structure must
be considered. Modeling superalloy substrates with composi-
tionally similar γ Ni-Cr-Al alloys has been performed in a pre-
vious study (19). Because superalloys have γ+γ' structures, a
natural extension of the previous study (19) is to model super-
alloy substrates with structurally similar γ+γ' Ni-Cr-Al alloys.
In considering γ+γ' Ni-Cr-Al alloys, two general changes in com-
position make them different from γ+γ' superalloys. First, the
bulk Al composition must be raised from 7-12 at.% to 17-19 at.%
to put the alloys in the γ+γ' phase field. Second, the bulk
Cr composition must be lowered from 9-23 at.% Cr to 0-10 at.%
Cr. These changes create larger differences in bulk Cr composi-
tion between β+γ alloy and γ+γ' alloy than bulk Al composition.
In real coating/superalloy systems, or β+γ/γ Ni-Cr-Al systems,
the bulk Al composition difference is usually much larger than
the bulk Cr composition difference. In view of this, slightly
different behavior would be expected between β+γ alloy inter-

diffusion with Ni-Cr-Al substrates and Ni-Cr-Al $\gamma+\gamma'$ substrates.

It is the aim of this study to investigate interdiffusion in $\beta+\gamma/\gamma+\gamma'$ Ni-Cr-Al diffusion couples. By using $\beta+\gamma/\gamma+\gamma'$ Ni-Cr-Al couples to model real coating/superalloy interdiffusion, the information obtained from the study can be used to better understand coating/substrate interdiffusion in the real system. Furthermore, it is the aim of this study to compare $\beta+\gamma/\gamma+\gamma'$ (Ni-Cr-Al) interdiffusion to $\beta+\gamma$ (Ni-Cr-Al-Zr)/γ (Ni-Cr-Al) interdiffusion investigated in a previous study (19), in order to determine which model system best represents real coating/superalloy interdiffusion.

Purpose of This Study

The purpose of the present study is twofold:

1. To examine the effect of $\beta+\gamma$ alloy composition and $\gamma+\gamma'$ alloy composition on $\beta+\gamma/\gamma+\gamma'$ (Ni-Cr-Al) interdiffusion; and

2. To compare these results with interdiffusion in $\beta+\gamma$ (Ni-Cr-Al-Zr/γ (Ni-Cr-Al) diffusion couples.

To accomplish this purpose, several $\beta+\gamma$ alloys representative of coating compositions and several $\gamma+\gamma'$ alloys spanning the $\gamma+\gamma'$ phase field were cast, annealed, and fabricated into diffusion couples. Subsequent analysis including concentration/ ·distance profiles in each phase, and measurements of growth

layer kinetics provided insight into the diffusional interaction. Determination of the NiCrAl phase diagram at 1200°C allowed quantitative diffusion paths to be determined which provided further insight into the interdiffusion process.

The results were utilized to determine the critical parameters governing $\beta+\gamma/\gamma+\gamma'$ interdiffusion. Variations in $\beta+\gamma$ alloy composition and $\gamma+\gamma'$ alloy composition allowed changes in diffusion path to occur which affected the amount of Cr and Al that diffused into the $\gamma+\gamma'$ alloy. Using high bulk Al $\gamma+\gamma'$ alloys caused different interdiffusion behavior to occur as compared to γ alloys. This behavior, however, could be beneficial, not detrimental, if made to occur in real coating/superalloy systems. Finally, these results, as well as previous results (11,18,19), can be used to better design coating substrate systems so that the quality, performance, and life of the coating and substrate can be improved.

Experimental Procedure

The Ni-Cr-Al alloys chosen for use in this study consisted of four β+γ alloys, two γ+γ' alloys, and one γ alloy. Alloy designations and compositions are given in Table 1. The phases present and volume fractions are given in Table 2. β+γ alloy C2 was cast to represent the coating alloy used in earlier coating studies (11,18-19). Alloy C1 contained approximately the same bulk Al composition as alloy C2 with a higher bulk Cr composition. Alloy C3 contained approximately the same bulk Cr composition as alloy C2 with a lower bulk Al composition. Alloy C4 was an attempt at obtaining an alloy with the same phase compositions (on the same tie line) as alloy C1. The γ+γ' alloys were chosen to span the γ+γ' phase field. They were made to contain the same bulk Al compositions with different bulk Cr compositions. Alloy S3 was intended to be a γ+γ' alloy, but resulted in a γ alloy of slightly lower bulk Al composition than alloys S1 and S2.

Alloy and Diffusion Couple Preparation

All alloys used in this study were prepared from pressed elemental powders. The Ni powder was obtained from International Nickel Co., type 123, of nominal purity 99.7% Ni. The Al powder was obtained form Alcoa, type 1202, of nominal purity 99.99% Al. The Cr powder was obtained from Alfa Products, type 00077, of nominal purity 99.95% Cr. After mixing and pressing of the powders, the alloys were arc melted in an argon atmosphere on a

TABLE 1

Compositions of the β+γ and γ+γ' Alloys
Used in Diffusion Couples

Alloy Designation	Alloy Composition[1]	
	Nominal	Bulk EDAX[2]
β + γ Alloys		
C1	Ni-19.8Cr-24.7Al	Ni-20.0Cr-24.1Al
C2	Ni-14.9Cr-24.7Al	Ni-15.3Cr-23.9Al
C3	Ni-14.9Cr-20.8Al	Ni-15.1Cr-20.3Al
C4	Ni-26.0Cr-16.9Al	Ni-26.4Cr-17.1Al
γ + γ Alloys		
S1	Ni-7.4Cr-18.1Al	Ni-7.4Cr-17.1Al
S2	Ni-3.7Cr-18.1Al	Ni-3.5Cr-17.0Al
γ Alloy		
S3	Ni-18.1Al	Ni-16.5Al[3]

1. All compositions in atomic percent
2. See Appendix A - Bulk Composition Analysis for details
3. Ni-16.2Al by electron microprobe analysis

TABLE 2

Phase Constitution and Measured Volume Fractions For the β+γ and γ+γ' Alloys Used in Diffusion Couples

Alloy	Phases Present		Volume Fraction of γ or γ'	
	As Cast	Homogenized (1200°C)	Measured	Calculated[1]
C1	β + γ	β + γ	30.0 ± 4.0%γ	31.0
C2	β + γ	β + γ	31.0 ± 4.0%γ	33.0
C3	β + γ	β + γ	61.0 ± 3.0%γ	59.0
C4	β + γ	β + γ	70.0 ± 4.0%γ	68.0
S1	γ	γ + γ'	26.0 ± 3.0%γ'	--
S2	γ	γ + γ'	19.0 ± 3.0% γ'	--
S3	γ	γ	--	--

1. Obtained from measured phase diagram using bulk EDAX compositions

water cooled copper hearth using a non-consumable tungsten electrode. The first melting step consisted of repeated melting of the alloy into an approximately 40mm diameter button. The second melting step consisted of melting the button into a 15mm diameter rod, 50mm in length. The final melting step consisted of melting the 15mm diameter rod into a 10mm diameter rod, approximately 90mm in length.

After melting, the alloys were annealed to obtain a homogeneous microstructure. The $\beta+\gamma$ alloys were annealed at 1250°C for 150 hours followed by a 200 hours anneal at 1200°C. Electron microprobe analysis showed no composition variations in the β and γ phases that were not within the standard deviation of the measurements. The $\gamma+\gamma'$ alloys were annealed at 1250°C for 50 hours followed by a 100 hours anneal at 1200°C. Alloy microstructures and their location on the NiCrAl phase diagram (1200°C) are shown in Figures 1 and 2.

After homogenization, the alloys were sectioned into approximately 10mm diameter by 3.2mm thick disks. The disks were polished through 0.05 alumina and then fabricated into diffusion couples. The fabrication involved placing the various $\beta+\gamma/\gamma+\gamma'$ alloys next to one another in a Mo canister. The canister and contents were annealed at 1200°C ($\pm$2°C) in a flowing Ar atmosphere for 100, 200, and 300 hours. The lower thermal expansion of the Mo canister caused a compressive stress to be placed on the couples. The compressive stress plus the highly polished disk surfaces allowed diffusion bonding to occur over approxi-

15

C2(Ni-15.3Cr-23.9Al)

C1(Ni-20 0Cr-24 1Al)

C3(Ni-15.1Cr-20.3Al)

C4(Ni-26.4Cr-17.1Al)

50at.%Al

β

γ'

γ

Cr
50at.%

Ni
100at.%

250μm
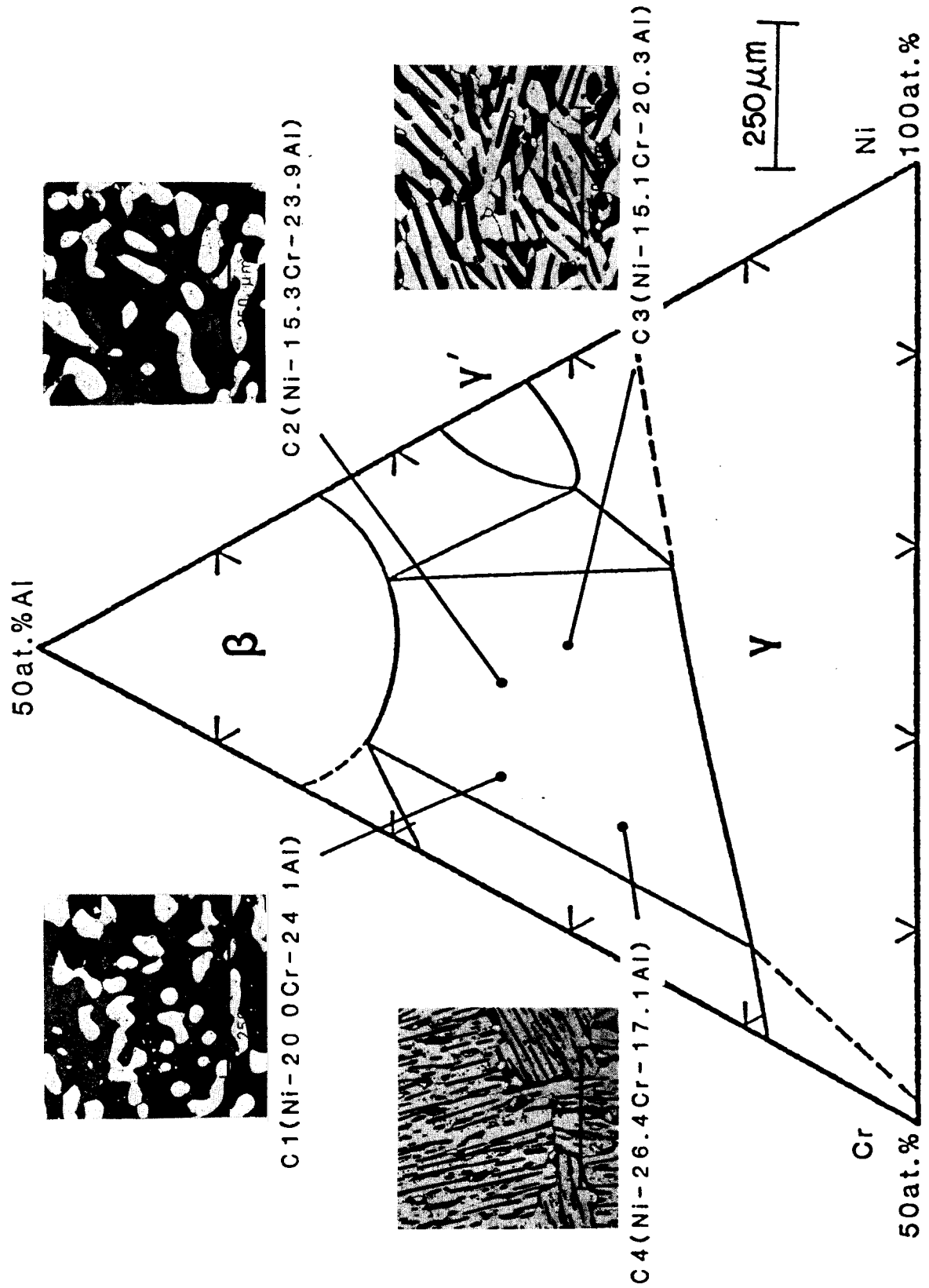
Figure 1   Coating alloy microstructures and their location on the NiCrAl phase diagram (1200°C).

16
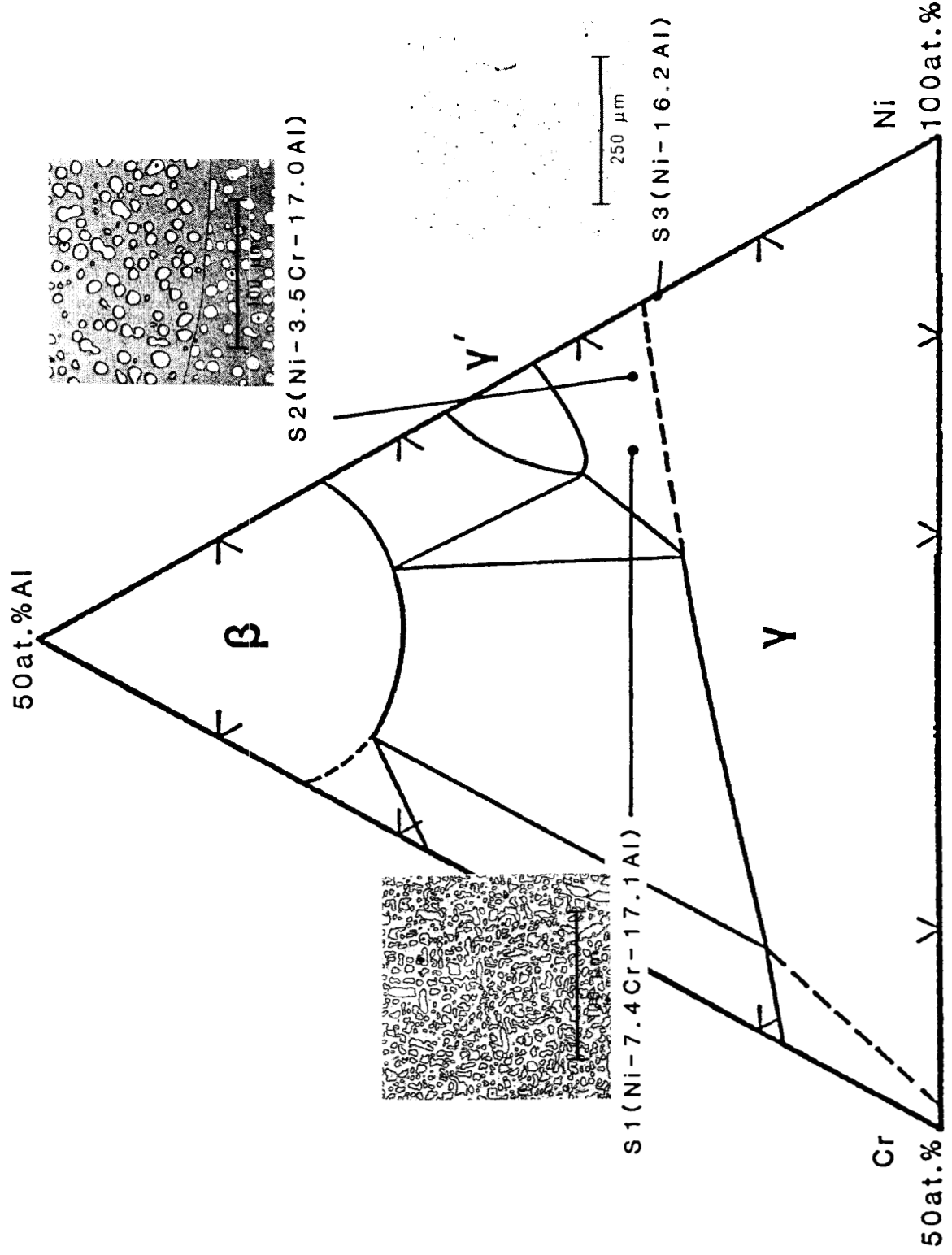
Figure 2. Substrate alloy microstructures and their location on the NiCrAl phase diagram (1200°C).

mately 80% of the couple. Following each 100 hours anneal, the diffusion couples were sectioned for microstructural investigation, phase growth measurements, and electron microprobe analysis. Microstructural investigation and phase growth measurements involved etching the sample with Marble's Reagent (32). Electron microprobe analyses were performed on unetched samples.

Experimental Results

To investigate coating/substrate interdiffusion using $\beta+\gamma/\gamma+\gamma'$ Ni-Cr-Al alloys, diffusion couples of homogenized alloys were utilized. The alloy sections were sufficiently thick so that no diffusion occurred at the outside ends of the couple. Thus, all results presented pertain to an infinite diffusion couple. The series of couples used to investigate interdiffusion were characterized by a common $\beta+\gamma$ or $\gamma+\gamma'$ alloy joined to selected alloys of the other phase field. Table 3 lists the series of couples studied. Depending on the composition of the terminal alloys, the couples developed complex, multiphase diffusion structures with a variety of interfaces, including: $\beta+\gamma/\gamma$, $\beta+\gamma/\gamma'$, $\beta+\gamma/\gamma+\gamma'$, $\gamma/\gamma+\gamma'$, γ/γ', $\gamma'/\gamma+\gamma'$, and $\gamma+\gamma'/\gamma$. A summary of the interfaces developed in each individual couple is presented in Table 3. Along with microstructural investigation, phase growth measurements, concentration/distance profiles at 200 hours in the phases in the diffusion zone, and diffusion paths were utilized to determine and explain the critical parameters governing the interdiffusion phenomena. The results of this work for each series of couples is presented below.

Series 1. C1, C2, C3, C4/S1(Ni-7.4Cr-17.1Al)

1. C1(Ni-20.0Cr-24.1Al)/S1. Interdiffusion resulted in growth of $\beta+\gamma$ into the $\gamma+\gamma'$ alloy, (i.e., the $\beta+\gamma$ structure expanded

19

TABLE 3

Summary of the Interfaces Developed
in the Diffusion Couples

Series	Couple[1,2]	$\beta+\gamma/$ γ	$\beta+\gamma/$ γ'	$\beta+\gamma/$ $\gamma+\gamma'$	$\gamma/$ $\gamma+\gamma'$	γ/γ'	$\gamma'/$ $\gamma+\gamma'$	γ/γ'
	C1/S1	--	--	Y	--	--	--	--
	C2/S1	--	--	Y	--	--	--	--
1	C3/S1	Y	--	--	Y	--	--	--
	C4/S1	Y	--	Y	--	--	--	--
	C1/S2	--	Y	--	--	--	Y	--
	C2/S2	--	Y	--	--	--	Y	--
2	C3/S2	Y	--	--	--	Y	Y	--
	C4/S2	Y	Y	--	--	--	Y	--
	C1/S3	--	Y	--	--	--	Y	Y
3	C2/S3	--	Y	--	--	--	Y	Y
	C3/S3	Y	--	--	--	Y	Y	Y

[1]See Table 1 for alloy identification.

[2]All diffusion times were 200 hours.

[3]Y = interface was present.

with time of interdiffusion). The diffusion zone, shown in Figure 3, consisted of the $\beta+\gamma$ alloy (C1), the $\beta+\gamma$ growth layer, and the $\gamma+\gamma'$ alloy (S1). Concentration/distance (hereafter referred to as C/D) profiles for Cr in the β and γ phases, and the calculated bulk Cr C/D profile* are shown in Figure 4. Likewise, C/D profiles for Al in the β and γ phases and the calculated bulk Al C/D profile are shown in Figure 5. C/D profiles in the $\gamma+\gamma$ regions were not measured because the γ and γ' phases could not be distinguished unetched, and the size of the γ' was on the order of the electron microprobe spot size (3-5 microns). From Figure 4 it can be seen that the Cr concentration in the β and γ phases begins to decrease well back ($\sim -600\mu m$) from the original interface (hereafter referred to as O.I.). The Cr concentration in the γ phase decreases much more sharply than the Cr concentration in the β phase. The bulk Cr decreases very little until near the O.I. where it decreases sharply. In the $\beta+\gamma$ growth layer, the Cr C/D profiles in the phases, and the bulk Cr C/D profile begin to level off (i.e. the change in concentration with distance, or the gradient, becomes less steep). The Al C/D profile in the β phase (Figure 5) is approximately constant, while the Al C/D profile in the γ phase increases slightly toward the O.I. - indicating uphill Al diffusion. This is not suprising, however, because all phase concentrations in the C/D profiles

* See Appendix D - Diffusion Paths and Diffusion Path Determination for details.

21

(a)

C1   O.I.   S1

50at.% Al

β

γ'

C1

b   c

a

S1

Cr   γ   Ni

50at.%   100at.%
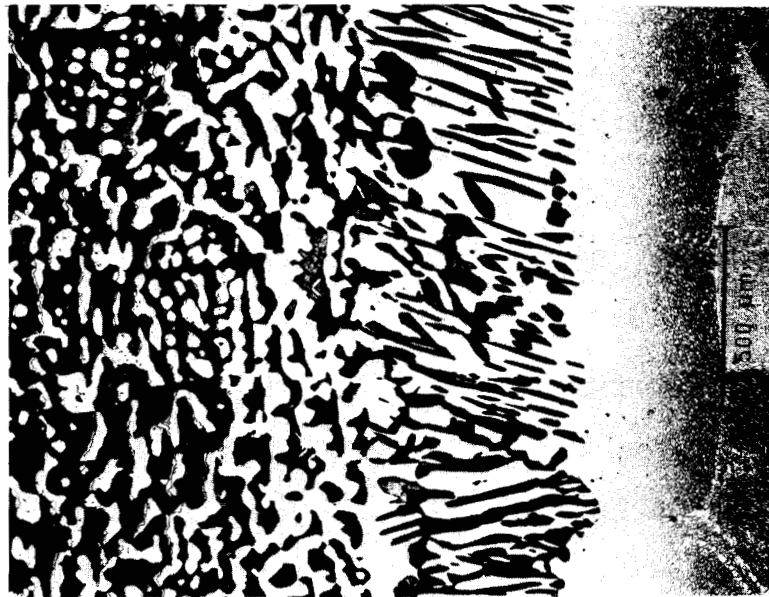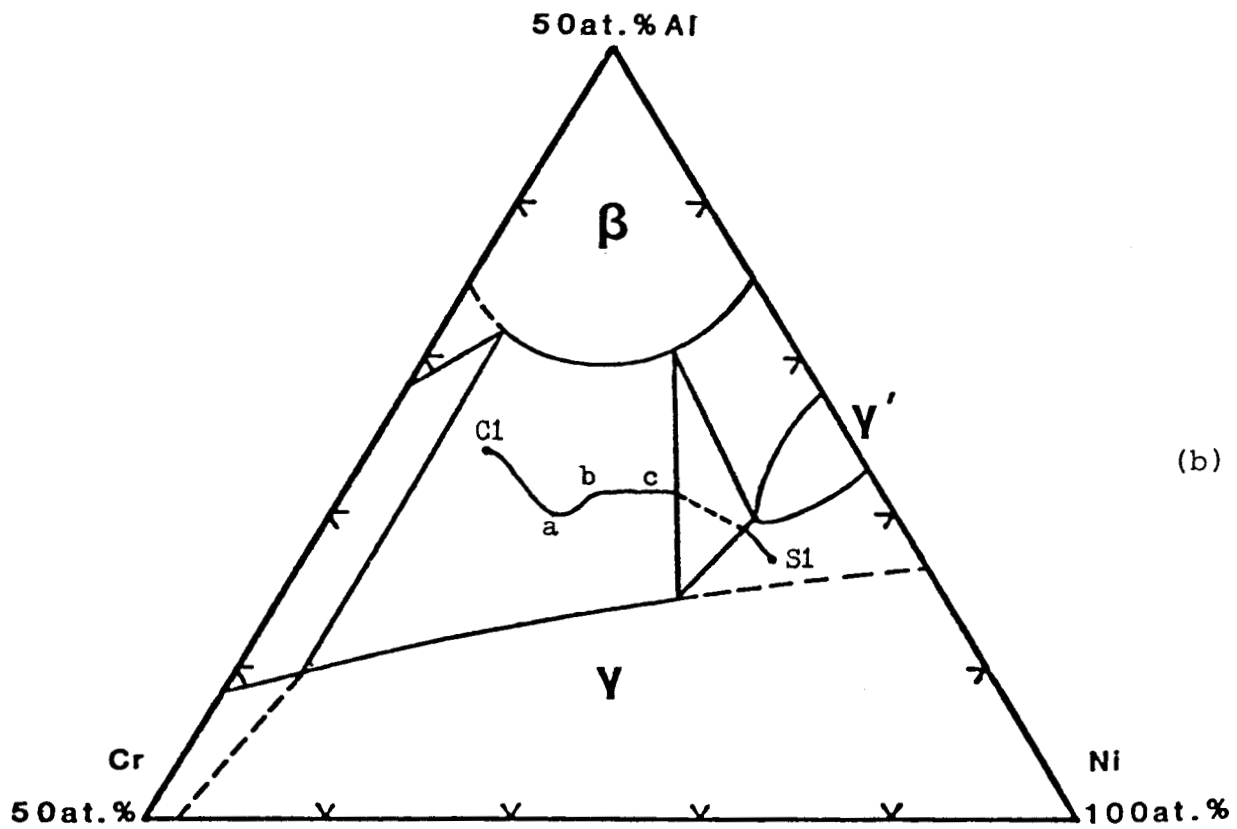
Figure 3. (a) Diffusion zone microstructure (200 hrs.);
and (b) diffusion path for couple Cl(Ni-20.0Cr-24.1)Al/
Sl(Ni-7.4Cr-17.1Al)

22
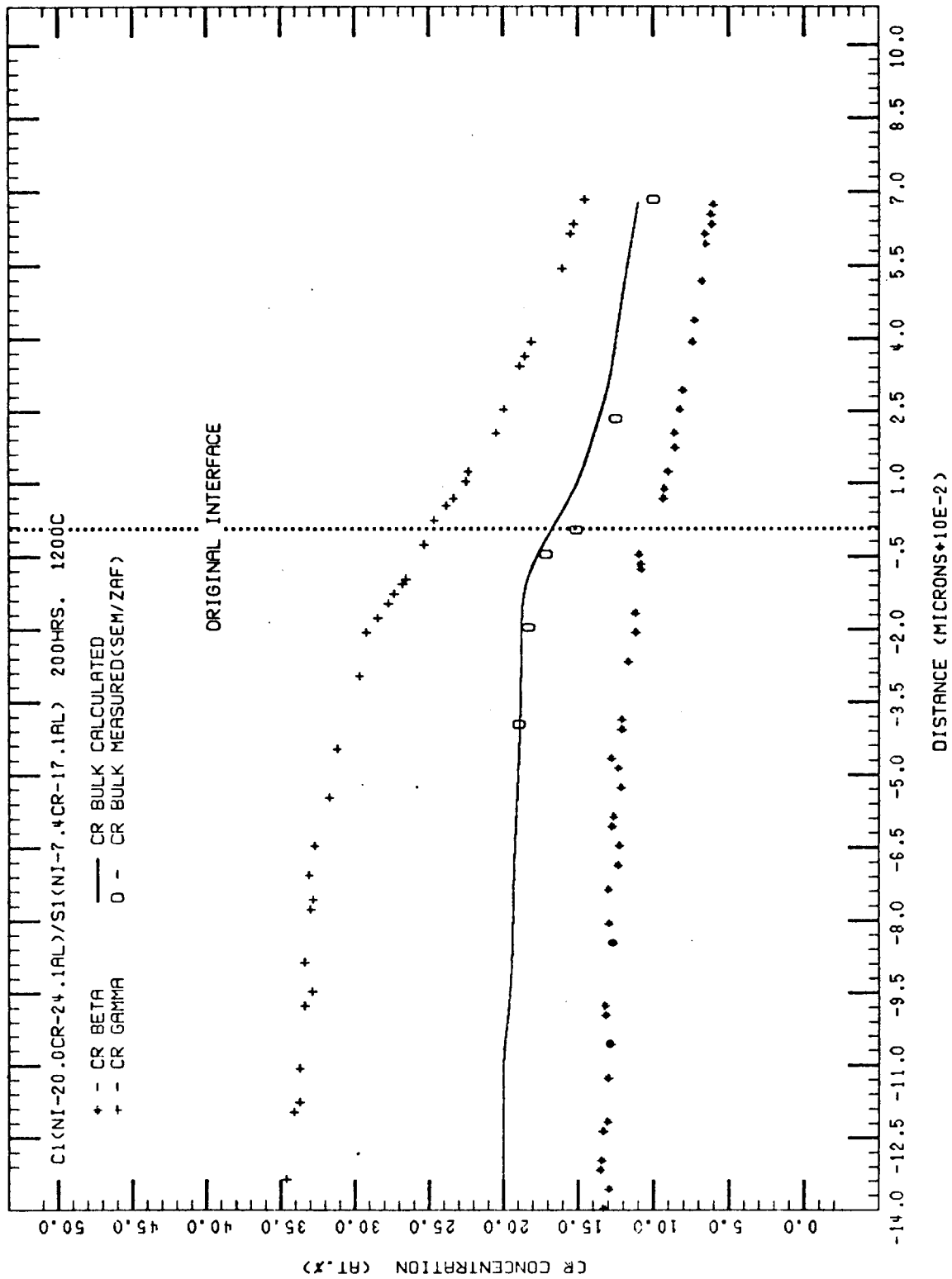
Figure 4. Cr concentration/distance profiles in the β and γ phases and the calculated bulk Cr profile for couple C1/S1.

23
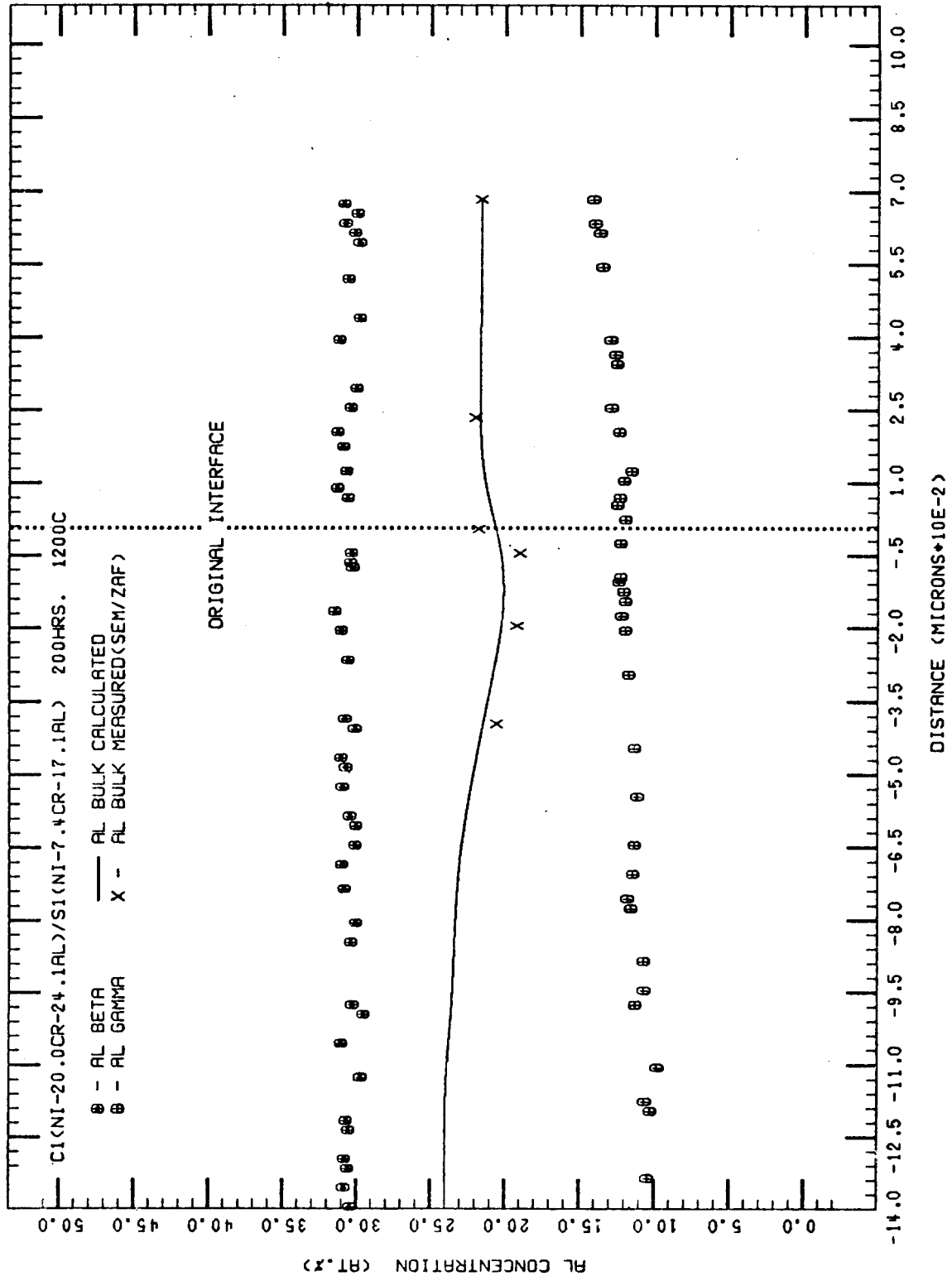
Figure 5. Al concentration/distance profiles in the β and γ phases and the calculated bulk Al profile for couple C1/S1.

24

were found to lie on the respective phase boundaries of the phase diagram, indicating local equilibrium was being maintained. As the $\beta+\gamma$ phase field is transversed toward the Ni-Al side of the phase diagram,** the $\gamma/\beta+\gamma$ phase boundary exhibits a rise in Al concentration from approximately 9.0 at.% Al to 14.5 at.% Al. The rise in Al concentration of the $\gamma/\beta+\gamma$ phase boundary is reflected in the rise of Al concentration in the γ phase C/D profile. The bulk Al C/D profile begins to decrease well back in the $\beta+\gamma$ alloy (~ -1000μm from the O.I.) and continues to decrease until the O.I. at which it increases and then levels to an approximately constant value. The increase in bulk Al at the O.I. corresponds to the point where the bulk Cr is decreasing sharply.

The diffusion path, shown in Figure 3, reflects the diffusion zone microstructure and the resulting changes in the C/D profiles. The Al decreases sharply at first, as seen by the first segment of the diffusion path (Cl-a). Over the same path segment, the bulk Cr changes very little. The decrease in bulk Al composition comes from the fact that the volume fraction of β is decreasing from approximately 70% in the alloy (well removed from the diffusion zone) to approximately 44% near the O.I. This reduction in the vol. fraction of β is also why the bulk Al C/D profile decreases toward the O.I.. Over the same distance that the bulk Al C/D profile is decreasing, the bulk Cr C/D profile decreases very little. Thus, the diffusion path

**See Figure C-1, pg. C-4.

segment C1-a shows very little change in bulk Cr composition. Only near the O.I. does the bulk Cr composition begin to decrease sharply. The sharp decrease in the bulk Cr C/D profile leads to an increase in the bulk Al C/D profile and this is reflected in the diffusion path by segment a-b. Considering the diffusion zone microstructure, it becomes apparent why the bulk Al C/D profile must rise. Transversing from the O.I. into the $\beta+\gamma$ growth layer shows an almost discontinuous change in the volume fraction of β from 44 vol.% near the O.I. to 48 vol.% in the $\beta+\gamma$ growth layer. The volume fraction of β remains constant throughout the growth layer. Because the β volume is constant, the bulk Al C/D profile is constant in the $\beta+\gamma$ growth layer. The bulk Cr C/D profile continues to decrease in this region. These results are evident in the diffusion path segment b-c where there is little change in the bulk Al composition, while the bulk Cr composition continues to decrease.

At the three-phase interface ($\beta+\gamma/\gamma+\gamma'$) the diffusion path enters the $\beta+\gamma+\gamma'$ triangle on the $\beta+\gamma$ side at approximately 21 at.% Al. It exits the triangle on the $\gamma+\gamma'$ side at approximately 19 at.% Al. The diffusion path reaches the $\gamma+\gamma'$ alloy (S1) composition by cutting tie-lines in the $\gamma+\gamma'$ field - as seen in the diffusion zone microstructure by a gradual reduction in the volume fraction of γ' away from the three-phase interface.

2.   C2(Ni-15.3Cr-23.9Al)/S1.   Interdiffusion resulted in a simi-

lar diffusion zone microstructure to couple C1/S1 - consisting

of β+γ alloy (C2), β+γ growth, and γ+γ' alloy (S1) as shown in

Figure 6.   C/D profiles for Cr and Al in the β and γ phases and

the calculated bulk Cr and Al C/D profiles are shown in Figures

7 and 8, respectively.   The C/D profiles were similar in appear-

ance to those of couple C1/S1.   The Cr concentration in the γ

phase decreased less sharply than in couple C1/S1.   This is be-

cause the equilibrium Cr concentration in the γ phase of alloy

C2 is approximately 24.0 at.% Cr, compared to 34.0 at.% Cr in

the γ phase of alloy C1.   Thus the Cr concentration has to de-

crease from 24.0 at.% Cr to 14.0 at.% Cr (at the three-phase

interface) and this results in a less steep Cr gradient.   Similar

to couple C1/S1, the bulk Cr C/D profile decreases at the O.I.

while the bulk Al C/D profile increases.   The decrease in bulk

Cr and increase in bulk Al at the O.I. is not as sharp as for

couple C1/S1.   This would be expected because alloy C2 has a

lower bulk Cr composition than alloy C1.   Thus, the Cr chemical

potential gradient in the couple is less than in C1/S1, and

therefore, the bulk composition gradients in the C/D profiles

are smaller.

The diffusion path, shown in Figure 6, is similar in appear-

ance in the β+γ phase field to the path of couple C1/S1.   The

bulk Al decreases first, corresponding to reductions in the

volume fraction of β toward the O.I. in the couple.   The bulk

Cr decreases slightly over this section of path.   At the O.I.
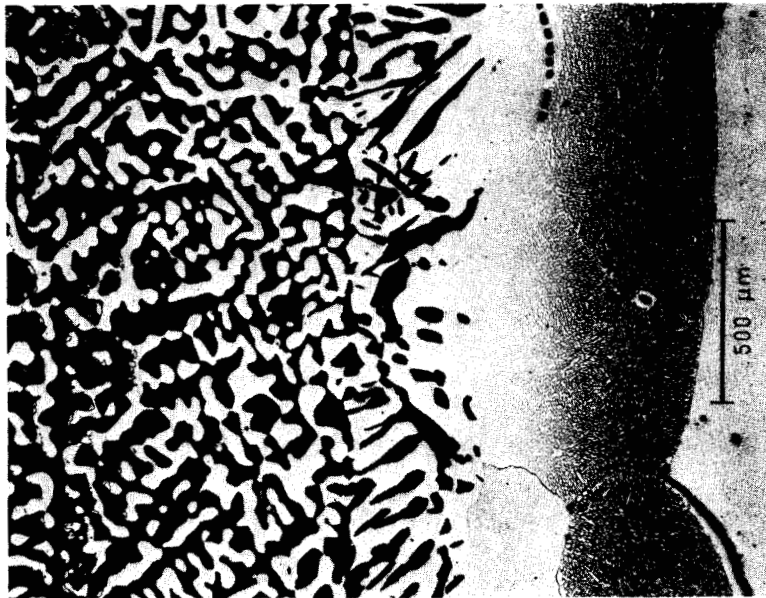
(a)

C2   O.I.   S1
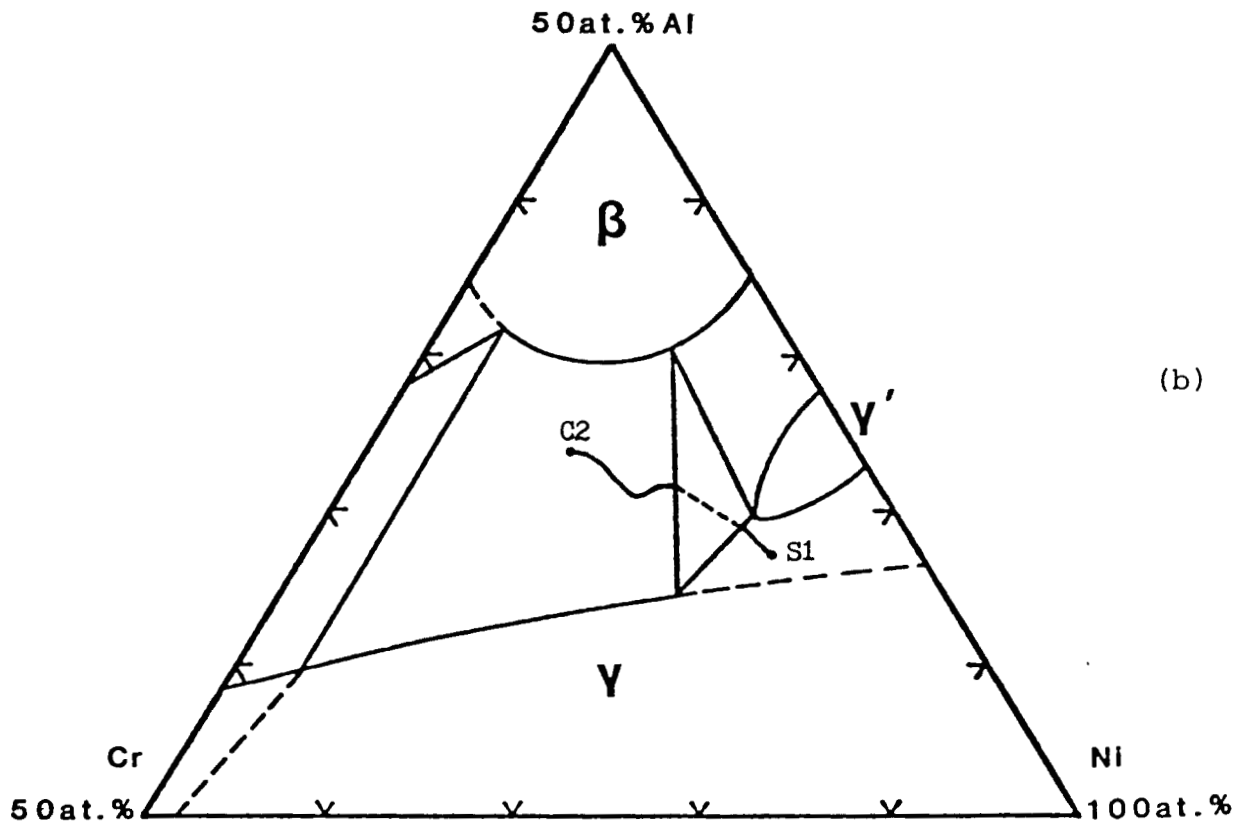
(b)

Figure 6. (a) Diffusion zone microstructure (200 hrs.); and (b) diffusion path for couple C2(Ni-15.3Cr-23.9Al)/ S1(Ni-7.4Cr-17.1Al)

28
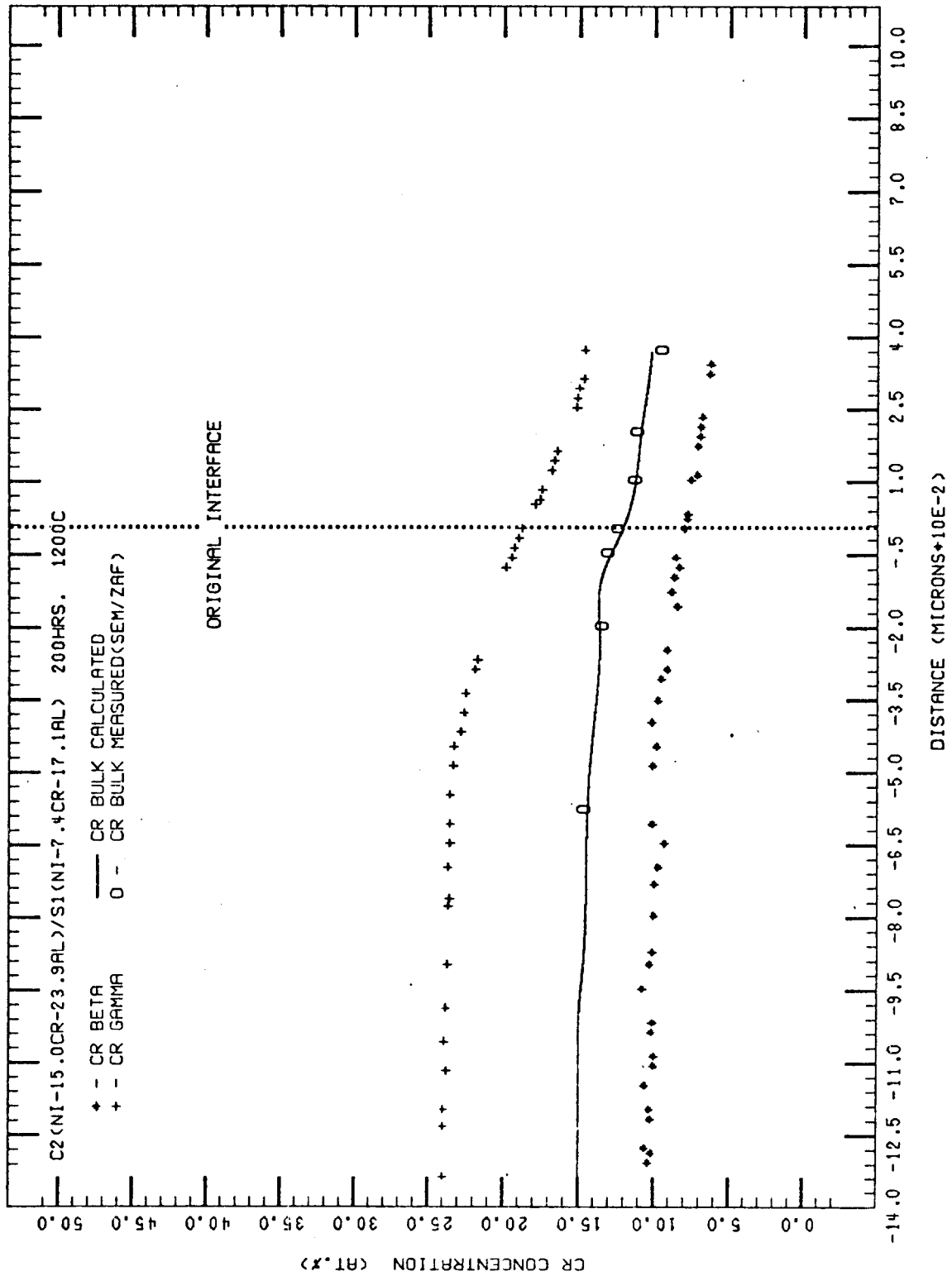
Figure 7. Cr concentration/distance profiles in the β and γ phases and the calculated bulk Cr profile for couple C2/S1.
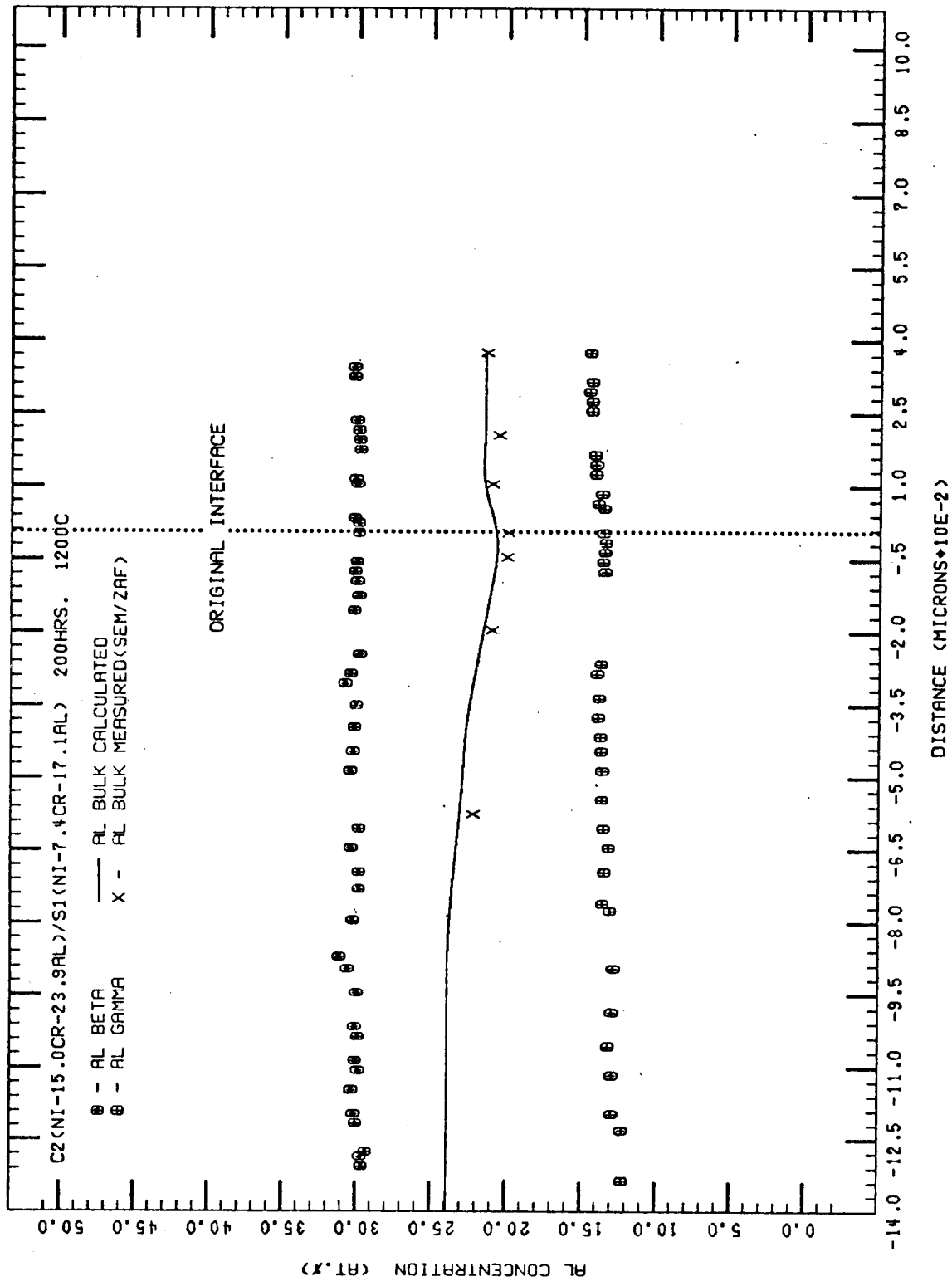
Figure 8. Al concentration/distance profiles in the β and γ phases and the calculated bulk Al profile for couple C2/S1.

30

the β volume fraction rises from approximately 45 vol.% to 48 vol.% in the β+γ growth layer. This discontinuous change in β volume fraction causes the diffusion path to inflect and increase to higher Al composition. In the β+γ growth layer, the volume fraction of β remains constant, and thus the path shows a straight segment of constant bulk Al composition. The bulk Cr composition continues to decrease along this path segment. At the three phase interface, the diffusion path enters the β+γ+γ' triangle on the β+γ side at approximately the same Al composition as couple C1/S1. The path exits the triangle on the γ+γ' side at the same point where the path of couple C1/S1 exits the triangle, and cuts tie lines until it reaches the terminal alloy (S1) composition.

3.   C3(Ni-15.1Cr-20.3Al)/S1.   Interdiffusion resulted in growth of γ into the γ+γ' alloy. The diffusion zone, shown in Figure 9, consists of the β+γ alloy (C3), the γ growth layer, and the γ+γ' alloy (S1). C/D profiles for Cr and Al in the β and γ phases, the γ growth layer, and the calculated bulk Cr and Al C/D profiles are shown in Figures 10 and 11, respectively. Similar to couples C1/S1 and C2/S1, the bulk Al C/D profile decreases toward the O.I. while the bulk Cr C/D profile stays relatively constant. The decrease in bulk Al corresponds to a reduction in the volume fraction of β toward the O.I.. At distances near the O.I., the bulk Cr C/D profile begins to decrease and the bulk Al C/D profile begins to increase. The increase in bulk Al corresponds to the fact that a very narrow β+γ layer is grown

31

C3   O.I.   S1

50at.%Al

β

γ'

C3

S1

γ

Cr
50at.%   Ni
                                       100at.%
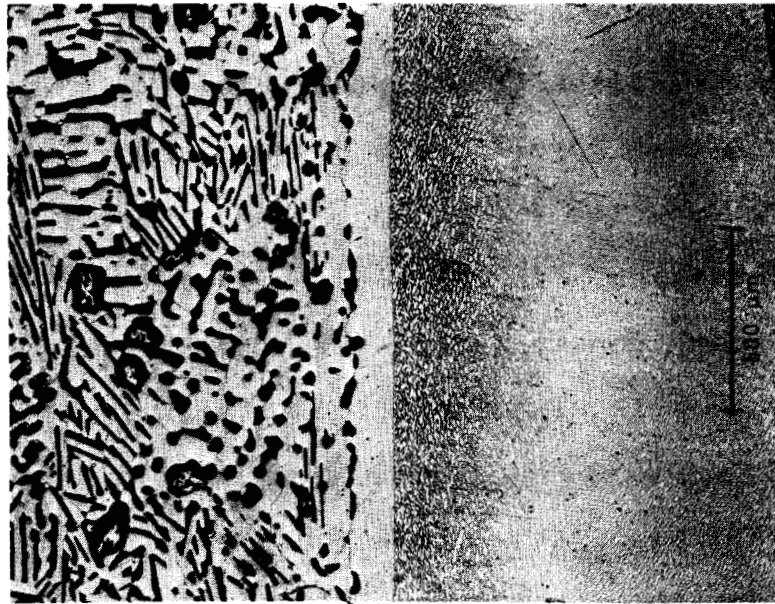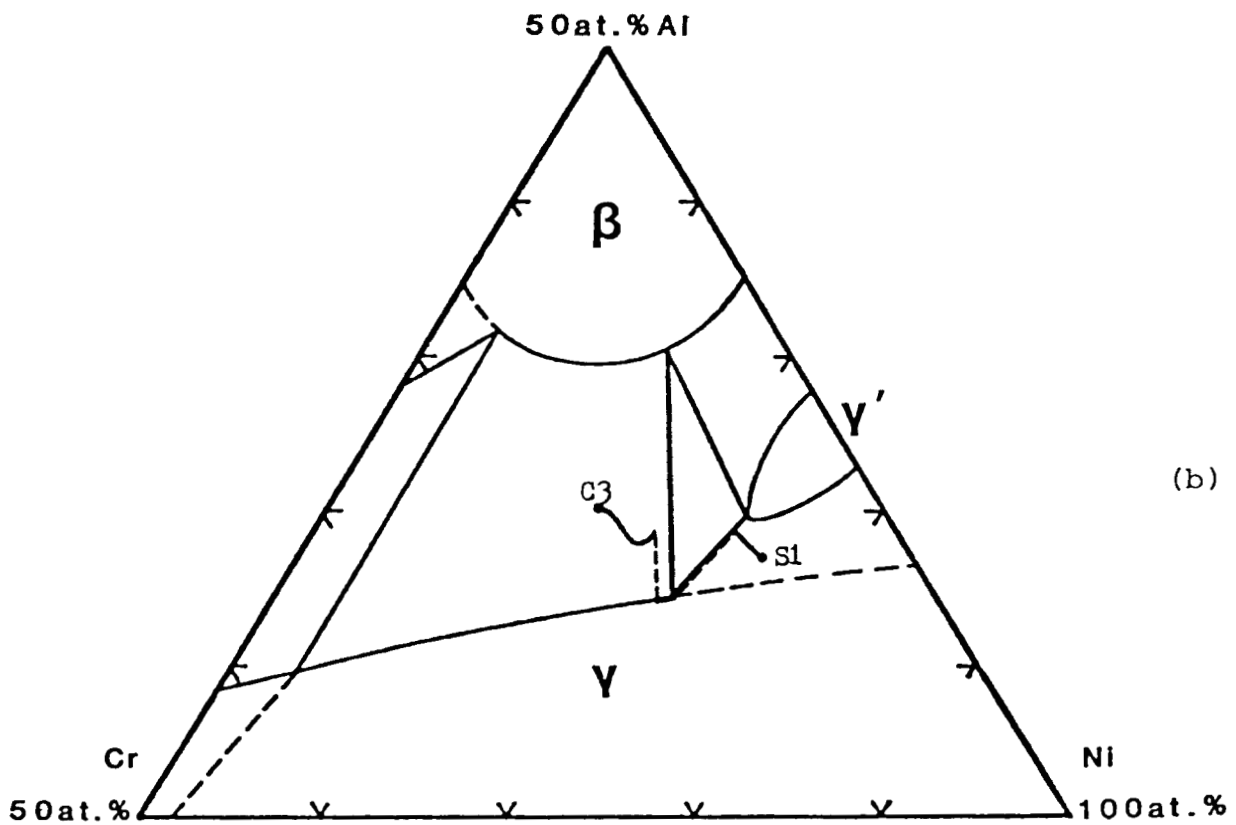
(b)

Figure 9. (a) Diffusion zone microstructure (200 hrs.);
and (b) diffusion path for couple C3(Ni-15.1Cr-20.3Al)/
S1(Ni-7.4Cr-17.1Al)
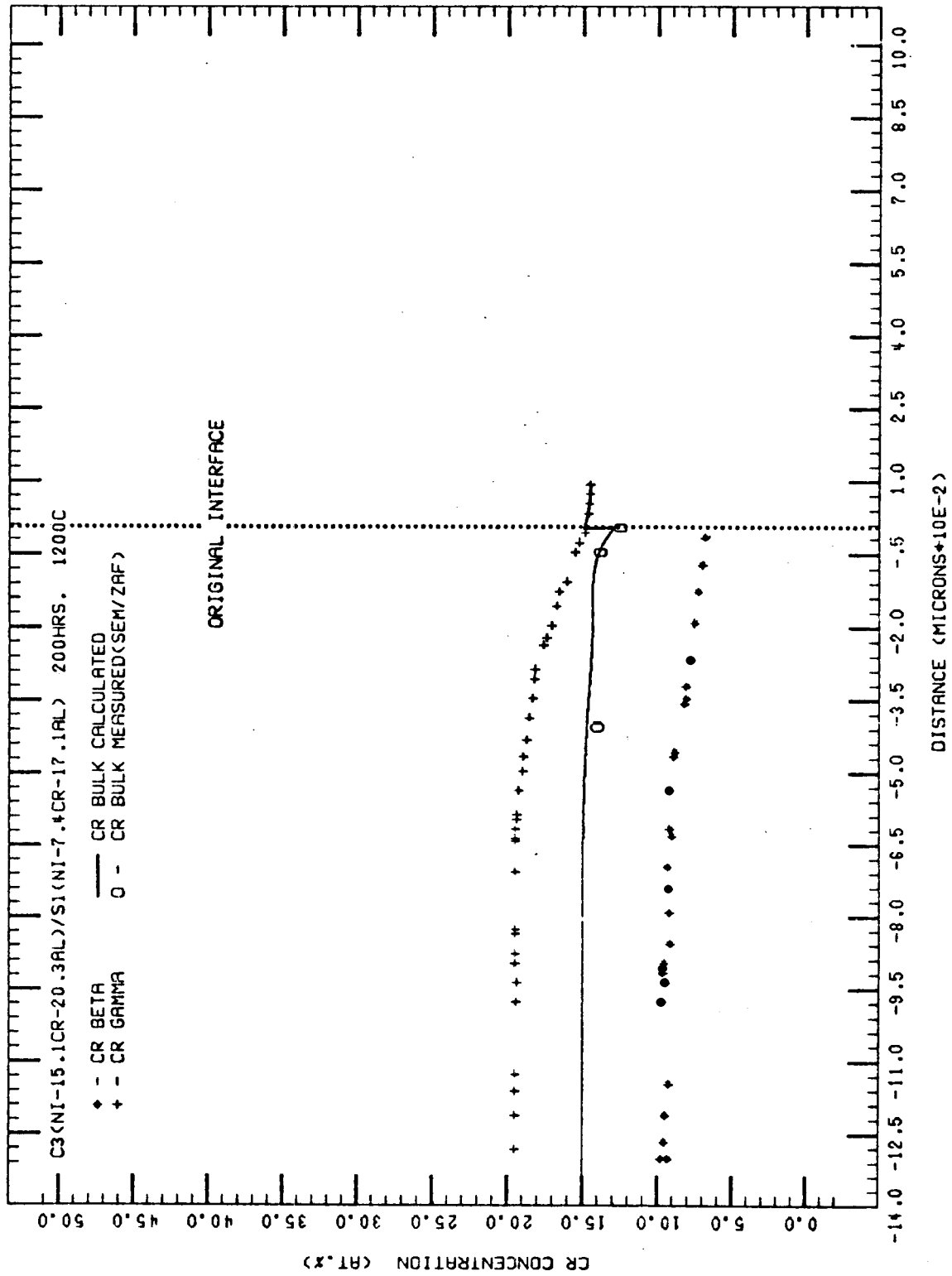
Figure 10. Cr concentration/distance profiles in the β and γ phases and the calculated bulk Cr profile for couple C3/S1.
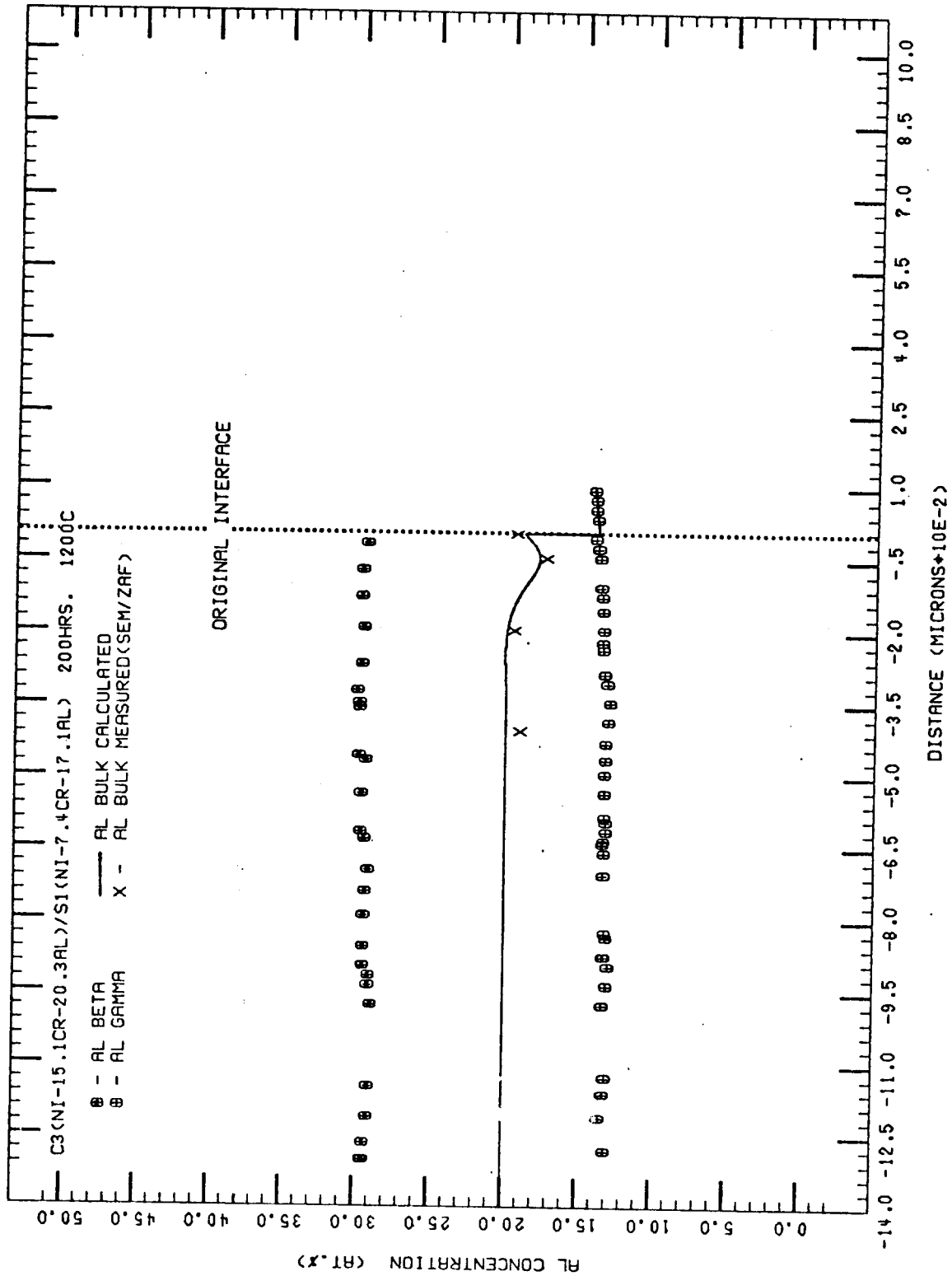
Figure 11. Al concentration/distance profiles in the β and γ phases and the calculated bulk Al profile for couple C3/S1.

34

at the O.I.. The layer can be seen as pertubations of β into the γ growth layer at the O.I.. The volume fraction of β changes from approximately 20 vol.% on the β+γ side of the O.I. (~-20μm) to 35 vol.% at the O.I., and this volume fraction change is reflected in the increase of the bulk Al C/D profile. At the O.I. the bulk Cr C/D profile discontinuously increases and becomes coincident with the Cr composition in the γ growth layer. Likewise at this point, the bulk Al C/D profile discontinuously decreases and becomes coincident with the Al composition in the γ growth layer.

The diffusion path, shown in Figure 9, shows some similar features in the β+γ phase field to the paths of couples C1/S1 and C2/S1. First, the bulk Al decreases while the bulk Cr stays relatively constant. Second, the path does rise like the other paths because a β+γ layer is grown at the O.I. Past the rising segment of path though, the similar features in paths stop. At the O.I., the very narrow β+γ growth layer changes discontinuously into a γ growth layer. The path thus follows a tie line to the γ/β+γ phase boundary (represented by a dashed line) and proceeds to follow the γ/β+γ phase boundary toward the γ corner of the β+γ+γ' triangle. The point where the path follows the tie line corresponds to the point where the bulk Cr C/D profile discontinuously increases and the bulk Al C/D profile discontinuously decreases, both becoming coincident with their respective concentrations in the γ growth layer. Thus the bulk Cr and Al discontinuities

simply correspond to a discontinuous transition from β+γ to γ in the couple. At the γ corner of the β+γ+γ' triangle, the path proceeds up the γ+γ' side and exits into the γ+γ' phase field at the same point where the paths of couples C1/S1 and C2/S1 exited the triangle. (These points were determined by measuring the γ' volume fraction at the three-phase interface.) The path then cuts tie lines until it reaches the composition.

4. C4(Ni-26.4Cr-17.1Al)/S1. Interdiffusion resulted in reces-sion of β in the β+γ alloy (i.e., the β phase dissolved at the O.I., creating a γ layer which thickened with time of interdif-fusion) and growth of β+γ into the γ+γ' alloy. The diffusion zone, shown in Figure 12, consists of the β+γ alloy (C4), a γ phase layer (which resulted from the β recession), the β+γ growth layer, and the γ+γ' alloy (S1). C/D profiles for Cr and Al in the β and γ phases, and the calculated bulk Cr and Al C/D pro-files are shown in Figures 13 and 14, respectively. The behavior of this couple is similar to the behavior of couples C1/S1 and C2/S1 in that a β+γ growth layer resulted from interdiffusion. The β+γ growth layer formed at the expense of the β phase in β+γ alloy. C/D profiles in the β and γ phases in the β+γ alloy showed no concentration gradients. Only at the β+γ alloy/γ interface (i.e., at the start of the γ layer that resulted from β recession) did the C/D profiles start to show concentration gra-dients. The bulk Cr and Al C/D profiles likewise were constant in the β+γ alloy. Similar to couple C3/S1, at the β+γ alloy/γ interface, the bulk C/D profiles show discontinuities - the Cr
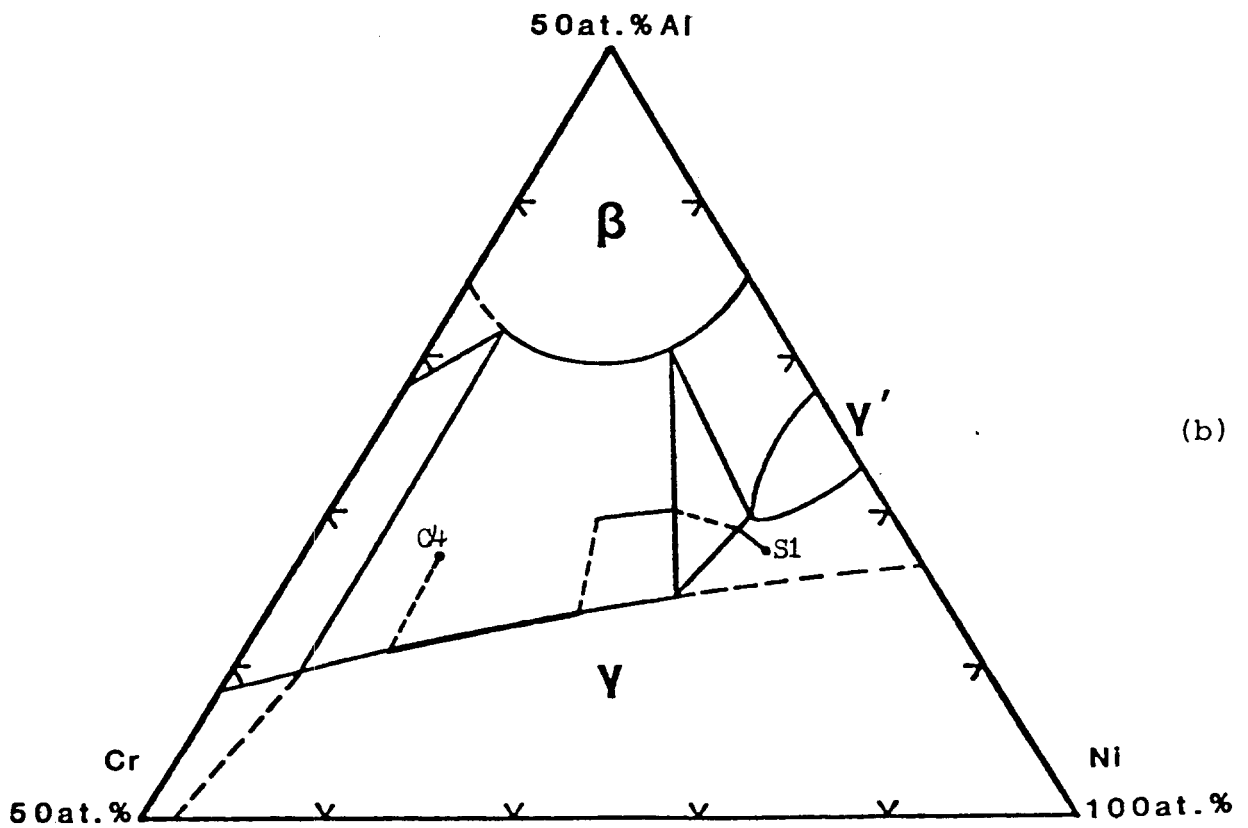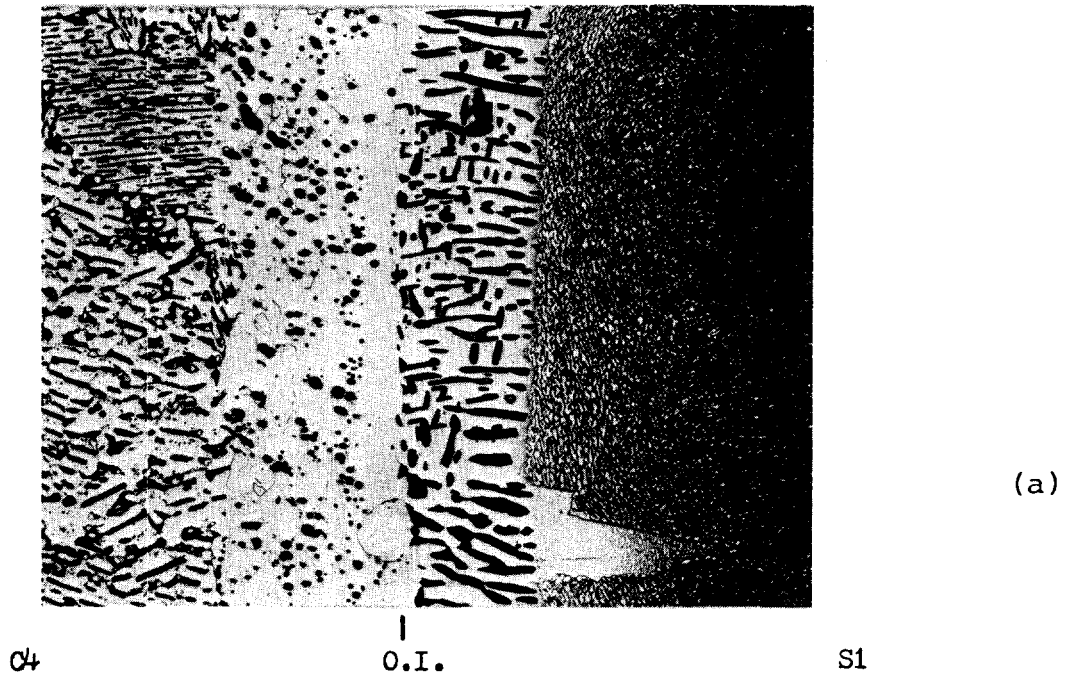
Figure 12. (a) Diffusion zone microstructure (200 hrs.);
and (b) diffusion path for couple C4(Ni-26.4Cr-17.1Al)/
S1(Ni-7.4Cr-17.1Al)
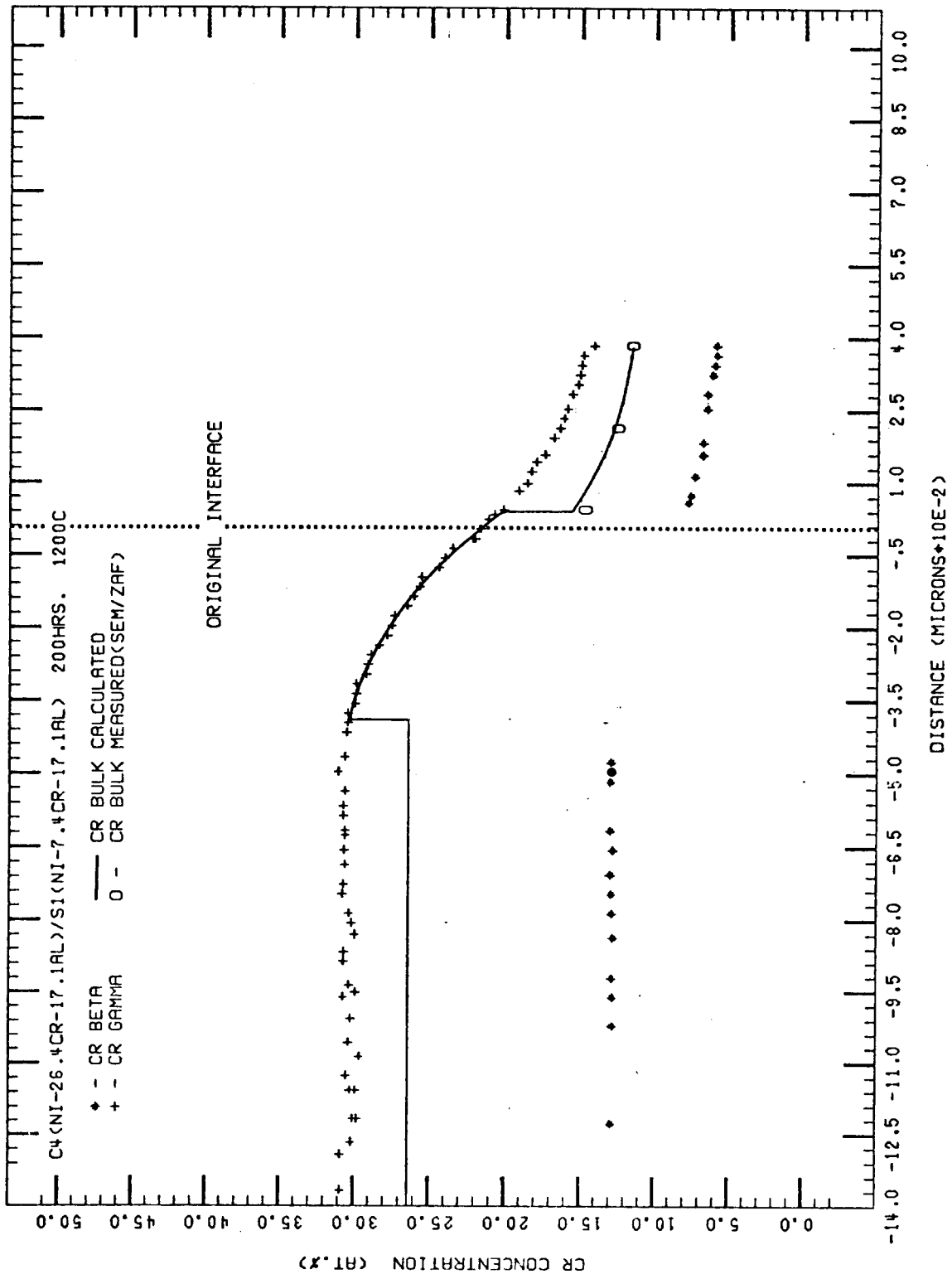
Figure 13. Cr concentration/distance profiles in the β and γ phases and the calculated bulk Cr profile for couple C4/S1.

38
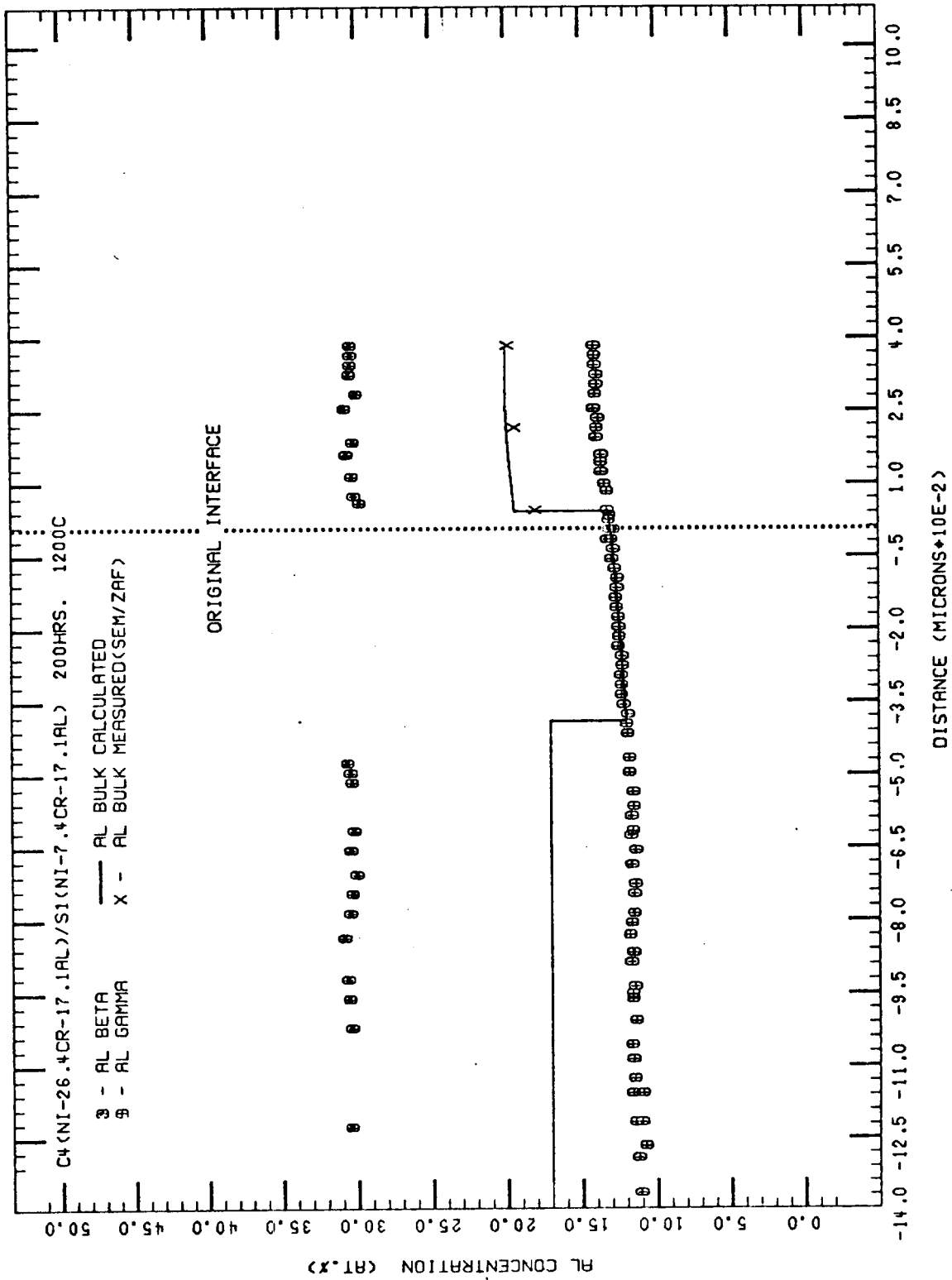
Figure 14. Al concentration/distance profiles in the β and γ phases and the calculated bulk Al profile for couple C4/S1.

increases and becomes coincident with the Cr concentration in the γ layer, and the Al decreases and becomes coincident with the Al concentration in the γ layer. These discontinuities signify that the diffusion path is following a tie line in the β+γ phase field to the γ/β+γ phase boundary. This can be seen in the diffusion zone as a discontinuous change in β volume fraction from approximately 30 vol.% in the β+γ alloy to 0 vol.% in the γ layer.

The bulk C/D profiles stay coincident with the γ phase concentrations in the γ layer until slightly past the O.I. (+40μm) at which point they again change discontinuously. The bulk Cr C/D profile decreases while the bulk Al C/D profile increases. These discontinuities arise from the formation of the β+γ growth layer at the O.I. They signify that, at the γ/β+γ growth layer interface, the diffusion path is proceeding from the γ/β+γ phase boundary into the β+γ phase field along a tie line. In the β+γ growth layer, the volume fraction of β remains constant and this leads to a relatively constant bulk Al C/D profile. The bulk Cr C/D profile continues to decrease in the β+γ growth layer.

The diffusion path, shown in Figure 12, reflects the changes that occur in the diffusion zone microstructure and the C/D profiles. The dashed line from the bulk composition of alloy C4 to the γ/β+γ phase boundary reflects the β+γ alloy/γ interface in the diffusion zone, and the first discontinuity in the bulk Cr and Al C/D profiles. During interdiffusion, the β phase dis-

solves in the β+γ alloy, creating a γ layer and a β+γ alloy/γ interface. This interface, being planar, and the fact that no concentration gradients are present in the β and γ phases up to the β+γ alloy/γ interface, means the diffusion path proceeds from the bulk composition of alloy C4 to the γ/β+γ phase boundary along the equilibrium tie line of alloy C4. The path proceeds along the γ/β+γ phase boundary and then follows a tie line (represented by another dashed line) into the β+γ phase field. The path proceeds through the β+γ phase field and enters the β+γ+γ' triangle at a lower Al composition than couples C1/S1 and C2/S1. The path exits the triangle on the γ+γ' side at the same Al composition where the other couples in the series exited the triangle. It then cuts tie lines and ends at the bulk composition of alloy S1.

5. Growth Layer Kinetics. Measured β+γ growth for couples C1/S1, C2/S1 and C4/S1, and measured γ growth for couple C3/S1, all versus time, are shown in Figure 15. The curves through the data points follow the equation:

$$X = Ct^y \qquad (1)$$

where X represents the length of the growth layer, C is a constant, t is time, and y is an exponent. If parabolic growth kinetics prevailed, y should be equal to 0.5. Using standard linear regression techniques, the constant C and exponent were calculated for each couple. The exponents ranged from 0.37
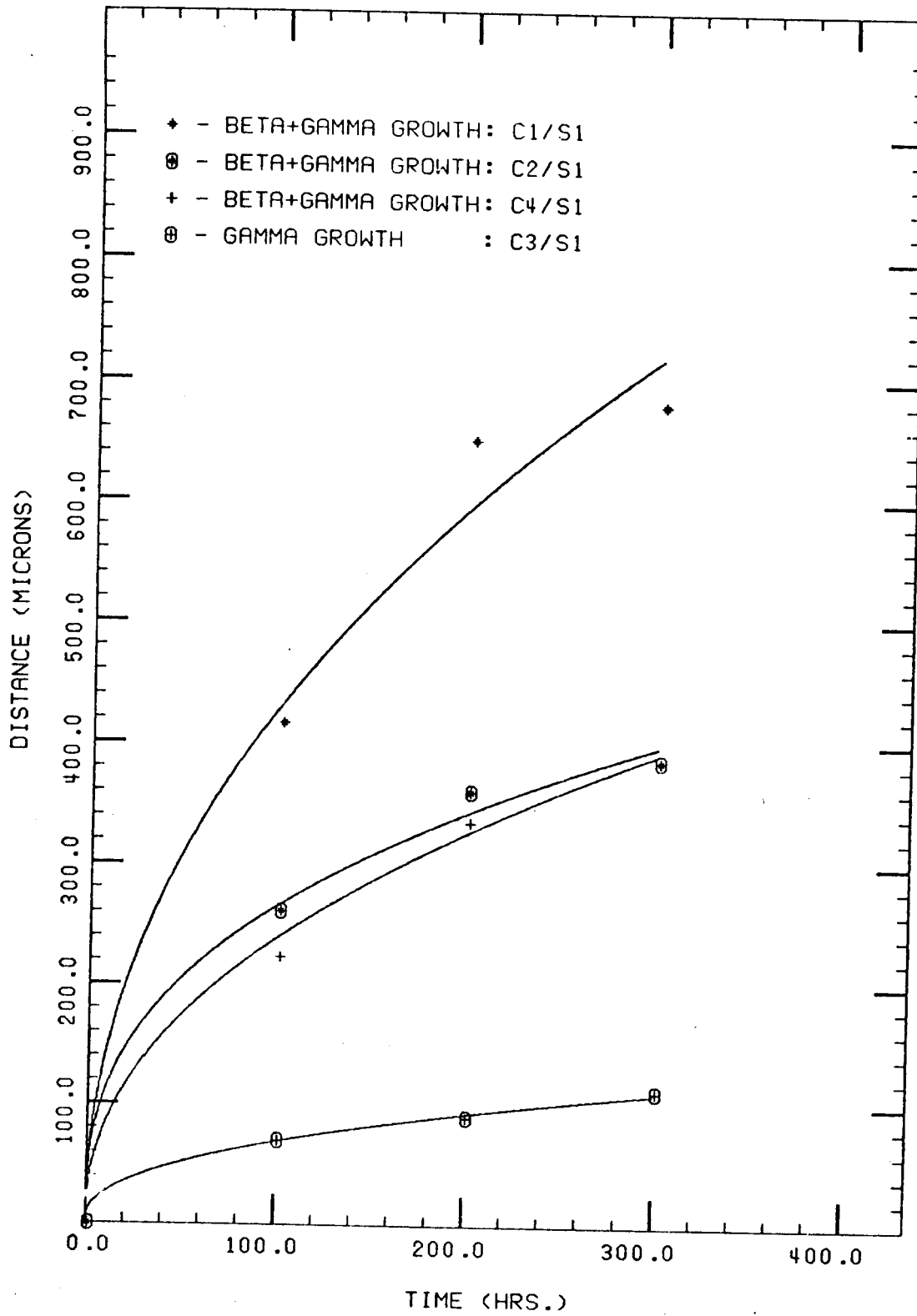
Figure 15.   Measured β+γ growth vs. time for couples C1/S1,
             C2/S1, and C4/S1, and measured γ growth vs.
             time for couple C3/S1.

(C2/S1) to 0.47 (C1/S1). Comparing the data at 200 hours, it can be seen that C1/S1 had the largest β+γ growth layer (650μm), followed by C2/S1 (360μm) and C4/S1 (330μm). The amount of growth of the γ layer at 200 hours in couple C3/S1 was much less than the amount of β+γ growth at 200 hours in each of the other couples.

Series 2. C1, C2, C3, C4/S2(Ni-3.5Cr-17.0Al)

1.   C1/S2. Interdiffusion resulted in the formation of two layers: a β+γ growth layer and a γ' growth layer. The diffusion zone, shown in Figure 16, consists of the β+γ alloy (C1), the β+γ growth layer, the γ' growth layer, and the γ+γ' alloy (S2). The diffusion zone of this couple is similar to the diffusion zone of couple C1/S1 except that a γ' layer also results from interdiffusion. C/D profiles for Cr and Al in the β, γ, and γ' phases, and the calculated bulk Cr and Al C/D profiles are shown in Figures 17 and 18, respectively. The C/D profiles in the phases and the bulk C/D profiles are similar to those of couple C1/S1. The sharp decrease in the bulk Cr C/D profile and the sharp increase in the bulk Al C/D profile at distances near the O.I. results from an almost discontinuous change of β volume fraction from 38 vol.% in the β+γ alloy, near the O.I., to 48 vol.% at the start of the β+γ growth layer. The β volume fraction is less near the O.I. in this couple than in couple C1/S1. In the β+γ growth layer the volume fraction of β increases over the first 150μm from 48 vol.% to 66 vol.% and then remains con-
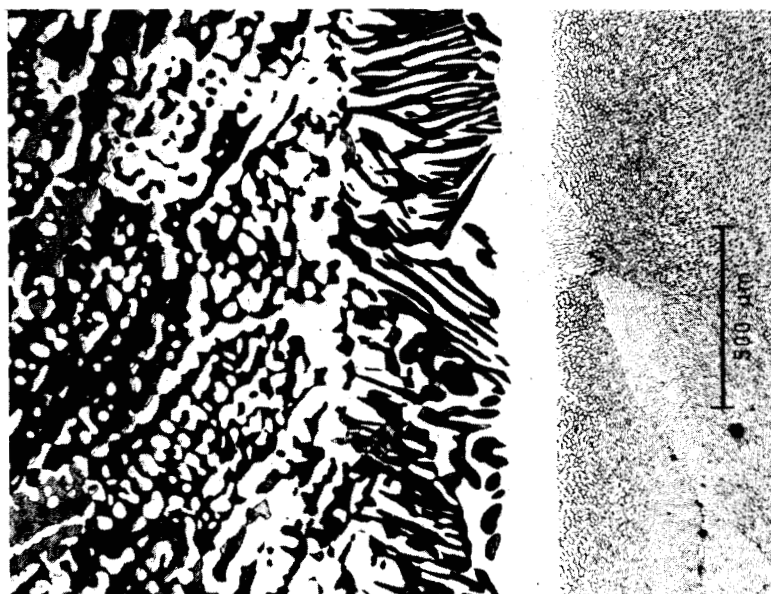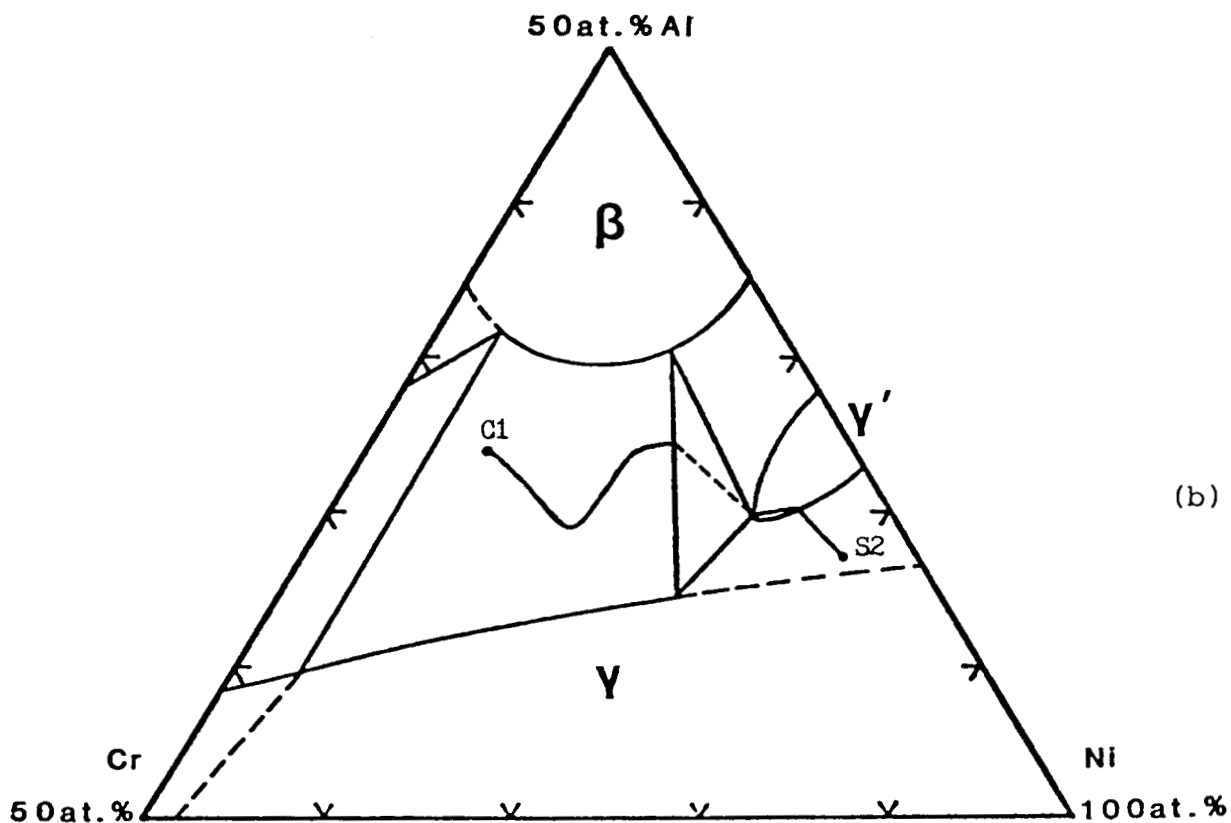
Figure 16. (a) Diffusion zone microstructure (200 hrs.);
and (b) diffusion path for couple C1(Ni-20.0Cr-24.1Al)/
S2(Ni-3.5Cr-17.0Al)
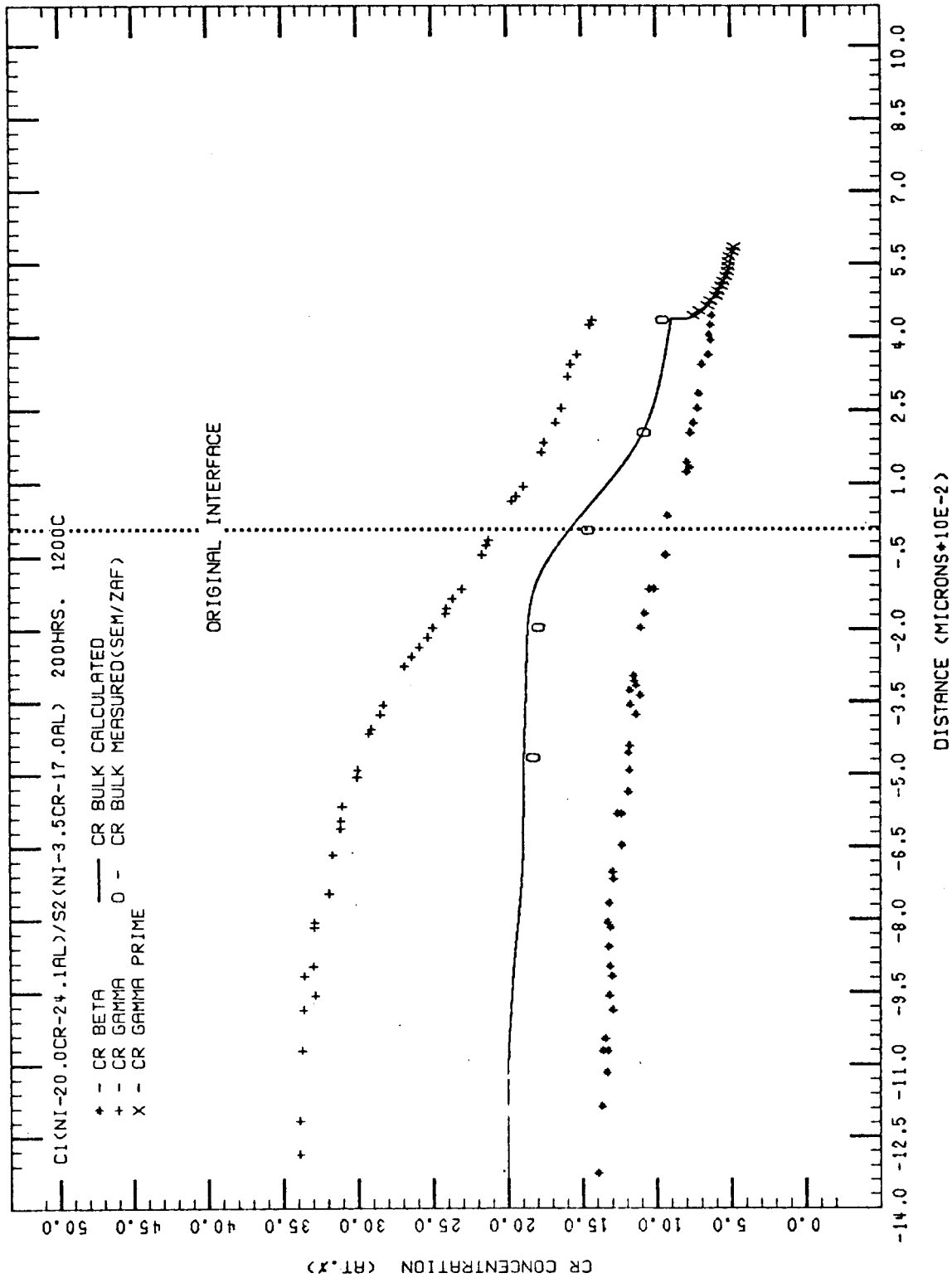
Figure 17. Cr concentration/distance profiles in the β, γ, and γ' phases and the calculated bulk Cr profile for couple C1/S2.
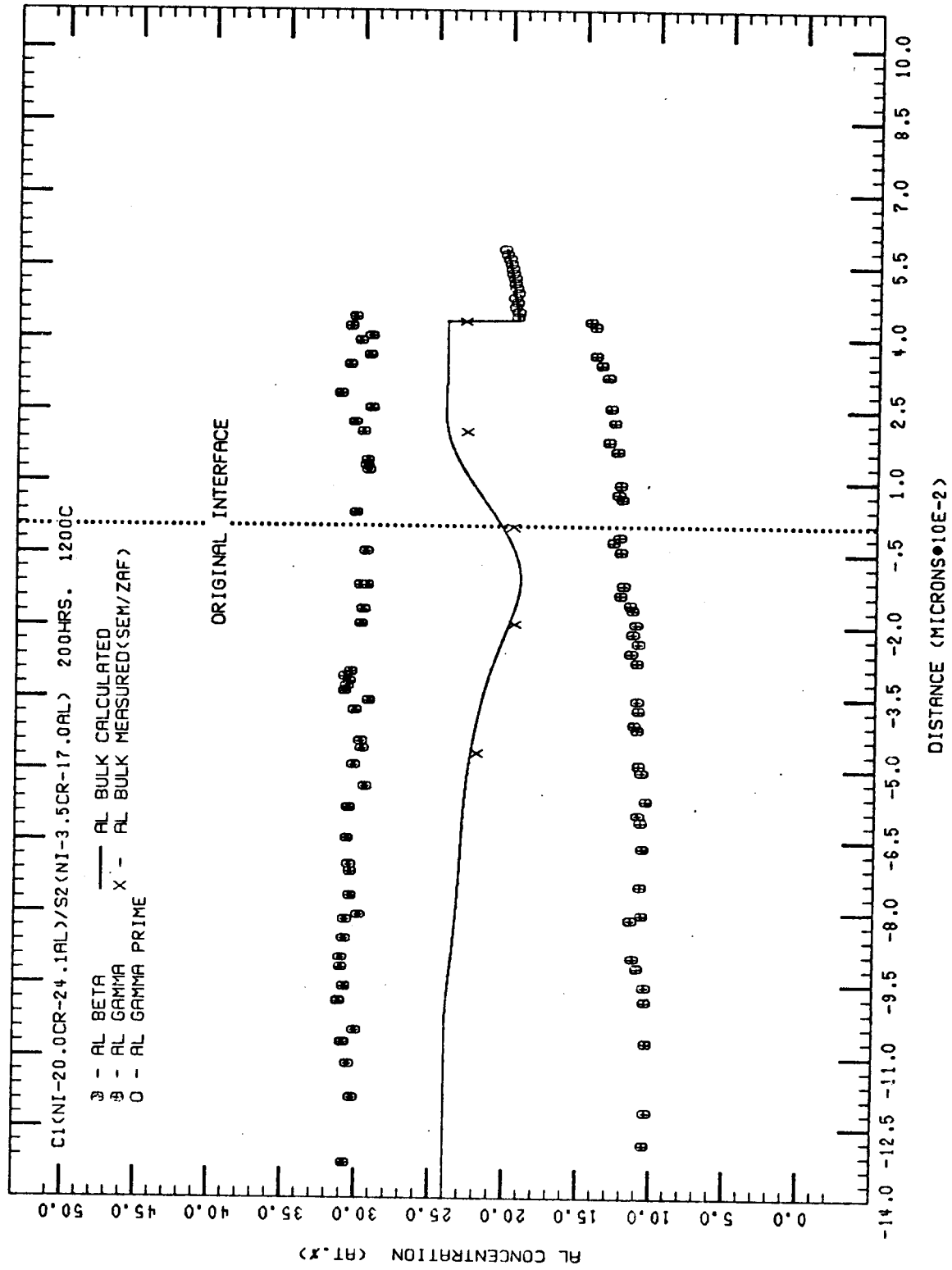
Figure 18. Al concentration/distance profiles in the β, γ, and γ' phases and the calculated bulk Al profile for couple C1/S2.

stant up to the β+γ/γ' interface. Thus, the bulk Al C/D profile does increase in the β+γ growth layer and then levels off to a constant value. At the β+γ/γ' interface the bulk Cr and Al C/D profiles change discontinuously and become coincident with their respective concentrations in the γ' growth layer. The Cr concentration in the γ' layer decreases sharply initially and then levels off. The Al concentration in the γ' layer increases slightly over the same distance.

The diffusion path, shown in Figure 16, has similar features in the β+γ phase field to that of couple C1/S1. The bulk Al decreases first while the bulk Cr stays relatively constant. The decrease in bulk Al is greater in this couple than in couple C1/ S1 because the volume fraction of β near the O.I. is less than the volume fraction of β near the O.I. in couple C1/S1. The path in the β+γ phase field stays "V" shaped longer than the path for couple C1/S1 because the volume fraction of β increases in the β+γ growth layer over the first 150μm. Only in approximately the last 200μm of the β+γ growth layer does the volume fraction of β remain constant and thus the path does not level off as fast as it did for couple C1/S1.

The path enters the β+γ+γ' triangle at a higher Al composition than the path of C1/S1. This is because the volume fraction of β is greater at the three-phase interface in this couple, than in C1/S1. As the path moves through the triangle (represented by a dashed line which indicates an interface of no spatial extent) the compositions of Cr and Al must change

discontinuously. These discontinuous changes in composition can be seen in the bulk Cr and Al C/D profiles at the $\beta+\gamma/\gamma'$ interface. (It should be noted that the couples of Series 1 also show discontinuities in bulk composition at the $\beta+\gamma/\gamma+\gamma'$ interface present in the couples. These were not shown in the C/D figures because bulk compositions in the $\gamma+\gamma'$ alloy were not determined.) The path exits the triangle into the γ' phase field. In the γ' phase field the path increases in Al composition slightly, while the Cr composition continues to decrease. At the $\gamma'/\gamma+\gamma'$ interface in the couple, the path exits the γ' phase field into the $\gamma+\gamma'$ phase field and cuts tie lines (as seen by a gradual reduction in the volume fraction of γ' away from the $\gamma'/\gamma+\gamma'$ interface in Figure 16) until it reaches the composition of S2.

2.   C2/S2. Interdiffusion resulted in a similar diffusion zone microstructure to couple C1/S2 - consisting of the $\beta+\gamma$ alloy (C2), $\beta+\gamma$ growth, γ' growth, and the $\gamma+\gamma'$ alloy (S2), as shown in Figure 19. C/D profiles for Cr and Al in the β, γ, and γ' phases, and the calculated bulk Cr and Al C/D profiles are shown in Figures 20 and 21, respectively. The C/D profiles in the $\beta+\gamma$ regions are similar to those of couple C2/S1. The bulk Al C/D profile shows similar behavior to the bulk Al C/D profile of C2/S1, but two differences can be noted. First, it decreases to slightly lower values near the O.I. because the reduction in the volume fraction of β is slightly greater near the O.I..

C2   O.I.   S2

(a)

50at.%Al

β

C2

γ′

S2

γ

Cr   Ni

50at.%   100at.%
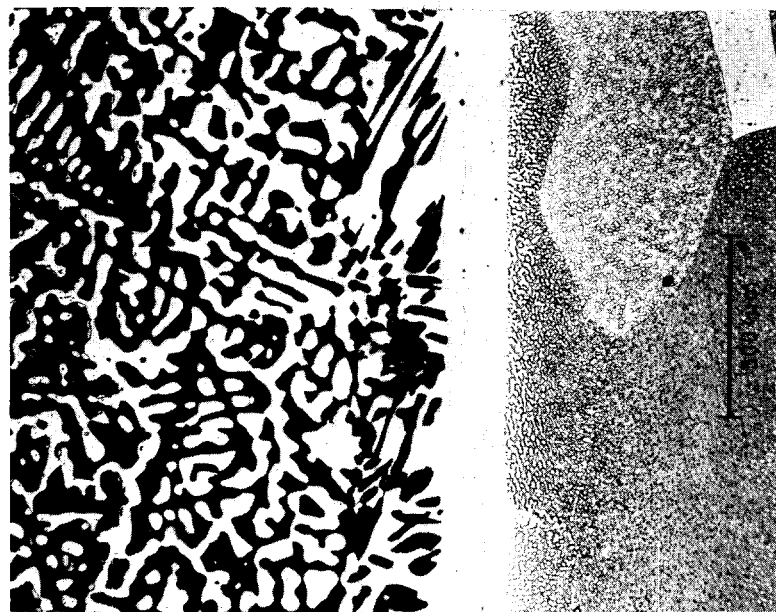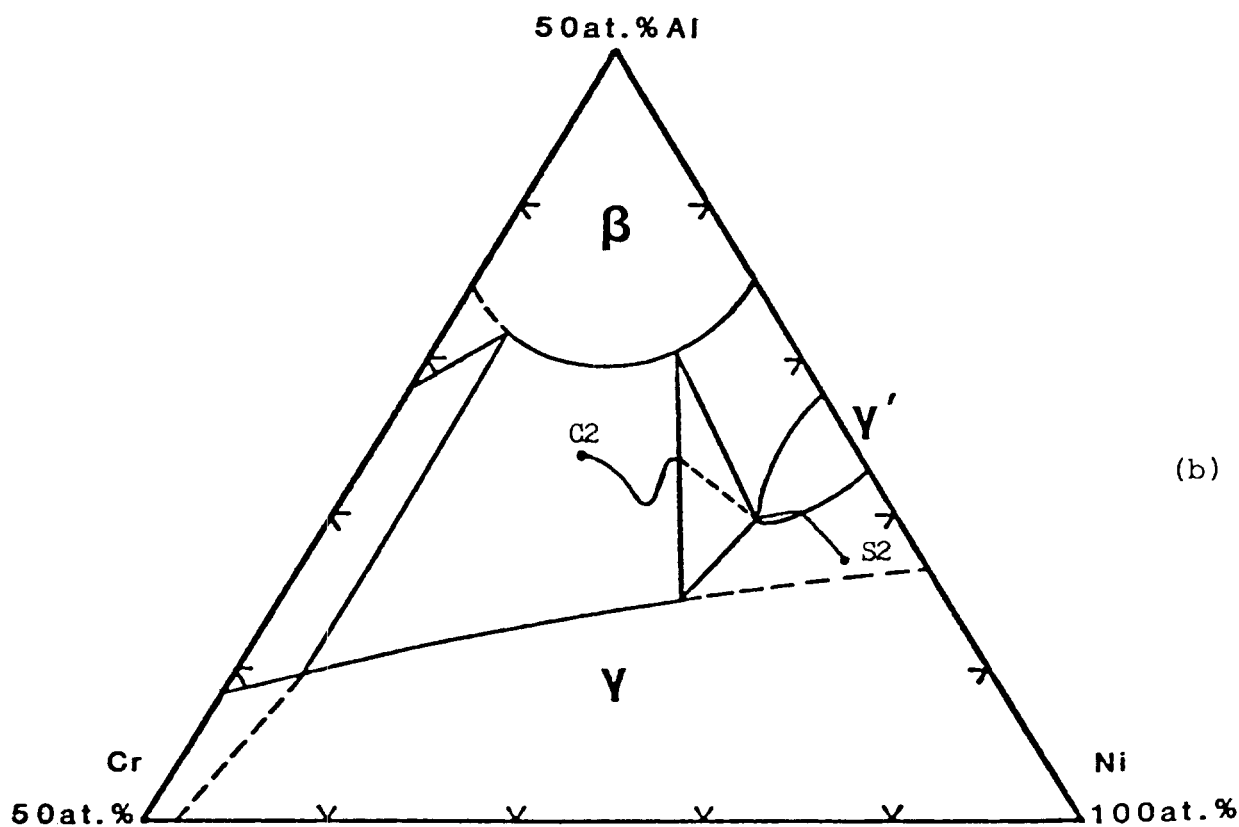
(b)

Figure 19. (a) Diffusion zone microstructure (200 hrs.);
and (b) diffusion path for couple C2(Ni-15.3Cr-23.9Al)/
S2(Ni-3.5Cr-17.0Al)
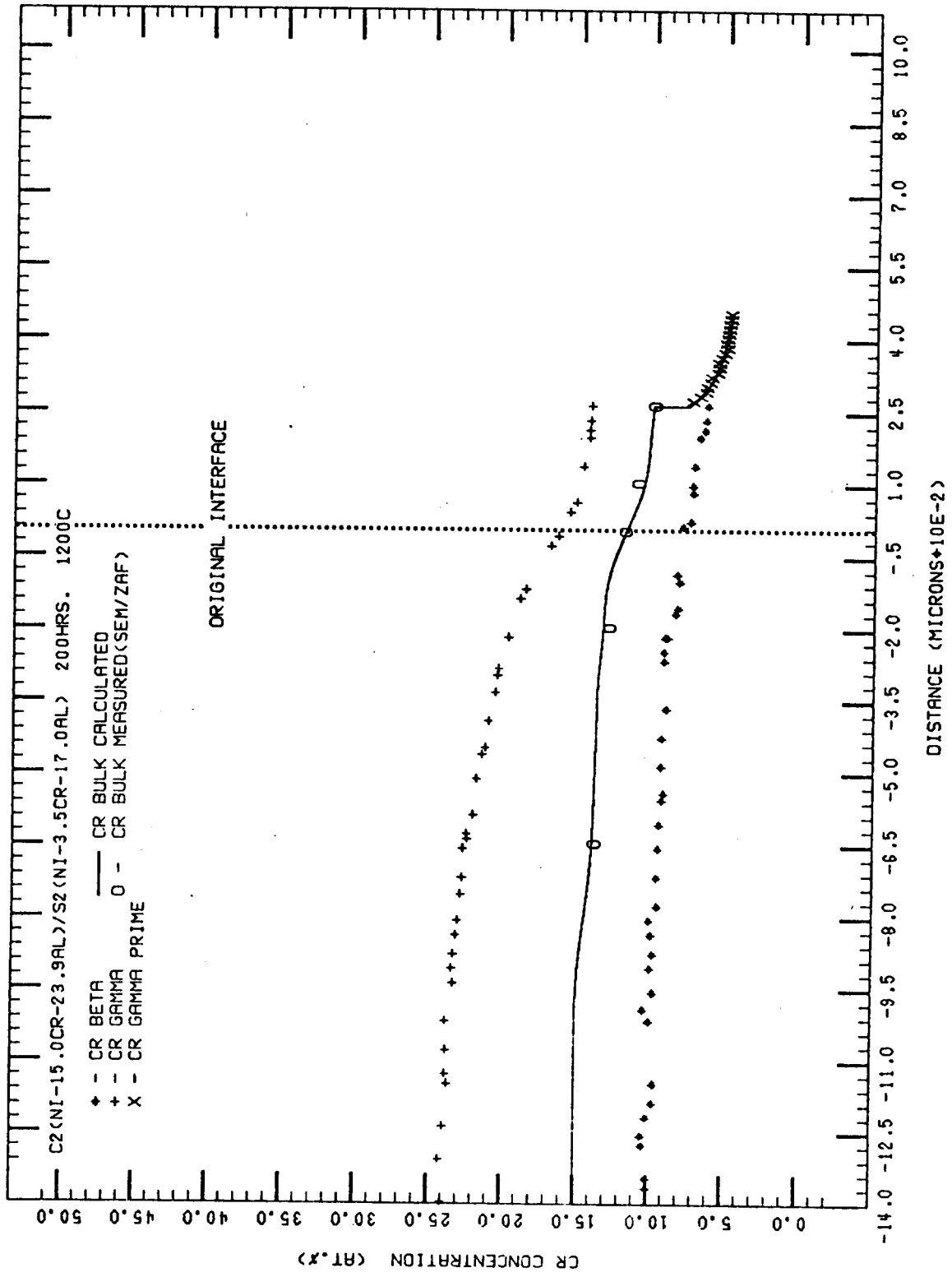
Figure 20. Cr concentration/distance profiles in the β, γ, and γ' phases and the calcualted bulk Cr profile for couple C2/S2.
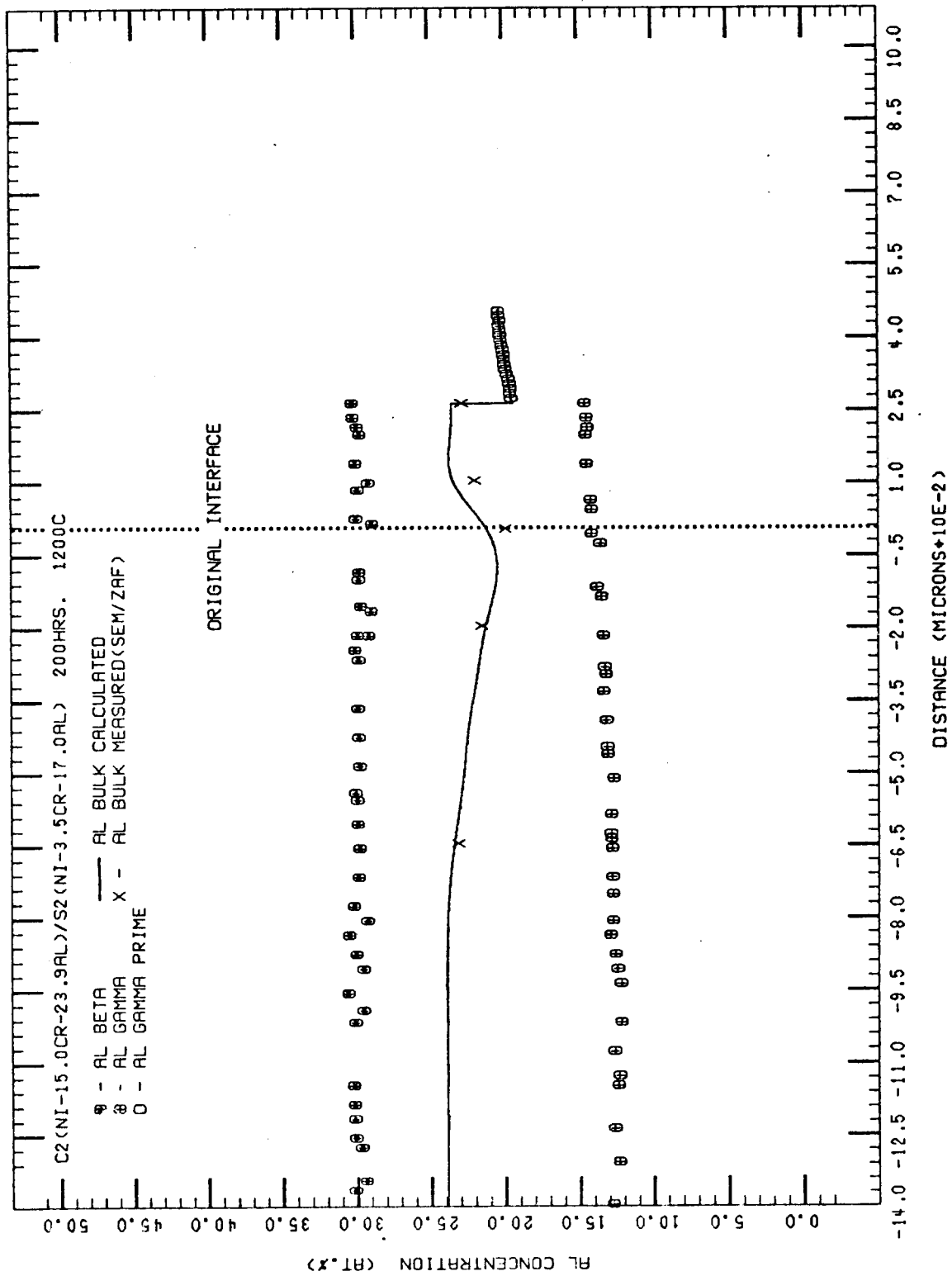
Figure 21. Al concentration/distance profiles in the β, γ, and γ' phases and the calcualted bulk Al profile for couple C2/S2.

Second, it increases sharply and levels off to a higher Al composition because the volume fraction of β in the β+γ growth layer is higher. At the β+γ/γ' interface the bulk Cr and Al C/D profiles change discontinuously and become coincident with their respective concentrations in the γ' growth layer.

The diffusion path shown in Figure 19, exhibits a "V" shape similar to that of couple C1/S2. Comparing the section of path in the β+γ field to that of couple C2/S1 shows that the path decreases to slightly lower Al compositions in the first segment and then rises and enters the β+γ+γ' triangle, at a higher Al composition - both facts in accord with the differences found between the bulk Al C/D profiles of the two couples. The constant Al composition segment of path, which was large in couple C1/S1 and C2/S1, is very small, if nonexistent, in this couple. The volume fraction of β changes discontinuously from 42 vol.% on the β+γ alloy side of the O.I. to 49 vol.% on the β+γ growth layer side of the I.O.. The volume fraction of β continues to increase from 49 vol.% to 59 vol.% at 150μm in the β+γ growth layer. Past 150μm, the volume fraction of β remains constant. Because of the constant β volume fraction, the bulk Al composition remains constant past 150μm. The bulk Cr composition past 150μm changes little and is very near the Cr composition at the β+γ side of the β+γ+γ' triangle. Thus, although the bulk Al stays constant over the last 100μm of the β+γ growth layer, when plotted with the bulk Cr compositions on the phase diagram, it

52

translates to a very small path segment of constant Al composition.

The path exits the triangle into the γ' phase field. The path segment through the γ' phase field is the same as the path segment through the γ' phase field in couple C1/S2. It exits the γ' phase field into the $\gamma+\gamma'$ phase field at the same Cr and Al composition where the path of C1/S2 exited the γ' phase field. The path then cuts tie lines in the $\gamma+\gamma'$ phase field until it reaches the bulk composition of alloy S2.

3. C3/S2. Interdiffusion resulted in similar microstructural features to couple C3/S1 and couples C1/S2 and C2/S2. First, a γ growth layer formed similar to C3/S1, and second a γ' growth layer formed similar to C1/S2 and C2/S2. The diffusion zone, shown in Figure 22, consists of the $\beta+\gamma$ alloy (C3), the γ growth layer, the γ' growth layer, and the $\gamma+\gamma'$ alloy (S2). C/D profiles for Cr and Al in the β, γ, and γ' phases, and the calculated bulk Cr and Al C/D profiles are shown in Figures 23 and 24, respectively. The bulk Cr C/D profile was similar to the bulk Cr C/D profile of couple C3/S1 with the exception that it decreases less sharply near the O.I.. The bulk Al C/D profile begins to decrease much further back in the $\beta+\gamma$ alloy ($\sim$-400μm) and to lower Al composition than did the bulk Al C/D profile of C3/S1. This decrease to lower Al composition is a result of greater reductions in the volume fraction of β up to the O.I.. A very narrow $\beta+\gamma$ layer is grown at the O.I.. This layer can

(a)

C3   0.I.   S2

50at.%Al

β

γ'

C3

S2

Cr   Ni

γ

50at.%   100at.%
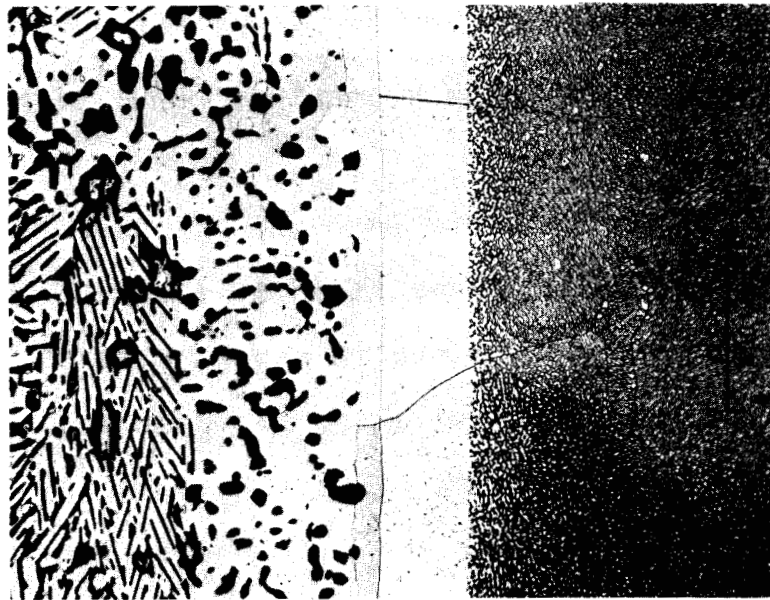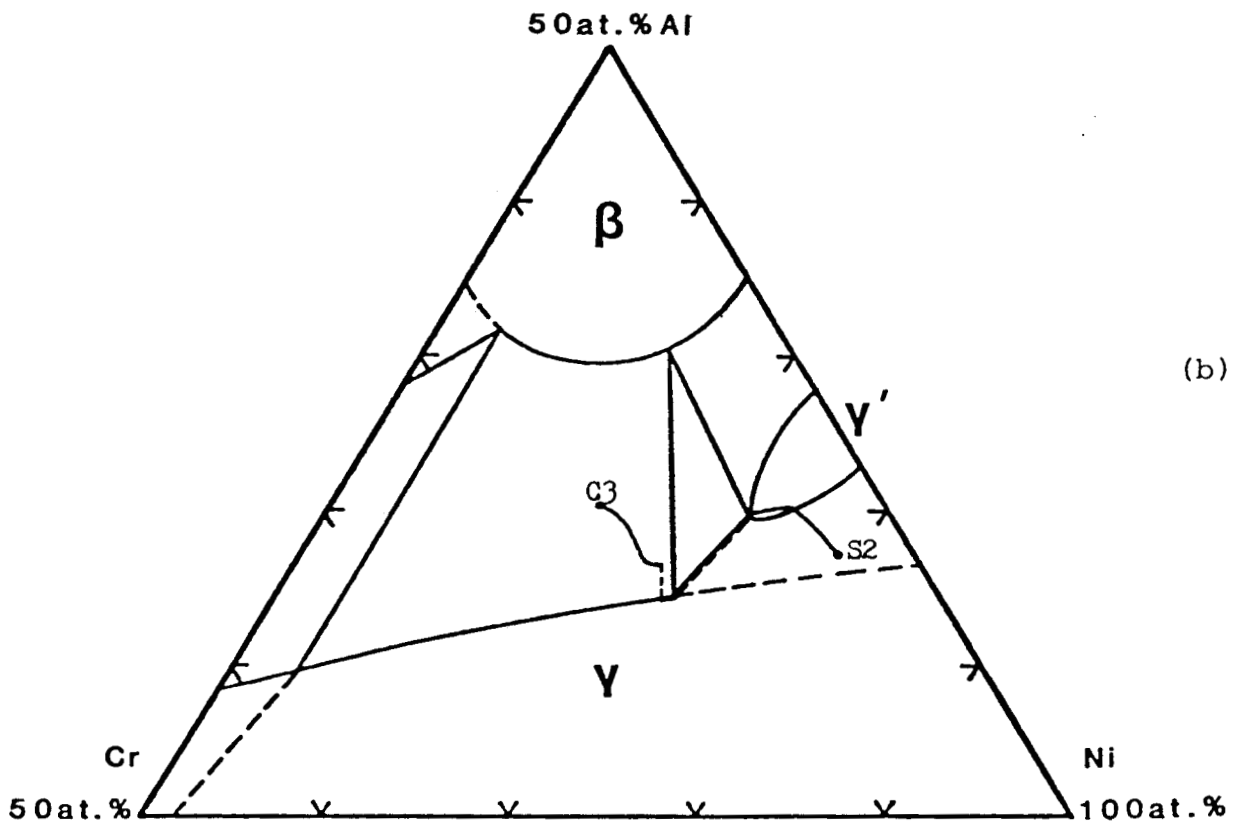
(b)

Figure 22. (a) Diffusion zone microstructure (200 hrs.);
and (b) diffusion path for couple C3(Ni-15.1Cr-20.3Al)/
S2(Ni-3.5Cr-17.0Al)

54
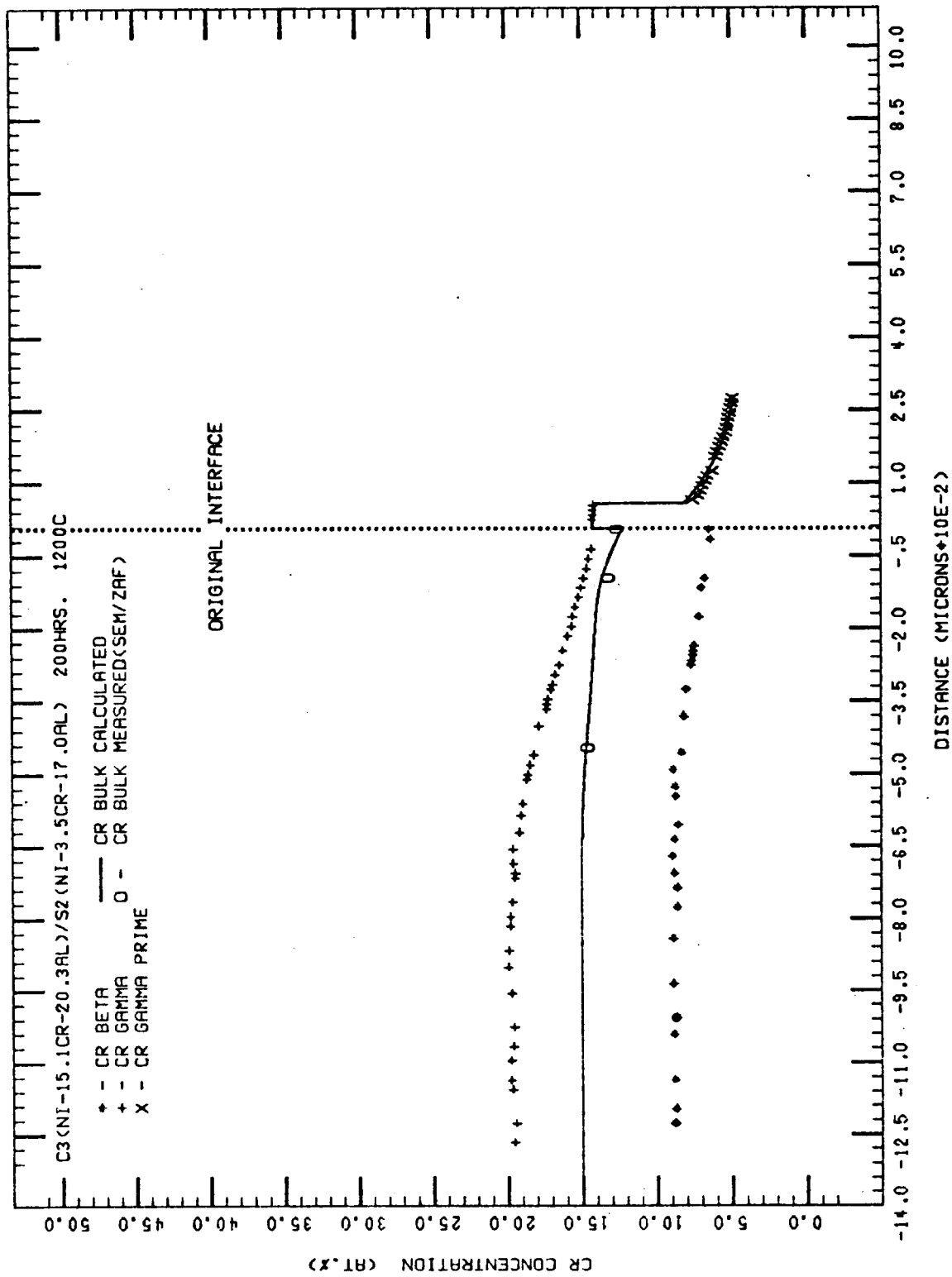
Figure 23. Cr concentration/distance profiles in the β, γ, and γ' phases and the calculated bulk Cr profile for couple C3/S2.
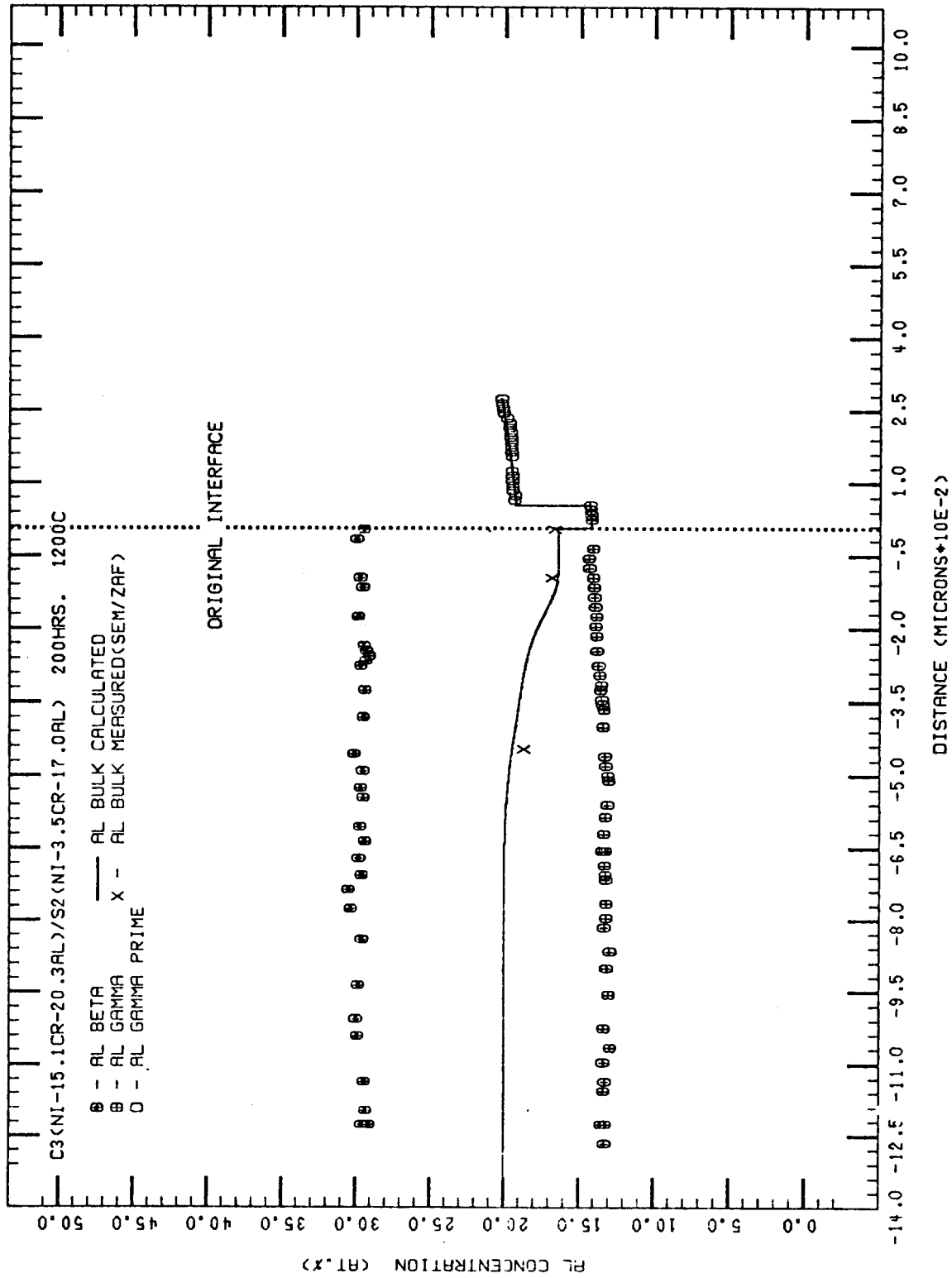
Figure 24. Al concentration/distance profiles in the β, γ, and γ' phases and the calculated bulk Al profile for couple C3/S2.

be seen as pertubations of β into the γ growth layer at the O.I..
However, the volume fraction of β at the O.I. is similar to the
volume fraction of β near the O.I. in the β+γ alloy (0 to -50μm),
and thus the bulk Al C/D profile does not increase at the O.I..

At the β+γ/γ growth layer interface, the bulk Cr C/D pro-
file increases discontinuously and becomes coincident with the
Cr concentration in the γ growth layer. Likewise the bulk Al
C/D profile decreases discontinuously and becomes coincident with
the Al concentration in the γ growth layer. The bulk composi-
tions stay coincident with the γ growth layer concentrations
until the γ/γ' interface at which point they again change dis-
continuously. The bulk Cr decreases almost 7.0 at.% and becomes
coincident with the Cr concentration in the γ' growth layer.
The bulk Al increases 5.0 at.% and becomes coincident with the
Al concentration in the γ' layer. The presence of the γ/γ' in-
terface in the couple, and the bulk composition discontinuities
at the interface, signify the diffusion path is moving up the
γ+γ' side of the β+γ+γ' triangle from the γ corner to the γ'
corner.

The diffusion path, shown in Figure 22, has some similar
features in the β+γ phase field to the path of C3/S1. The bulk
Al decreases first, and to lower Al composition than the same
path segment in C3/S1. The path levels off slightly in Al com-
position because of a relatively constant β volume fraction
from -50μm to the O.I. in the couple. At the O.I., the narrow
β+γ growth layer changes discontinuously into a γ growth layer,

57

and thus the path follows a tie line in the β+γ phase field to the γ/β+γ phase boundary. The path follows the γ/β+γ phase boundary to the γ corner of the β+γ+γ' triangle, at which point it proceeds up the γ+γ' side to the γ' corner. In the γ'-phase field, the path is the same as for the other couples in the series. Likewise, the Cr and Al compositions at the γ'/γ+γ' interface are the same as the other couples in the series. This similarity in compositions means the path exits the γ' phase field into the γ+γ' phase field at the same point where the paths of the other couples exited the γ' phase field. The path then cuts tie lines in the γ+γ' phase field until it reaches the composition of S2.

4. C4/S2. Interdiffusion resulted in a similar diffusion zone microstructure to couple C4/S1, with the addition of a γ' growth layer. The diffusion zone, shown in Figure 25, consists of the β+γ alloy (C4), a γ layer which resulted from recession of β, the β+γ growth layer, the γ' growth layer, and the γ+γ' alloy (S2). C/D profiles for Cr and Al in the β, γ, and γ' phases, and the calculated bulk Cr and Al C/D profiles are shown in Figures 26 and 27, respectively. The C/D profiles show very similar behavior to those of couple C4/S1. The Cr and Al C/D profiles in the β and γ phases, and the bulk Cr and Al C/D profiles are constant up to the β+γ alloy/γ interface. At the β+γ alloy/γ interface, the Cr and Al concentrations in the γ layer begin to exhibit concentration gradients. The bulk Cr and Al
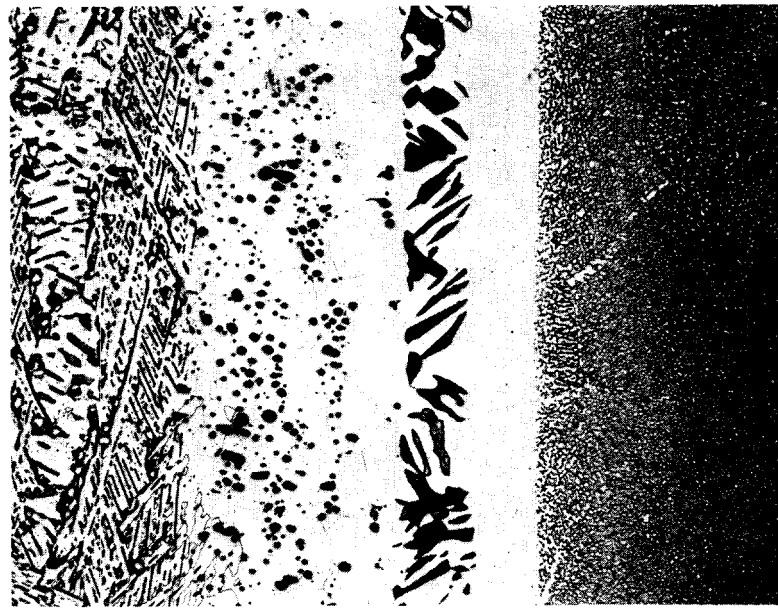
(a)
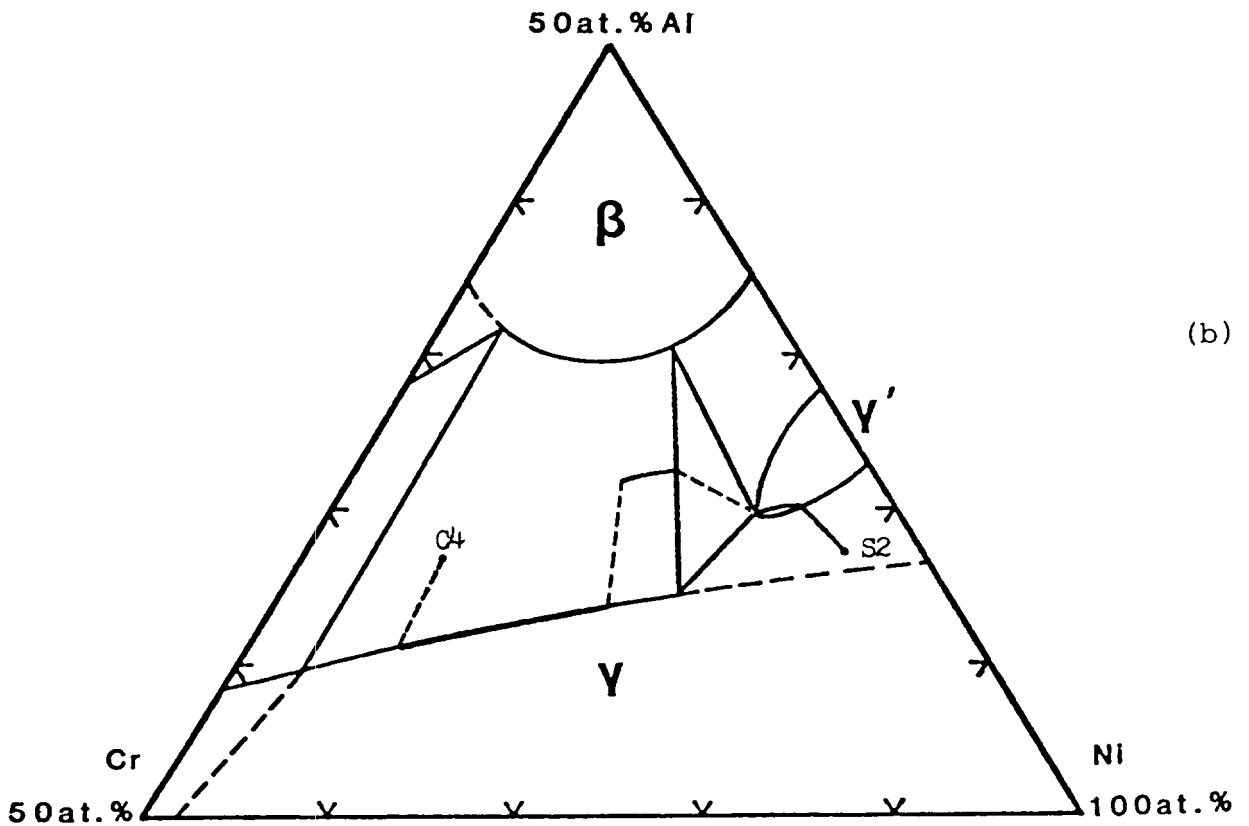
(b)

Figure 25. (a) Diffusion path microstructure (200 hrs.);
and (b) diffusion path for couple C4(Ni-26.4Cr-17.1Al)/
S2(Ni-3.5Cr-17.0Al)
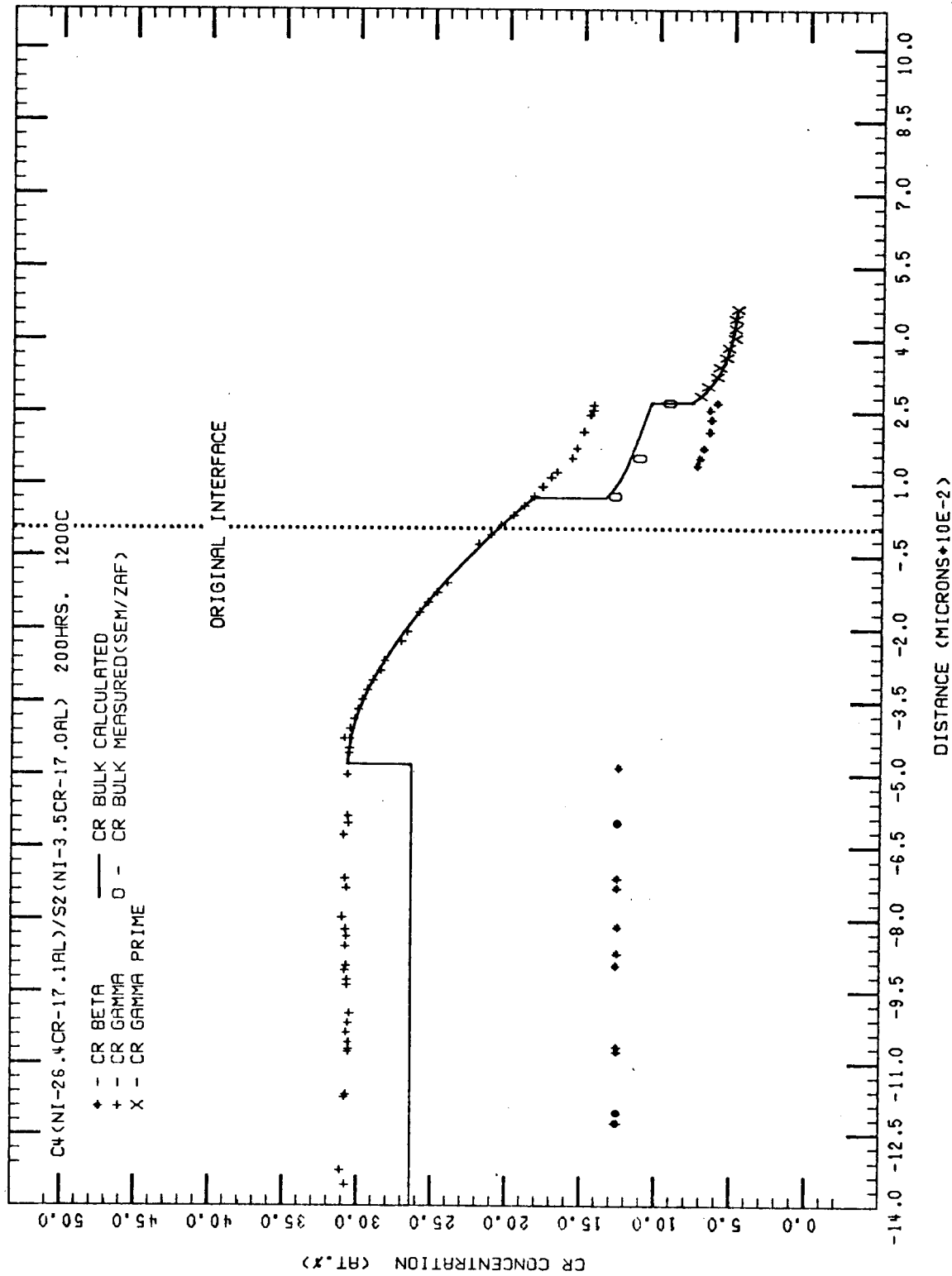
Figure 26. Cr concentration/distance profiles in the β, γ, and γ' phases and the calculated bulk Cr profile for couple C4/S2.

60
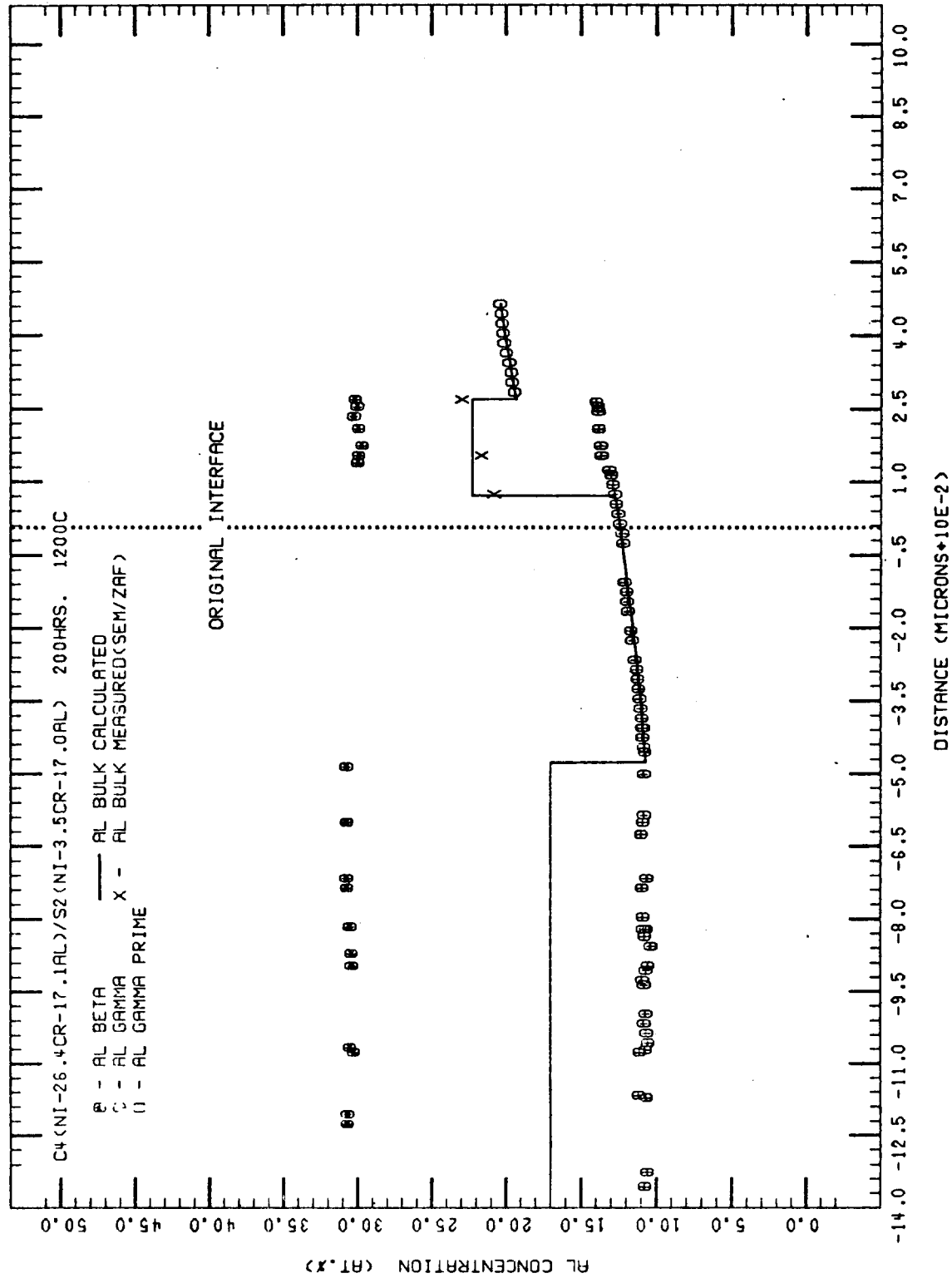
Figure 27. Al concentration/distance profiles in the β, γ, and γ' phases and the calculated bulk Al profile for couple C4/S2.

C/D profiles change discontinuously at the β+γ alloy/γ interface, the Cr increases and becomes coincident with the Cr concentration in the γ layer while the Al decreases and becomes coincident with the Al concentration in the γ layer. The bulk C/D profiles stay coincident with the γ layer concentrations until approximately +70.0μm at which point they change discontinuously again. The bulk Cr C/D profile decreases while the bulk Al C/D profile increases. In the β+γ growth layer, the β volume fraction is greater than the β volume fraction in the β+γ growth layer of couple C4/S1. Thus, the bulk Al C/D profile is higher in the β+γ growth layer than in C4/S1. At the β+γ/γ' interface, the bulk Cr and Al C/D profiles again change discontinuously and become coincident with the Cr and Al concentrations in the γ' growth layer. The Cr concentration decreases in the γ' layer while the Al concentration increases slightly.

The diffusion path, shown in Figure 25, is very similar to that of C4/S1. The path follows the equilibrium tie line of alloy C4 from the bulk composition of alloy C4 to the γ/β+γ phase boundary. This section of path is represented by the β+γ alloy/γ interface in the couple. The path proceeds along the γ/β+γ phase boundary and then follows a tie line into the β+γ phase field. This tie line section of path is represented by the γ/β+γ growth layer interface in the couple. The path follows the tie line to higher Al composition than did C4/S1, because the β volume fraction is greater in the β+γ growth layer than in C4/S1. Because of a higher β volume fraction the path

also enters the β+γ+γ' triangle at a higher Al composition than did C4/S1. The path exits the triangle into the γ' phase field. The section of path through the γ' phase field, and γ+γ' phase field, to the composition of S2, is the same as for the other couples in the series.

5.   Growth Layer Kinetics. Measured β+γ growth for couples C1/S2, C2/S2, and C4/S2, and measured γ growth for couple C3/S2, all versus time , are shown in Figure 28. Measured γ' growth versus time for all couples in the series is shown in Figure 29. Exponents for the curves through the β+γ growth data points in Figure 29 ranged from 0.37 (C2/S2) to 0.42 (C1/S2). Exponents for the curves through the γ' growth data points in Figure 29 ranged from 0.54 (C3/S2) to 0.79 (C1/S2). Comparing the β+γ growth at 200 hours it can be seen that C1/S2 had the largest β+γ growth layer (465μm), followed by C2/S2 (268μm) and C4/S2 (170μm). The growth of the γ layer at 200 hours in couple C3/S1 was appreciably less than the amount of β+γ growth at 200 hours in each of the other couples. Comparing the γ' growth at 200 hours it can be seen that C3/S2 had the largest γ' growth layer (230μm), followed by C4/S2 (190μm), C2/S2 (170μm), and C1/S2 (135μm).

Series 3. C1, C2, C3/S3 (Ni-16.2Al)

1.   C1/S3. Interdiffusion resulted in a similar diffusion zone microstructure to that of C1/S2, with the formation of a β+γ growth layer and a γ' growth layer. However, because alloy S3
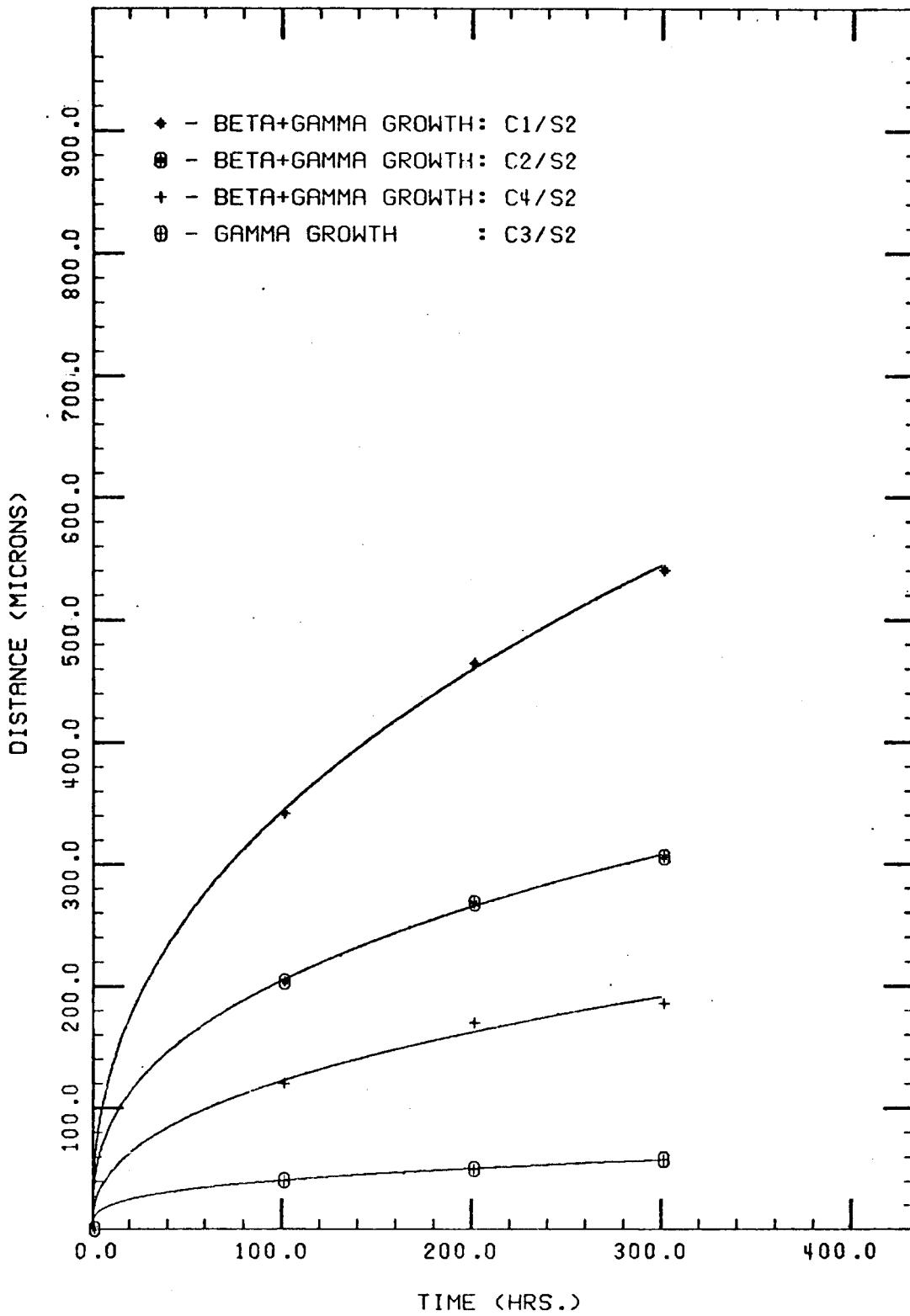
Figure 28. Measured β+γ growth vs. time for couples
C1/S2, C2/S2, and C4/S2, and measured
γ growth vs. time for couple C3/S2.
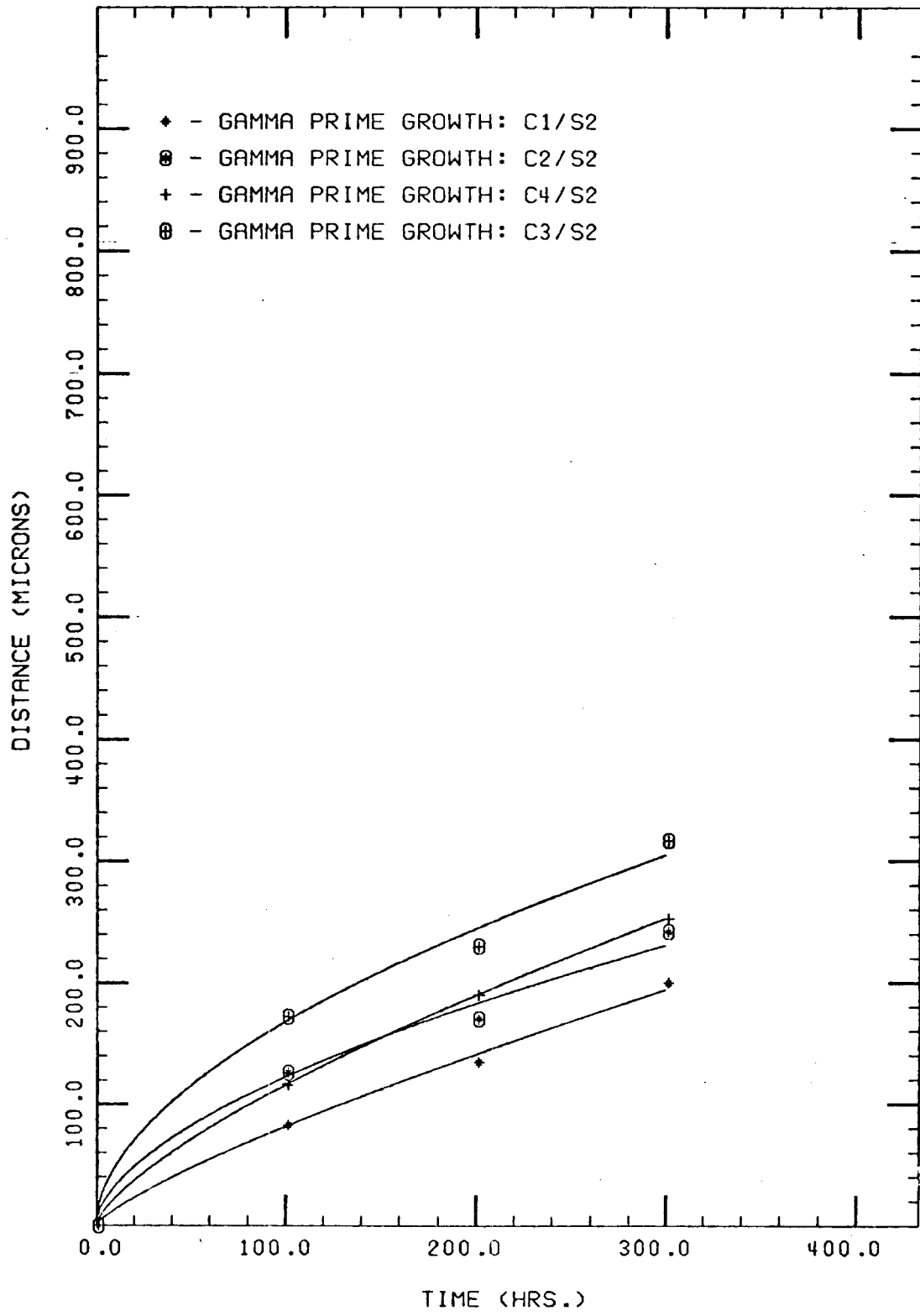
Figure 29. Measured γ' growth vs. time for couples C1/S2, C2/S2, C3/S2, and C4/S2.

resulted in a γ alloy after being cast and annealed, and not a $\gamma + \gamma'$ alloy, a $\gamma + \gamma'$ zone is also present in the microstructure. The diffusion zone microstructure, shown in Figure 30, consists of the $\beta + \gamma$ alloy (Cl), the $\beta + \gamma$ growth layer, the γ' growth layer, the $\gamma + \gamma'$ layer, and the γ alloy (S3). C/D profiles for Cr and Al in the β, γ, and γ' phases, and the calculated bulk Cr and Al C/D profiles are shown in Figure 31 and 32, respectively. The C/D profiles in the phases and the bulk C/D profiles exhibit similar features to the profiles of couples Cl/S1 and Cl/S2. The bulk Cr C/D profile decreases much more sharply at distances near the O.I. than in Cl/S1 and Cl/S2. Likewise, the bulk Al C/D profile increases sharply at distances near the O.I. and to higher compositions than in Cl/S1 and Cl/S2, because the volume fraction of β in the $\beta + \gamma$ growth layer is greater than the volume fractions of β in the $\beta + \gamma$ growth layers of Cl/S1 and Cl/S2. At the $\beta + \gamma / \gamma'$ interface the bulk Cr and Al C/D profiles change discontinuously and become coincident with the Cr and Al concentrations in the γ' growth layer. The Cr concentration decreases very sharply in the γ' layer. The Cr gradient in the γ' layer is much higher than the Cr gradient in the γ' layer of Cl/S2. The Al concentration in the γ' layer increases quite sharply, and exhibits a larger gradient than in the γ' layer of Cl/S2.

The diffusion path, shown in Figure 30, is very similar to the diffusion path of Cl/S2. In the $\beta + \gamma$ phase field it exhibits the same "V" shape as that of Cl/S2. The only noteable differ-

(a)

C1   O.I.   S3

(b)
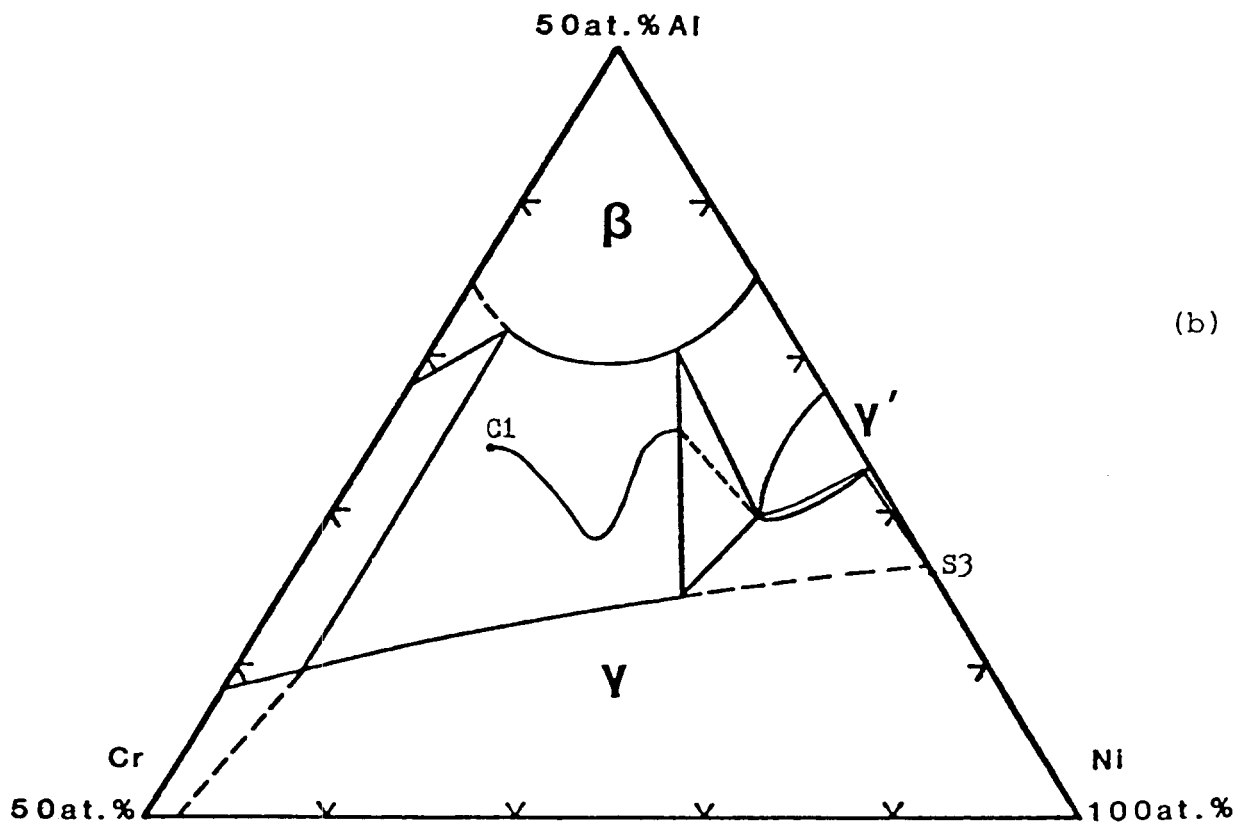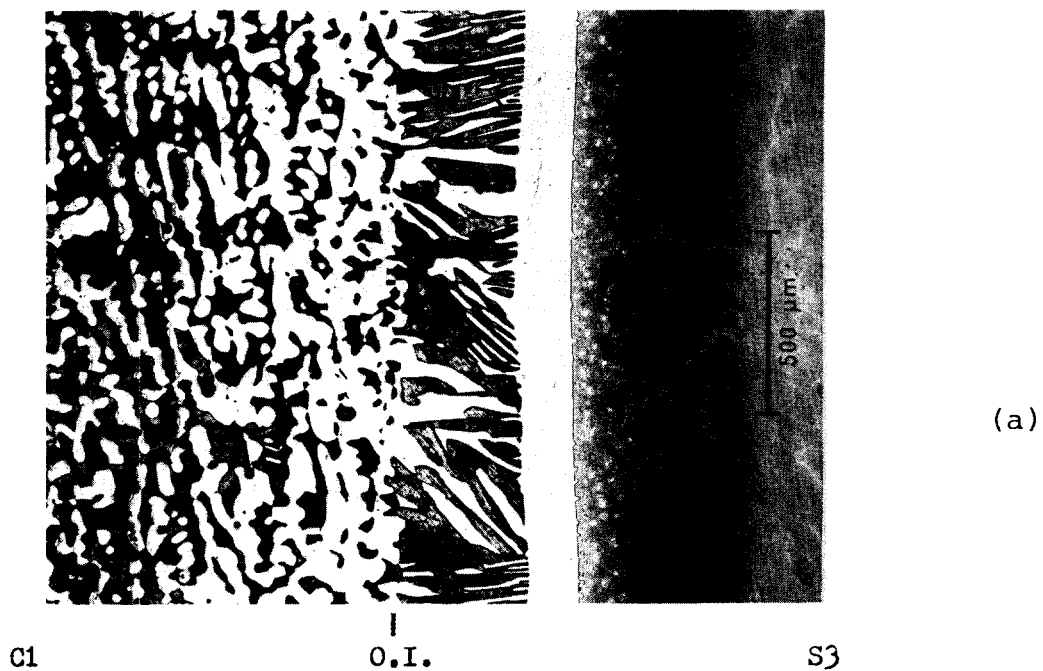
Figure 30. (a) Diffusion zone microstructure (200 hrs.); and (b) diffusion path for couple C1(Ni-20.0Cr-24.1Al)/ S3(Ni-16.2Al)
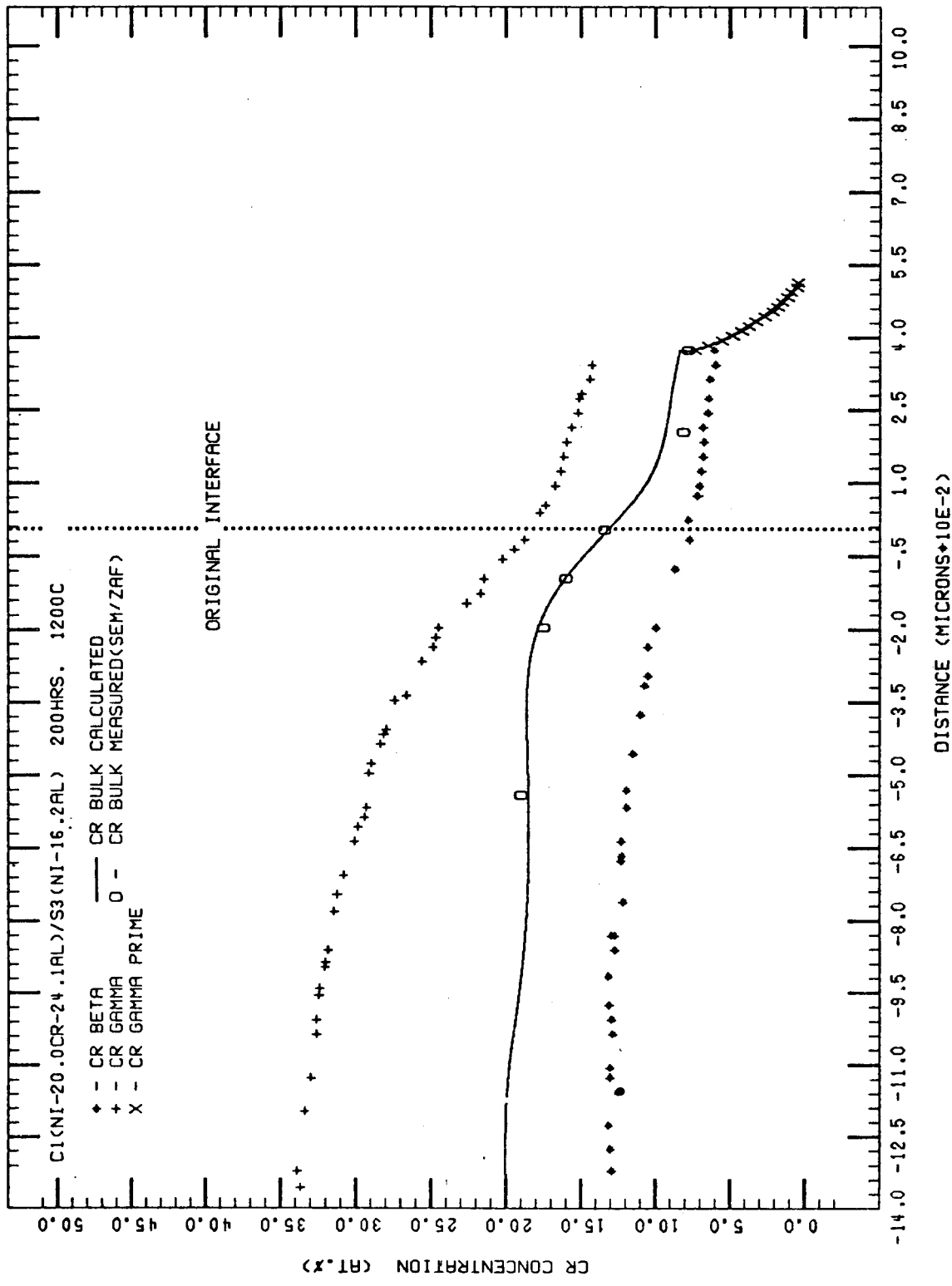
Figure 31. Cr concentration/distance profiles in the β, γ, and γ' phases and the calculated bulk Cr profile for couple C1/S3.
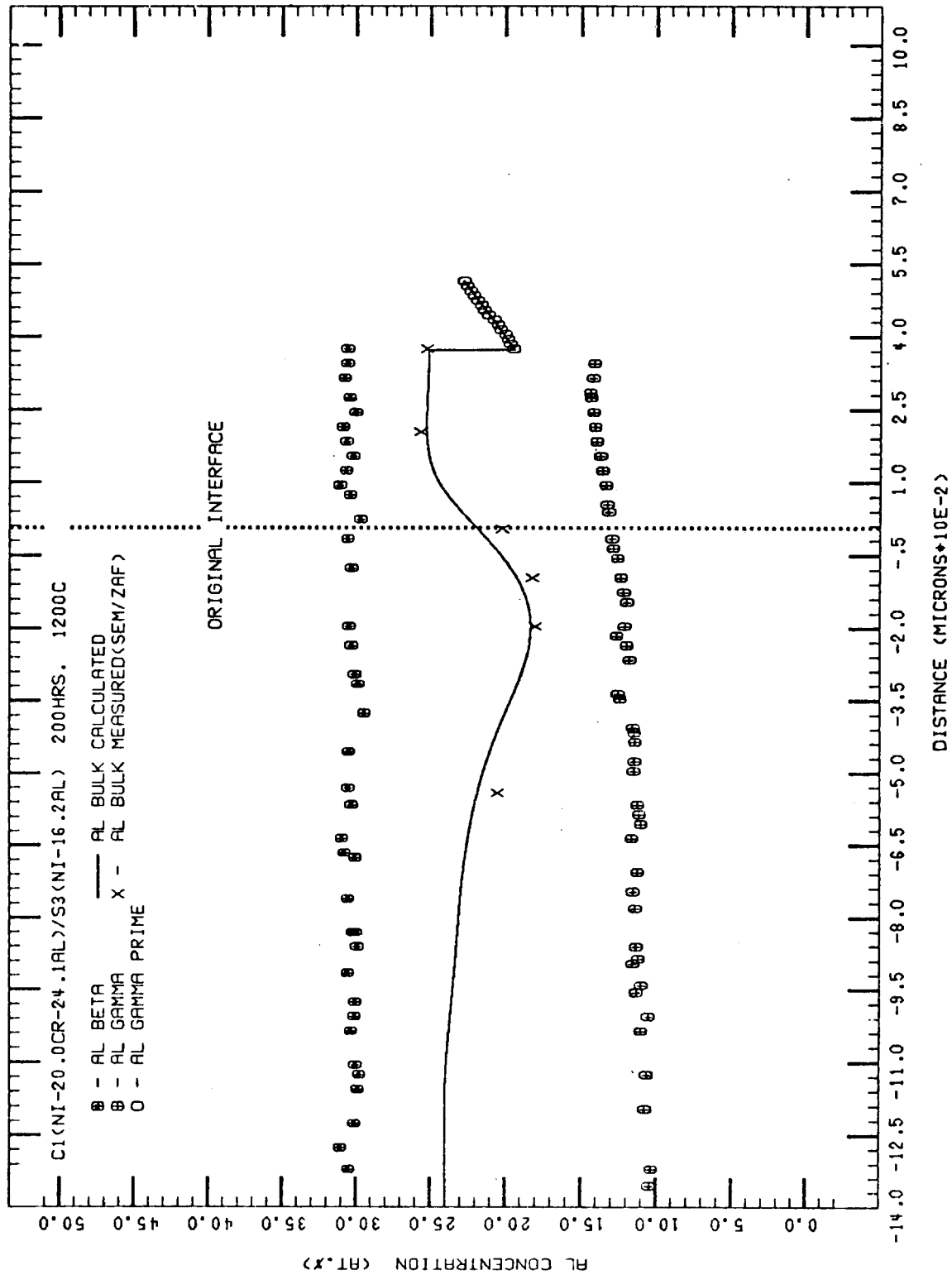
Figure 32. Al concentration/distance profiles in the β, γ, and γ' phases and the calculated bulk Al profile for couple C1/S3.

erence is that it enters the $\beta+\gamma+\gamma'$ triangle at a higher Al composition than did C1/S2, because the volume fraction of β in the $\beta+\gamma$ growth layer is higher than the β volume fraction in the $\beta+\gamma$ growth layer of C1/S2. The path exits the triangle into the γ' phase field. In the γ' phase field the path increases in Al composition from 19.5 at.% to approximately 22.3 at.%. This substantial increase in Al concentration is reflected in the increase of the Al C/D profile in the γ' growth layer. Over this same path segment the Cr decreases from 7.3 at.% to 0.5 at.%. This large decrease in Cr composition leads to a large Cr gradient in the γ' growth layer. The path exits the γ' phase field into the $\gamma+\gamma'$ phase field, very near the Ni-Al side of the phase diagram. It cuts tie lines through the $\gamma+\gamma'$ phase field (as seen in the diffusion zone by a gradual reduction in γ' volume fraction in the $\gamma+\gamma'$ layer) and exits the $\gamma+\gamma'$ phase field into the γ phase field where it reaches the composition of alloy S3, on the Ni-Al side of the phase diagram.

2.   C2/S3.   Interdiffusion resulted in the same diffusion zone microstructure as in C1/S3 - consisting of the $\beta+\gamma$ alloy (C2), the $\beta+\gamma$ growth layer, the γ' growth layer, the $\gamma+\gamma'$ layer, and the γ alloy (S3), as shown in Figure 33. C/D profiles in the β, γ, and γ' phases, and the calculated bulk Cr and Al C/D profiles are shown in Figures 34 and 35, respectively. The C/D profiles in the phases, and the bulk c/D profiles exhibit similar behavior to the profiles of couples C2/S1 and C2/S2. The bulk Al C/D profile rises to higher compositions in the $\bar{\beta}+\gamma$

(a)

C2   O.I.   S3

(b)
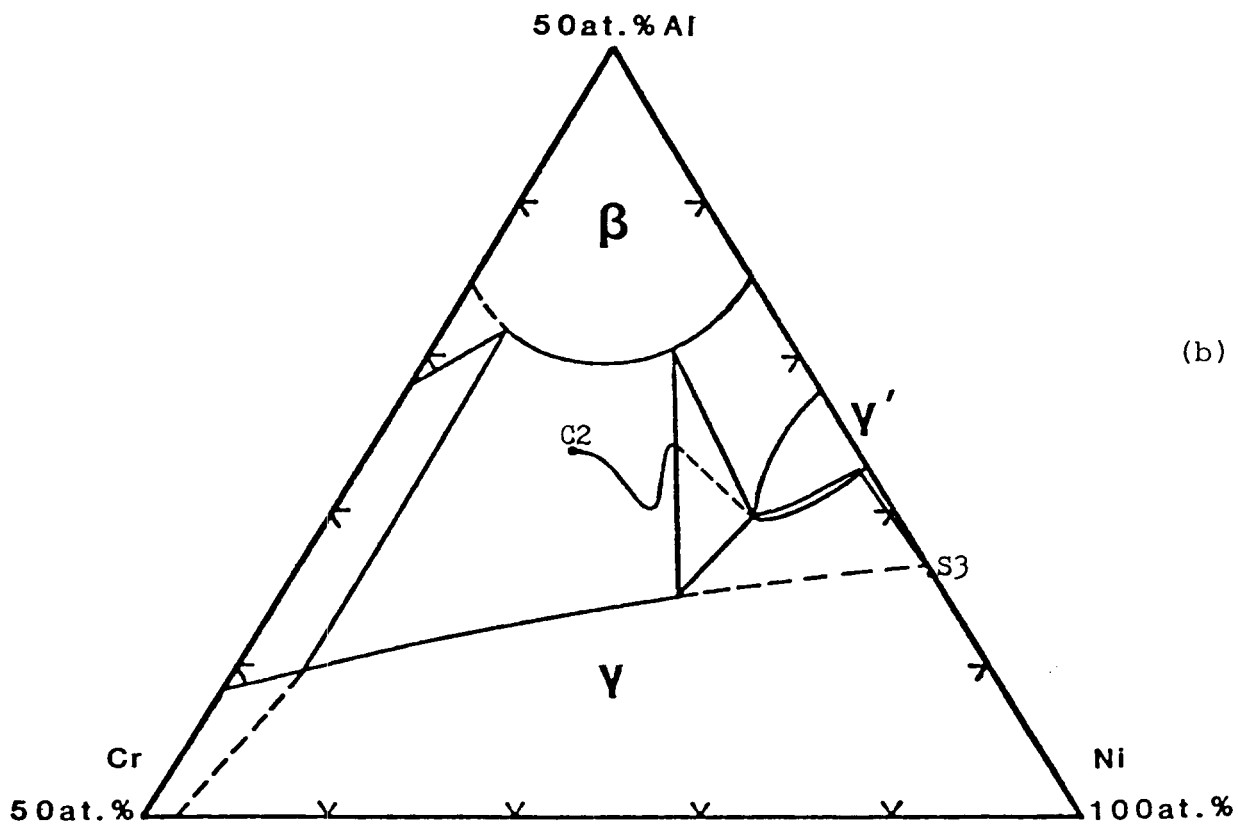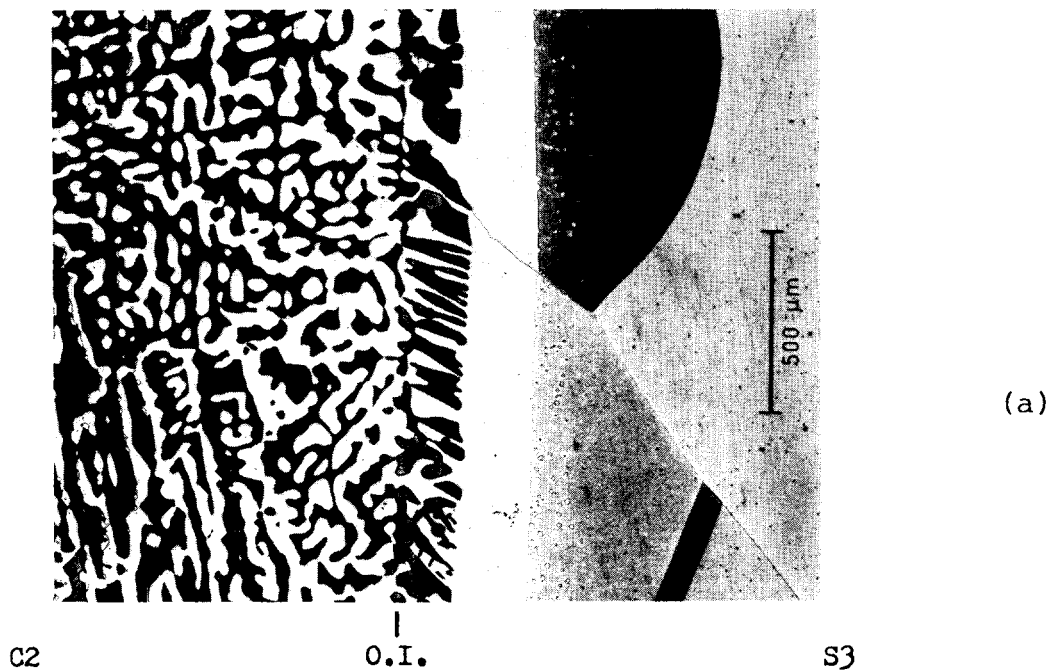
Figure 33. (a) Diffusion zone microstructure (200 hrs.); and (b) diffusion path for couple C2(Ni-15.3Cr-23.9Al)/ S3(Ni-16.2Al)

71
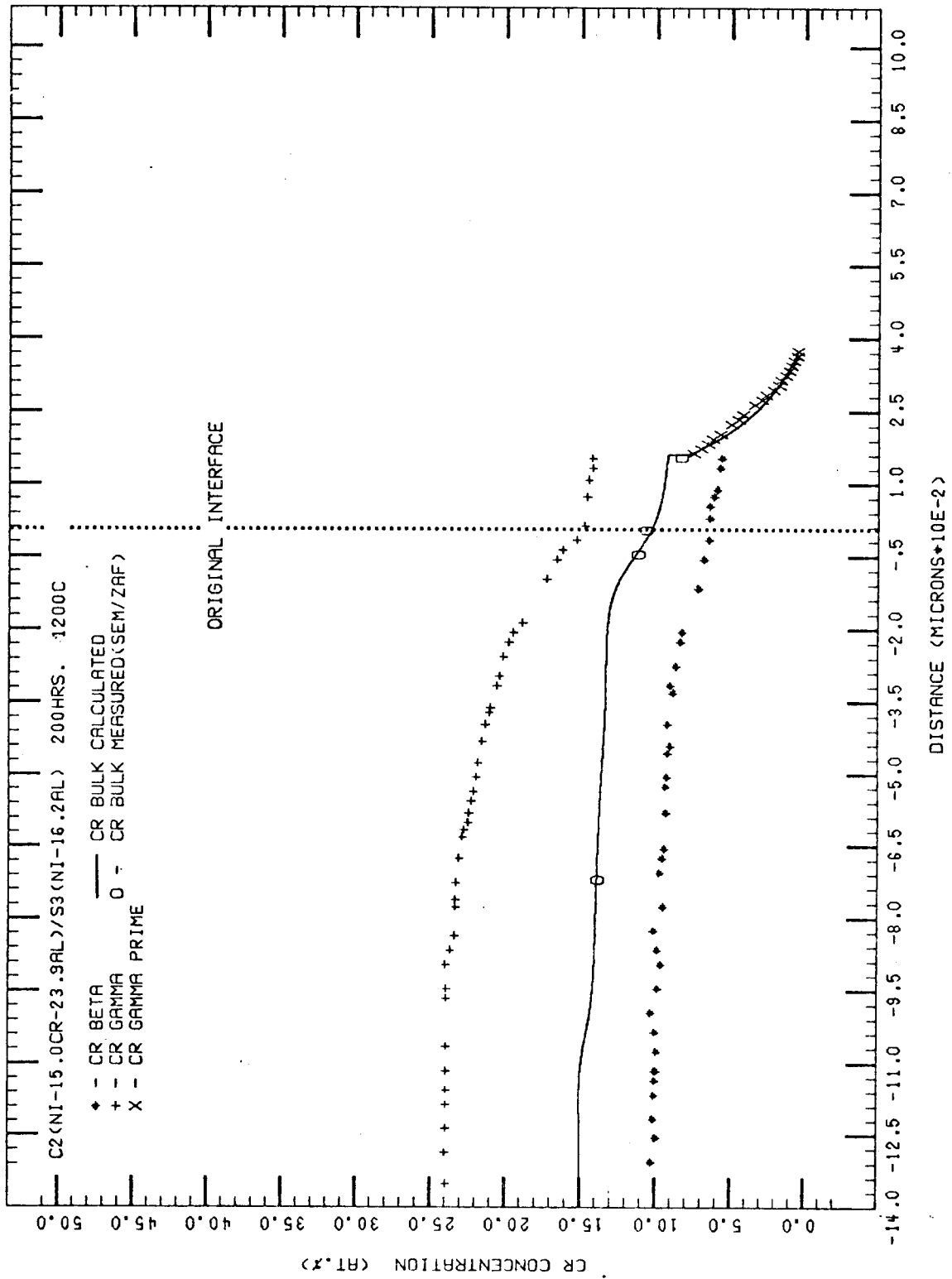
Figure 34. Cr concentration/distance profiles in the β, γ, and γ' phases and the calculated bulk Cr profile for couple C2/S3.
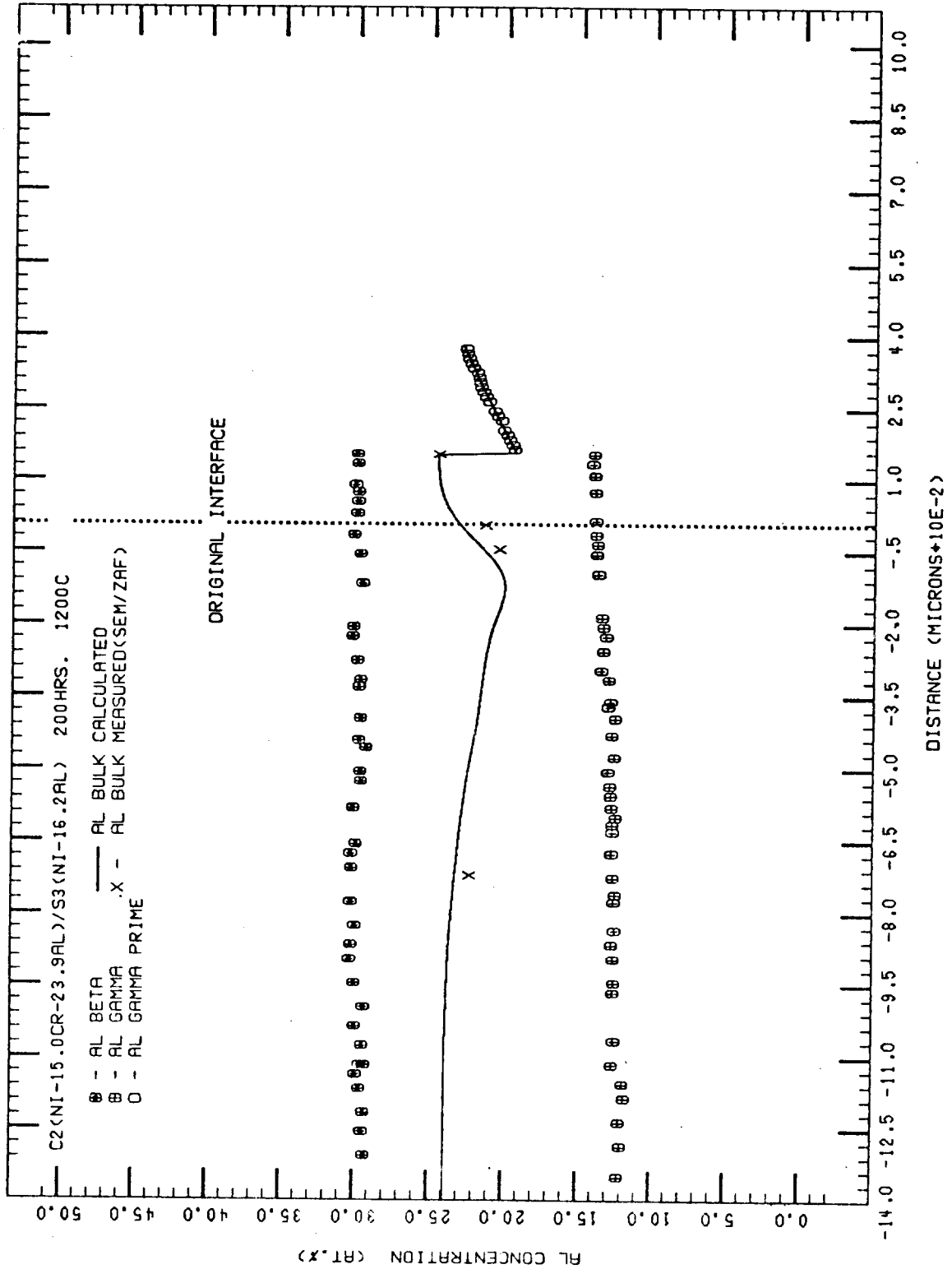
Figure 35. Al concentration/distance profiles in the β, γ, and γ' phases and the calculated bulk Al profile for couple C2/S3.

73

growth layer than it did in C2/S1 and C2/S2 because the volume fraction of β is higher in the $\beta+\gamma$ growth layer. At the $\beta+\gamma/\gamma'$ interface the bulk C/D profiles change discontinuously and become coincident with the concentrations in the γ' growth layer. The Cr concentration decreases rapidly in the γ' growth layer while the Al composition increases, similar to couple C1/S3.

The diffusion path, shown in Figure 33, is very similar to the diffusion path of C2/S2. The section of path in the $\beta+\gamma$ phase field exhibits the same "V" shape as did the path section in the $\beta+\gamma$ phase field in C2/S2. It enters the $\beta+\gamma+\gamma'$ triangle at a higher Al composition than C2/S2 because the volume fraction of β is higher in the $\beta+\gamma$ growth layer. The path exits the triangle into the γ' phase field. The section of path through the γ' phase field, $\gamma+\gamma'$ phase field, and γ phase field, to the bulk composition of S3, is the same as in C1/S3.

3.   C3/S3.   Interdiffusion resulted in different behavior than couples C3/S1 and C3/S2 exhibited in that a γ layer did not grow into alloy S3.   Instead, recession of β occurred, although a γ' growth layer and a $\gamma+\gamma'$ layer did form, similar to couples C1/S3 and C2/S3.   The diffusion zone shown in Figure 36, consists of the $\beta+\gamma$ alloy (C3), a γ layer which formed from β recession, the γ' growth layer, the $\gamma+\gamma'$ layer, and the γ alloy (S3).   C/D profiles in the β, γ, and γ' phases, and the calculated bulk Cr and Al C/D profiles are shown in Figures 37 and 38, respectively. The bulk Cr C/D profile begins to decrease slightly in the $\beta+\gamma$

(a)

C3   O.I.   S3
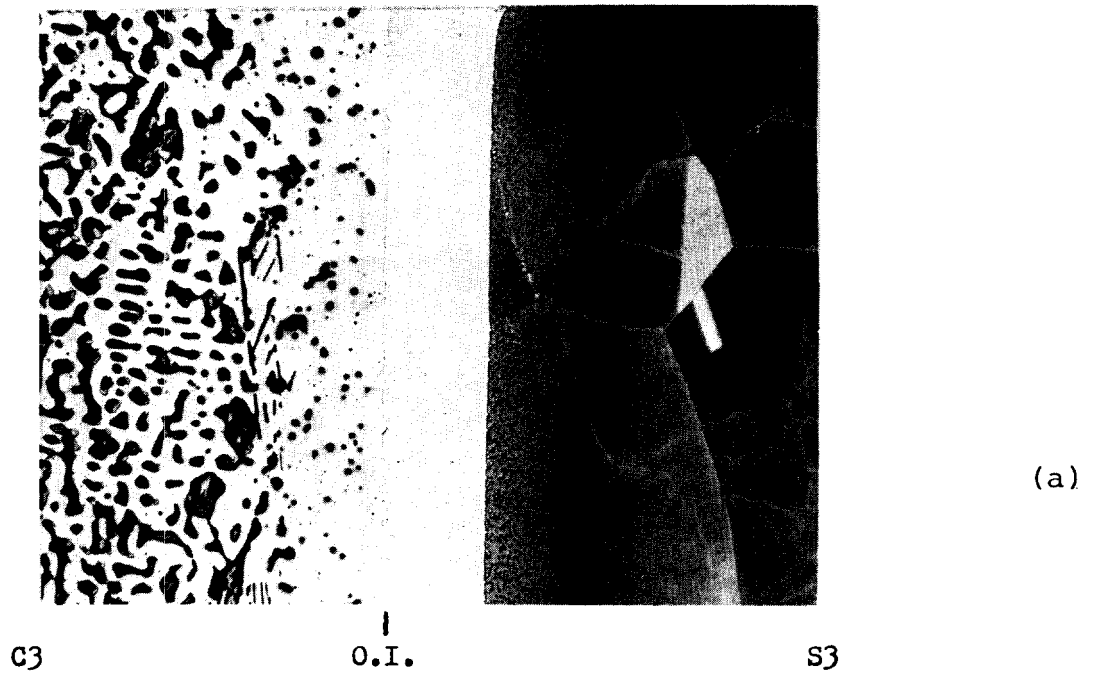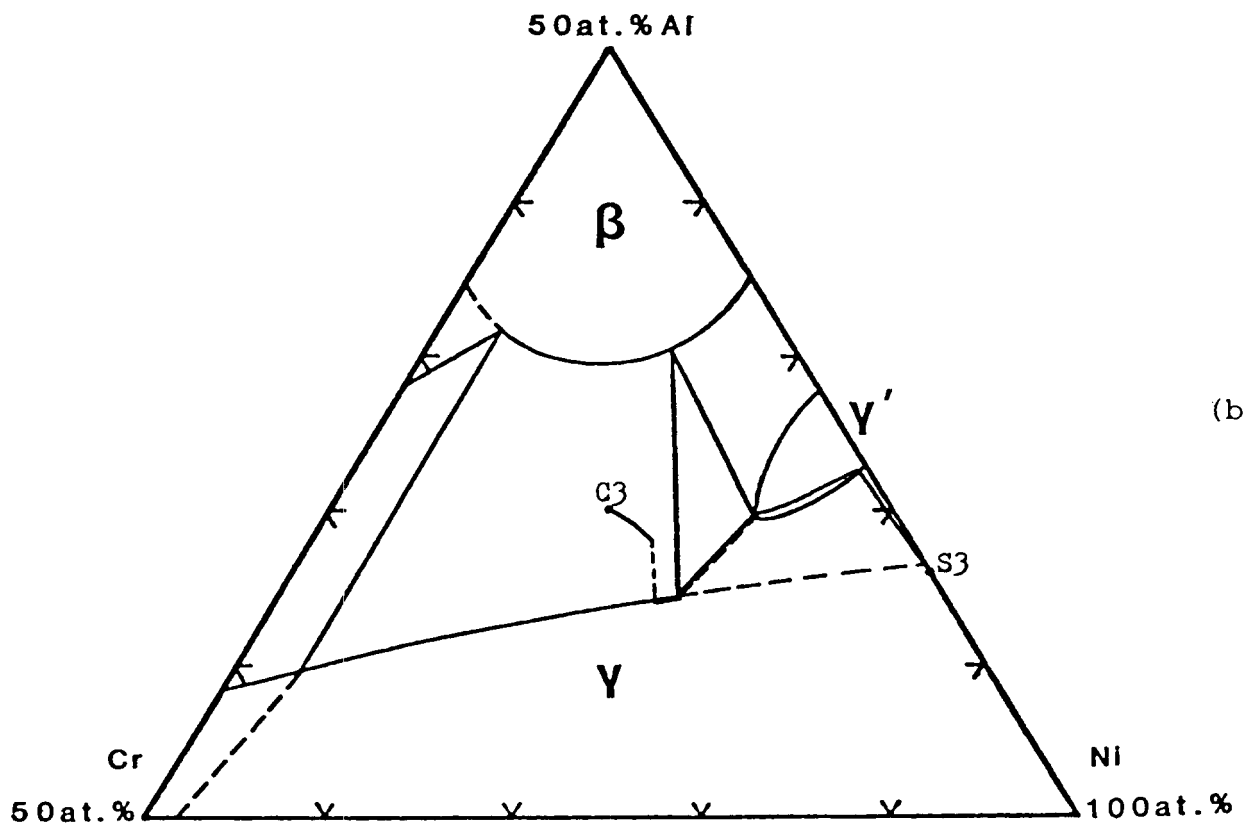
(b)

Figure 36. (a) Diffusion zone microstructure (200 hrs.);
and (b) diffusion path for couple
C3(Ni-15.1Cr-20.3Al)/S3(Ni-16.2Al)

75
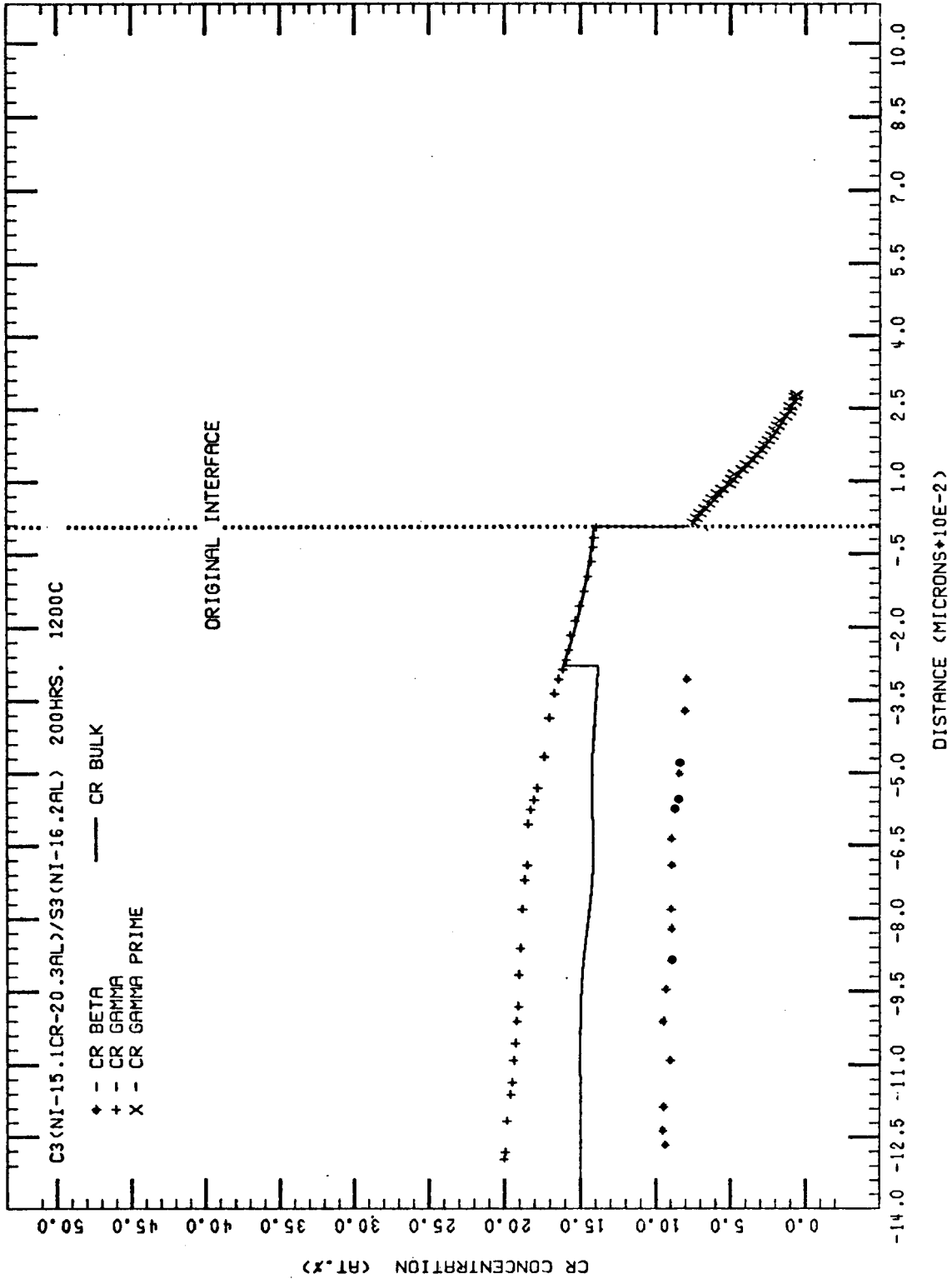
Figure 37. Cr concentration/distance profiles in the β, γ, and γ' phases and the calculated bulk Cr profile for couple C3/S3.
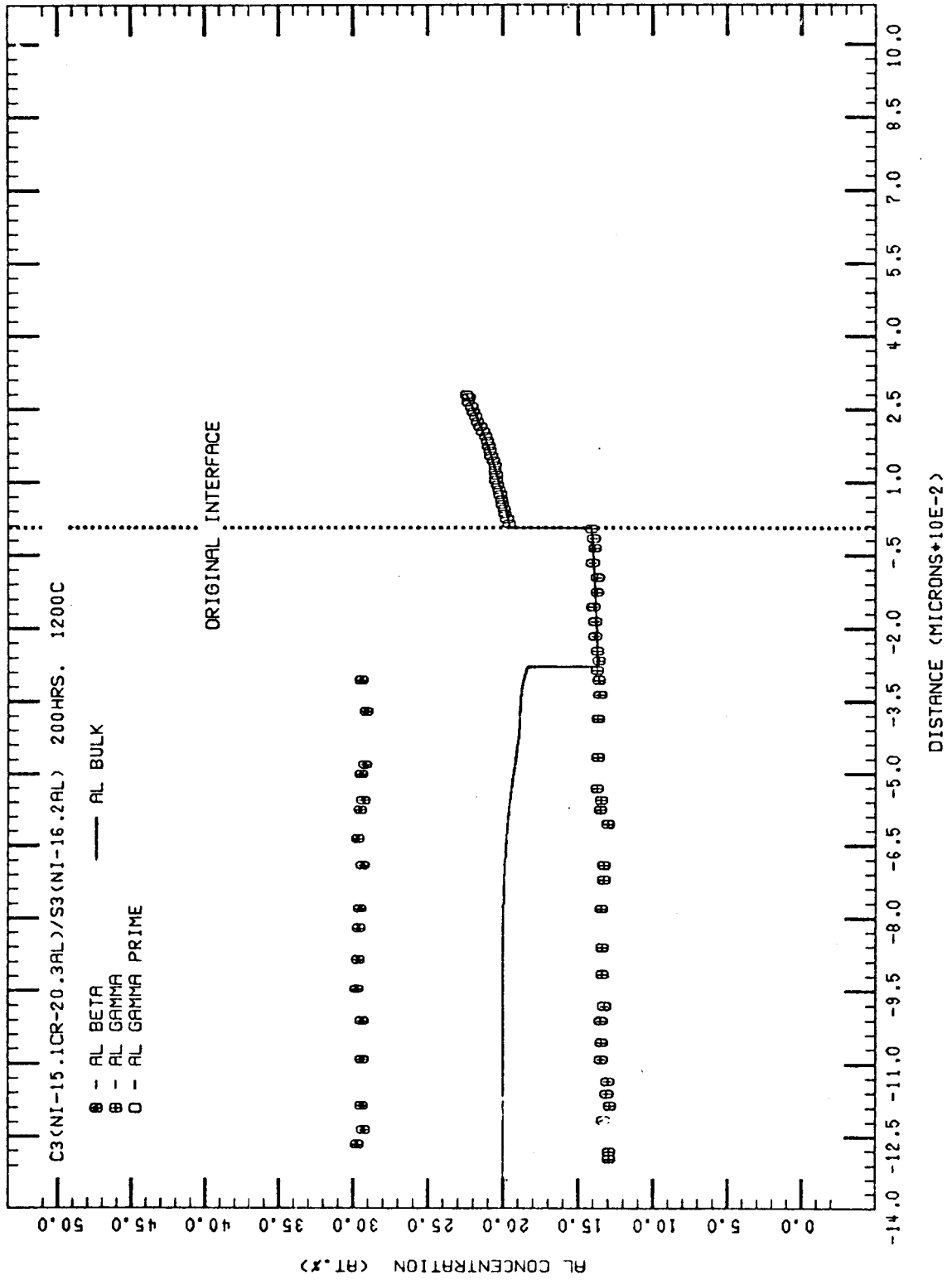
Figure 38. Al concentration/distance profiles in the β, γ, and γ' phases and the calculated bulk Al profile for couple C3/S3.

77

alloy at approximately -800μm from the O.I.. Likewise, the bulk Al C/D profile begins to decrease at the same distance. The bulk Cr C/D profile decreases very slowly over the next 500μm while the bulk Al C/D profile decreases slightly faster over the same distance. At -280μm the bulk C/D profiles change discontinuously and become coincident with the concentrations in the β layer. These discontinuities correspond to the diffusion path following a tie line in the β+γ phase field to the γ/β+γ phase boundary. The bulk C/D profiles stay coincident with the concentrations in the γ layer until the O.I. at which point they change discontinuously and become coincident with the concentrations in the γ' growth layer. These discontinuities correspond to the diffusion path proceeding up the γ+γ' side of the β+γ+γ' triangle from the γ corner to the γ' corner. In the γ' growth layer the Cr concentration decreases appreciably while the Al concentration increases, similar to couples C1/S3 and C2/S3.

The diffusion path, shown in Figure 36, reflects the changes that occur in the diffusion zone microstructure. Although recession of β resulted from interdiffusion, similar to couples C4/S1, and C4/S2, the path does not follow the equilibrium tie line of C3 from the bulk composition of C3 to the γ/β+γ phase boundary, like it did in C4/S1 and C4/S2. Instead it begins by moving to lower Al composition while the Cr composition decreases slightly. This path segment clearly cuts tie lines in the β+γ phase field. This is apparent in the C/D profiles and the diffusion zone microstructure. Unlike couples C4/S1 and C4/S2,

where the phase and bulk C/D profiles were constant in the β+γ
alloy up to the γ layer that formed from β recession, the phases
and bulk C/D profiles in this couple do exhibit concentration
gradients up to the β+γ alloy/γ interface. In the diffusion
zone, this can be seen as a measurable reduction in the β volume
fraction up to the β+γ alloy/γ interface. Thus, in C4/S1 and
C4/S2, the segment of path from the bulk composition of C4 to
the γ/β+γ phase boundary was simply represented by the equili-
brium tie line of alloy C4. In this couple, the path must cut
tie lines before it exits the β+γ phase field via a tie line. The
path proceeds along the γ/β+γ phase boundary until it reaches
the γ corner of the β+γ+γ' triangle. At this point it moves
up the γ+γ' side of the triangle to the γ' corner. The path
segment from the γ' corner to the bulk composition of S3 is the
same as in couples C1/S3 and C2/S3.

4.   Growth Layer Kinetics. Measured β+γ growth versus time for
couples C1/S3 and C2/S3 are shown in Figure 39. Measured γ'
growth for all the couples in the series is shown in Figure 40.
Exponents for the curves through the data points were not cal-
culated because only 100 hours and 200 hours data were available.
The 300 hours samples, which would have given the necessary third
data point, were not available. Comparing the β+γ growth at
200 hours it can be seen that C1/S3 had a larger β+γ growth
layer (335μm) than C2/S3 (170μm). Comparing the γ' growth at
200 hours, it can be seen that C3/S3 had the largest γ' growth
layer (285μm) followed by C2/S3 (186μm) and C1/S3 (140μm).
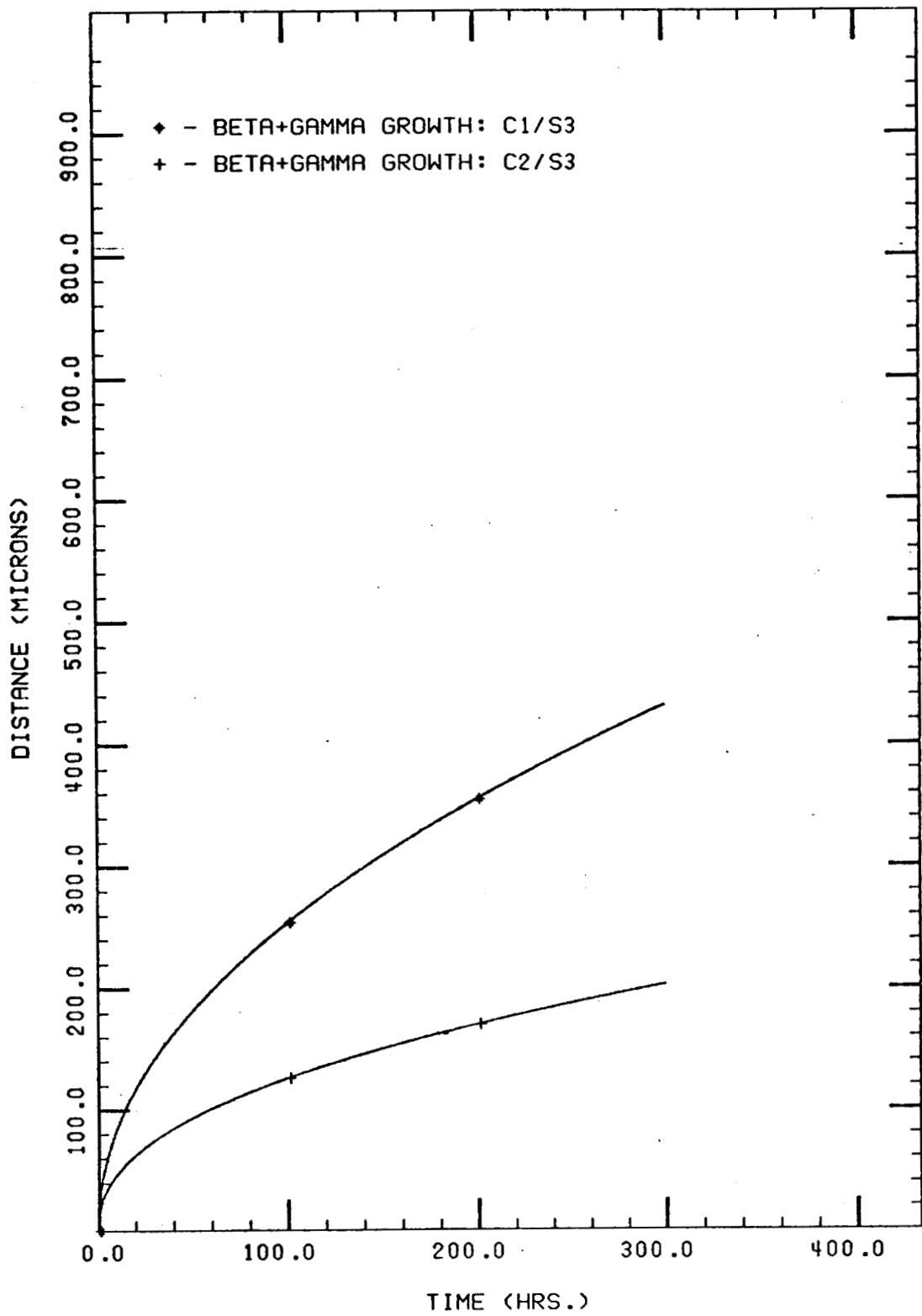
Figure 39. Measured β+γ growth vs. time for couples
C1/S3 and C2/S3.
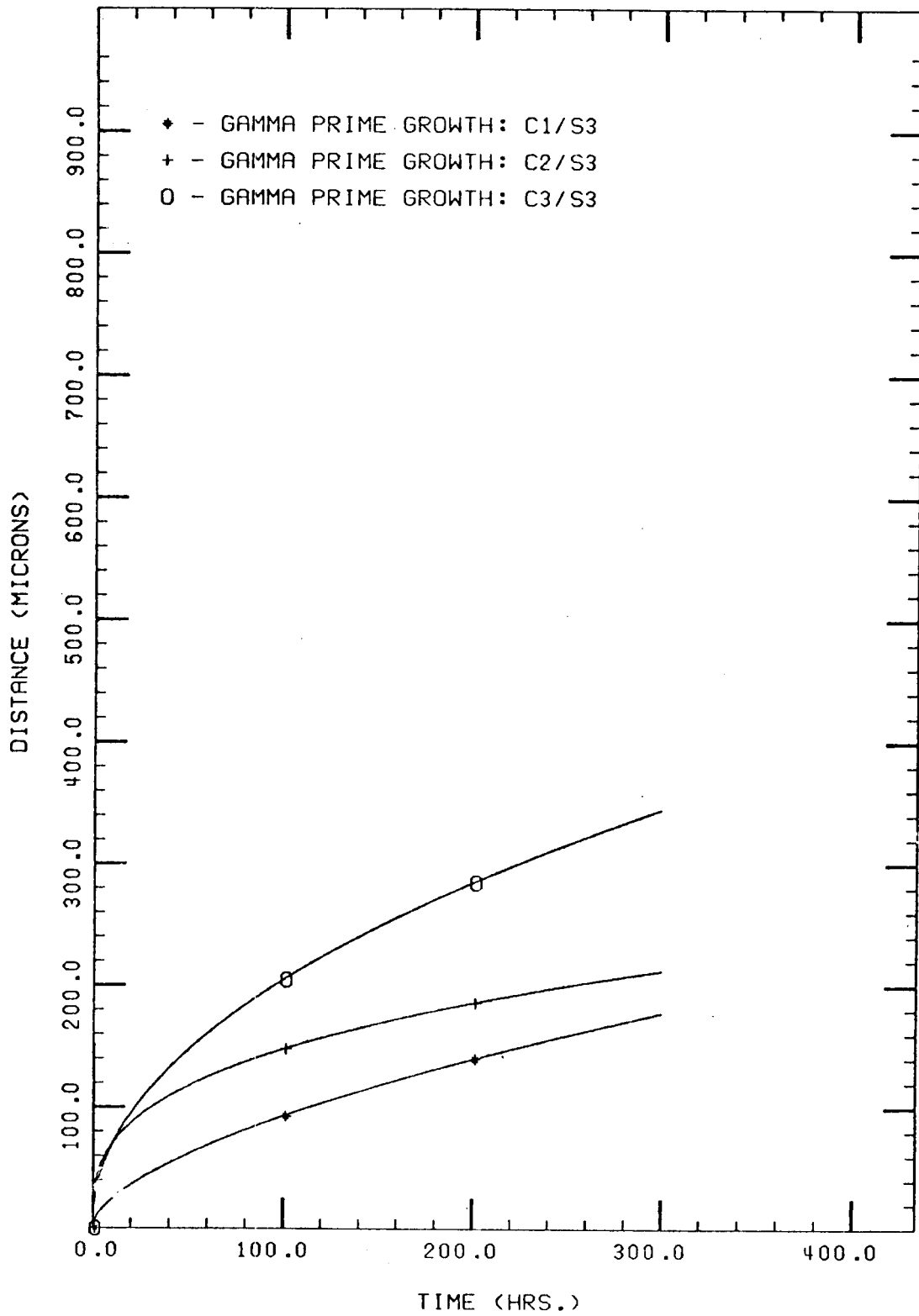
Figure 40. Measured γ' growth vs. time for couples
C1/S3, C2/S3, C3/S3.

Bulk Flow Analysis

In order to gain insight into the mechanisms governing the establishment of the diffusion structures in the diffusion zone, analyses of the direction (i.e., into the $\gamma+\gamma'$ alloy or into the $\beta+\gamma$ alloy) and amount of bulk Cr and Al flow in the diffusion couples were performed. Analyses of bulk flow in diffusion couples requires location of the Matano interface in the couple. The Matano interface serves to locate the plane in the couple where the mass lost from one side of the plane equals the mass gained on the other side of the plane. In general, the Matano plane is not coincident with the original interface because the interface can move during diffusion, as shown by Kirkendall (33). The Matano plane is determined according to the equation:

$$\int_{C_i^-}^{C_i^+} X dC = 0 \qquad i = 1,2,\ldots,n \qquad (1)$$

where X is measured from the Matano plane and C_i^- and C_i^+ are the bulk compositions at either end of the couple for component i. Breaking up Eqn. (1) into two integrals yields:

$$\int_{C_i^-}^{C_i^M} X dC = \int_{C_i^+}^{C_i^M} X dc \qquad i = 1,2,\ldots,n \qquad (2)$$

where C_i^M is the concentration of component i at the Matano plane. Positioning of the Matano plane should ideally be identical for all components (19).

The Matano interfaces for the couples in this study were located by graphical integration, according to Eqn. (2), of the calculated bulk Cr and Al concentration/distance profiles. The experimental accuracy of the calculated bulk Cr and Al concentration/distance profiles was estimated as being ± 2.0 at.% (Cr or Al). This accuracy was confirmed by measuring bulk concentrations at various distances in the diffusion zone with a scanning electron microscope line scan, KEVEX 8000 Series energy-dispersive X-ray analyzer, and subsequent Magic V ZAF correction routine. The measurements were always within 1.5 at.% (Cr or Al) of the calculated values. Taking this accuracy into account, however, leads to some error in graphically integrating the bulk profiles. Furthermore, bulk concentration/distance profiles were not determined in the $\gamma + \gamma'$ alloy adjacent to the growth layers. The gradual reduction in the γ' volume fraction from the growth layer (i.e., $\beta + \gamma$, γ, or γ')/$\gamma + \gamma'$ interface into the $\gamma + \gamma'$ alloy showed that Cr and Al diffusion had occurred past the growth layers. Thus, the amount of Cr and Al gained in these regions had to be estimated. To take into account the accuracy of the profiles, and the Cr and Al gained in the $\gamma + \gamma'$ alloy adjacent to the growth layers, repeated integrations of the profiles were made. The calculated Matano interfaces, $X^M_{Cr,Al}$, and the area on either side of the interface, $A_{Cr,Al}$, listed in Table 4, are averages of the repeated integrations.

From the data in Table 4 it can be seen for all couples that the amount of Cr and Al lost from the $\beta + \gamma$ alloy (i.e. A_{Cr}, A_{Al})

TABLE 4

Calculated Matano Interfaces and Loss of Cr and Al
From the $\beta+\gamma$ Alloys in the Diffusion Couples.

Couple[1]	A_{Cr} (at.%·μm)	X_{Cr}^{M} (μm)	A_{Al} (at.%·μm)	X_{Al}^{M} (μm)
C1/S1	2371 (+123)	138 (+85)	2675 (+123)	39 (+25)
C1/S2	2835 (+151)	100 (+46)	3085 (+134)	47 (+21)
C1/S3	3653 (+204)	80 (+26)	3828 (+130)	73 (+31)
C2/S1	1185 (+119)	62 (+19)	1719 (+111)	40 (+48)
C2/S2	1893 (+ 20)	67 (+ 4)	2133 (+ 58)	42 (+39)
C2/S3	2193 (+ 36)	25 (+ 7)	2535 (+154)	30 (+56)
C3/S1	651 (+126)	27 (+68)	145 (+ 37)	-22 (+32)
C3/S2	943 (+ 60)	47 (+32)	893 (+ 25)	-81 (+20)
C3/S3	1004 (+ 0)	2 (+ 0)	1582 (+118)	-14 (+20)
C4/S1	1383 (+ 0)	130 (+ 0)	1830 (+ 0)	-19 (+ 0)
C4/S2	1757 (+ 0)	150 (+ 0)	2136 (+ 0)	-48 (+ 0)

1. C1(Ni-20.0Cr-24.1Al)   S1(Ni-7.4Cr-17.1Al)
    C2(Ni-15.3Cr-23.9Al)   S2(Ni-3.5Cr-17.0Al)
    C3(Ni-15.1Cr-20.3Al)   S3(Ni-16.2Al)
    C4(Ni-26.4Cr-17.1Al)

NOTE: $X_{Cr,Al}^{M}$ are measured from original interface.

increases as the Cr composition of the $\gamma + \gamma'$ alloy decreases. As the Cr composition of the $\beta + \gamma$ alloy decreases, at constant Al composition (e.g. C1/S1 vs. C2/S1), the amount of Cr and Al lost from the $\beta + \gamma$ alloy decreases. Likewise, as the Al composiiton in the $\beta + \gamma$ alloy decreases, at constant Cr composition (e.g. C2/S1 vs. C3/S1) the amount of Cr and Al lost from the $\beta + \gamma$ alloy decreases.

The data in Table 4 also shows that the phase compositions, and not just the bulk compositions, play a role in determining the amount of Cr and Al lost from the $\beta + \gamma$ alloy. The amount of Cr and Al lost from C1 couples was higher than the amount of Cr and Al lost from C4 couples, even though alloy C4 had a higher bulk Cr composition (26 at.% Cr) than alloy C1 (20 at.% Cr). The β and γ phase Cr concentrations in alloy C1, however, are higher than the β and γ phase Cr concentrations in alloy C4. (The Al compositions in the phases were similar for both alloys.) Likewise, the amount of Cr and Al lost from C2 couples was higher than the amount of Cr and Al lost from C3 couples, even though both alloys had approximately the same bulk Cr composition (15 at.% Cr). Again, the β and γ phase Cr concentrations in alloy C2 are higher than the β and γ phase Cr concentrations in alloy C3. Thus the data shows that the phase compositions, and in particular, the Cr concentration in the phases, are important in determining the amount of Cr and Al lost from the $\beta + \gamma$ alloy.

The direction of Cr and Al flow can be deduced from the diffusion zone microstructure. Kirkendall porosity was always ob-

85

served on the $\beta + \gamma$ side of the original interface. The location of porosity in the $\beta + \gamma$ alloys is similar to the location of porosity found in similar $\beta + \gamma$ alloys of a previous study (19). In the previous study (19), the porosity was attributed to an intrinsic flux imbalance. An intrinsic flux imbalance will occur whenever the number of atoms diffusing in one direction is greater than the number diffusing in the reverse direction. Consequently, a net flux of vacancies, equal to, and opposite to the intrinsic flux imbalance must exist. Porosity results when the number of lattice imperfections is insufficient to absorb and equilibrate the vacancy flux. In the previous study (19), the intrinsic diffusivities of Ni, Cr, and Al were ranked as:

$$D_{AlAl} > D_{CrCr} > D_{NiNi}$$

The porosity was therefore attributed to high Al and Cr fluxes from the high Cr, high Al ($\beta + \gamma$ or γ) alloys into the low Cr, low Al γ alloys (19). The similar location of porosity in the $\beta + \gamma$ alloys of this study shows that high Cr and Al fluxes, in the direction of the $\gamma + \gamma'$ alloy, are responsible for the porosity. Therefore, the location of porosity in the $\beta + \gamma$ alloys of this study shows conclusively that Cr and Al diffusion is occurring in the direction of the $\gamma + \gamma'$ alloy.

γ-Phase Flux Analysis

The establishment of the diffusion structures in the β+γ/ γ+γ' couples, a result of bulk Cr and Al flow between the β+γ and γ+γ' alloys, occurs by Cr and Al diffusion in the phases. A way to gain insight into the mechanisms by which the bulk Cr or Al flow takes place is to examine the Cr or Al flux variation in the phases in the diffusion zone. The diffusion flux defines the amount of Cr or Al transported per unit area, per unit time. By determining the flux variation in the phases, the regions in the couple where maximum Cr or Al transport occurs can be found. Relating these regions to the changes in bulk Cr or Al flow that occurs in the diffusion zone then allows the mechanisms by which the structures form in the diffusion zone to be determined.

Following Onsager's initial formalism (34-36), the diffusion flux, J_i, of each component, i, is a linear function of all the concentration gradients, C_k, given by:

$$J_i = \sum_{k=1}^{n} D_{ik}' \nabla C_k \quad (i=1,2,\ldots,n) \quad (1)$$

The diffusion coefficients D_{ik}' are assumed to be functions of the concentrations, C_k. Kirkaldy (37) imposed the following conditions:

$$\sum_{i=1}^{n} J_i = 0 \quad (2)$$

$$\sum_{i=1}^{n} C_i = \text{constant} \quad (3)$$

87

These conditions allow n equations involving n^2 diffusion coefficients to be reduced to n-1 equations involving $(n-1)^2$ diffusion coefficients. Thus Eqn. (1) can be written as:

$$J_i = \sum_{k=1}^{n-1} D_{ik} \nabla C_k \qquad (4)$$

where $D_{ik} = D_{ik}' - D_{in}'$.

Considering a 3 component system, where diffusion occurs in the X direction only, Eqn. (4) expands to:

$$J_1 = -D_{11}\frac{\partial C_1}{\partial X} - D_{12}\frac{\partial C_2}{\partial X} \qquad (5)$$

$$J_2 = -D_{21}\frac{\partial C_1}{\partial X} - D_{22}\frac{\partial C_2}{\partial X} \qquad (6)$$

Eqns. (5) and (6) are valid in a single phase. In two-phase alloys, separate sets of equations are necessary for each phase (38).

Fluxes were calculated for Cr and Al in the γ phase of the couples in this study. Fluxes in the γ phase could be calculated because the four ternary diffusion coefficients as a function of Cr and Al concentration were determined at 1200°C from an earlier study (19). For the β and γ' phases, diffusion coefficient data were insufficient to allow flux calculations.

Analysis of ternary diffusion in the β+γ regions of the β+γ/γ+γ' couples in this study ideally requires that fluxes of Cr and Al be known in the β phase as well as in the γ phase. The need to have fluxes in the β phase can be alleviated if they can be shown to be smaller than the fluxes in the γ phase, and/

or, that they are not predominately responsible for transport of Cr and Al during interdiffusion. Available data on the 4 ternary diffusion coefficients in the β phase at 1025°C (39), and binary $\tilde{D}_{NiAl}$ data in the β phase at 1000°C - 1200°C (39-41), allow the 4 diffusion coefficients in the β phase at 1200°C to be assessed as being of the same order of magnitude as the 4 diffusion coefficients in the γ phase at 1200°C. The Al concentration gradient in the β phase in the couples was approximately zero (or very small). Thus any flux of Al in the β phase would have to be a result of the Cr concentration gradient in the β phase. The Cr concentration gradient in the β phase was at most an order of magnitude less than the Cr concentration gradient in the γ phase. Therefore, assuming the assessment of the order of magnitudes of the 4 diffusion coefficients in the β phase at 1200°C is correct, the flux of Cr and Al in the β phase can at best be an order of magnitude less than the flux of Cr and Al in the γ phase. Using this basis alone, most transport of Cr and Al would have to occur in the γ phase. Further support that the γ phase fluxes are predominately responsible for transport of Cr and Al during interdiffusion can be found from consideration of the diffusion zone microstructures of couples C4/S1 and C4/S2. The complete β dissolution in these couples shows that the β phase is not necessary as a mechanism of transport for Cr and Al to the layers that form during interdiffusion. The complete β dissolution also shows that the β phase simply dissolves during interdiffusion, giving up Cr and Al to be transported in

the γ phase. Therefore, the diffusion behavior in $\beta+\gamma/\gamma+\gamma'$ couples is primarily a result of diffusion in the γ phase. Thus, the diffusion behavior in $\beta+\gamma/\gamma+\gamma'$ diffusion couples can be rationalized in terms of fluxes in the γ phase.

A computer program was developed to calculate Cr and Al fluxes in the γ phase using Eqns. (5) and (6). First, a smooth curve representative of the concentration/distance data (Cr or Al) measured by the electron microprobe was produced by a cubic spline curve smoothing routine (42). The cubic spline smoothing routine (CSSR) allows point to point fluctuations in the experimental data to be eliminated. The benefit of the CSSR is it allows the concentration gradient at any position on the concentration profile to be calculated.

The Cr and Al concentration gradients from the smoothed curves were calculated using finite-difference techniques (43). The finite-difference (F-D) technique requires definition of grid points across the smoothed curves. The grid points are equally spaced across the curves, each point being associated with a specific Cr or Al concentration. A total of 1000-3000 grids where used in the present study. The gradients were calculated at each grid point using a second-forward difference (43):

$$y_i' = (-C_i(I+2)+4.0 \cdot C_i(I+1)-3.0 \cdot C_i(I))/2 \cdot DELX \qquad (7)$$

where:

y_i' = gradient at the Ith grid point (i=Cr or Al)

$C_i(I+2)$ = concentration of Cr or Al at the Ith + 2 grid point.

$C_i(I+1)$ = concentration of Cr or Al at the Ith + 1 grid point.

$C_i(I)$ = concentration of Cr or Al at the Ith grid point.

DELX = distance between successive grid points.

Once the gradients were calculated at each grid point, the 4 diffusion coefficients (19) were calculated using the Cr and Al concentrations at each grid point. The 4 diffusion coefficients as a function of Cr and Al concentration used in the program are given below:*

$$D_{AlAl} = 1.97 + 1.38 \, Al + 0.18 \, Cr + 0.0061 \, Al^2 - 0.0032 \, Cr^2$$

$$D_{AlCr} = 0.135 + 0.28 \, Al - 0.016 \, Cr + 0.035 \, Al^2 + 0.0004 \, Cr^2$$

$$D_{CrAl} = -1.41 + 0.33 \, Al + 0.47 \, Cr - 0.013 \, Al^2 - 0.0081 \, Cr^2$$

$$D_{CrCr} = 3.21 - 0.56 \, Al + 0.18 \, Cr + 0.07 \, Al^2 - 0.0037 \, Cr^2$$

Al,Cr = Al or Cr concentration (at.%)

*Taken from Reference 19

The calculated gradients and diffusion coefficients at each grid point were substituted into the following flux equations:

$$J_{Al}{}^{\gamma} = -D_{AlAl} \frac{dC_{Al}}{dX} - D_{AlCr} \frac{dC_{Cr}}{dX} \qquad (8)$$

$$J_{Cr}{}^{\gamma} = -D_{CrAl} \frac{dC_{Al}}{dX} - D_{CrCr} \frac{dC_{Cr}}{dX} \qquad (9)$$

and the flux of Cr and Al was calculated at each grid point. The flux at each grid point was then plotted, yielding a curve which showed the flux variation in the γ phase in the diffusion zone.

F-D techniques are a convenient method for calculating the concentration gradient at any given point on a concentration/dis-

tance profile. F-D techniques, however, are only an approxima-
tion to the true gradient that exists at any given point on the
profile. When the F-D technique is used, increasing the number
of grid points should give a closer and closer approximation of
the true gradient that exists at any given grid point. Thus,
if the calculated gradient at a given grid point is plotted
against the number of grid points, it should converge toward the
real gradient as the number of grid points increases. Therefore,
to check whether the F-D technique is properly executed, the num-
ber of grids must be increased to see if the calculated gradients
converge. This check was performed on the program, and conver-
gence of the calculated gradients occurred.

Possible Errors

There are three sources of error in calculating the γ-phase
Cr and Al fluxes in this study. The three sources of error are:

1. The accuracy of the concentration measurements.

2. The accuracy of the diffusion coefficients.

3. Determination of the concentration gradients by
   the cubic spline smoothing routine.

The accuracy of the concentration measurements is discussed in
Appendix B. The accuracy of the diffusion coefficients was veri-
fied in a previous study (19) by comparison of measured and pre-
dicted concentration/distance profiles. A computer model was
developed to simulate interdiffusion in γ / γ diffusion couples
(19). The computer model utilized finite-difference techniques

and the measured diffusion coefficients to predict measured concentration/distance profiles. Excellent agreement was found between the measured and predicted profiles, thus supporting the accuracy of the diffusion coefficients. The largest source of error in calculating the Cr and Al fluxes in this study comes from the calculation of the concentration gradients. The concentration gradients were calculated from curves smoothed through the experimental data by a cubic spline smoothing routine (CSSR). The CSSR used in this study was desired to eliminate the obvious point to point fluctuations in the experimental data. The point to point fluctuations in the experimental data were most obvious in the two-phase regions for both Cr and Al. Concentration measurements in two-phase regions were always carefully made in the center of a given phase. However, the possibility of the other phase being right underneath, or near, the phase being measured always existed, and thus fluctuations in the Cr and Al experimental data were inevitable. In one-phase regions, this difficulty was not encountered, and the fluctuations were much less than in the two-phase regions. In general, as the point to point fluctuations in the experimental data increased, larger smoothing parameters were necessary. To account for the fluctuations in the Cr and Al experimental data in this study, smoothing parameters in the range 0.5-7.0 were necessary, depending on the given couple.

Selection of the Cr and Al smoothing parameters were determined by observing the variation in the calculated Cr and Al

fluxes in the diffusion zone. The smoothing parameters were set
when the Cr and Al flux variation in the diffusion zone were
found to be smooth curves. Two regions of the calculated Cr and
Al fluxes (shown in Figure 41) were found to be sensitive to the
smoothing parameters. The first region was at distances well
back in the $\beta+\gamma$ alloys (-1400 to -800μm range, depending on the
couple) and the second region was at the three-phase interfaces
in the couple (i.e. fluxes on the positive side of the original
interface, in the last 10μm of the calculated flux profiles).
The Cr and Al fluxes in regions near the original interface (i.e.,
where the fluxes reached a maximum) were not as sensitive to the
smoothing parameters as the fluxes in the other two regions.

The Cr and Al fluxes in the -1400 to -800μm range were sen-
sitive to the smoothing parameters because of the point to point
fluctuations in the experimental data. The point to point fluc-
tuations in the experimental data arose from various measurement
errors, such as focusing, instrument drift, etc... The Cr and
Al experimental data in these regions were all within the stan-
dard deviation of the Cr and Al concentrations measured in the
γ-phase of homogenized alloys used for phase diagram determina-
tion. Therefore, in these regions, no concentration gradients
were present. However, the CSSR will only smooth a perfectly
horizontal curve through data points when all the data points
have the exact same value. When the data points do not have the
same value, such as from point to point fluctuations in the ex-
perimental data, but are known to fall along a horizontal line,

94

the CSSR will smooth a curve through the data points with some finite slope. Thus, in the -1400 to -800μm range, both the Cr and Al smoothed curves exhibited very small concentration gradients. These very small gradients lead to non-zero flux values in these regions. Changing the smoothing parameters did not appreciably effect the Cr fluxes in the regions, but did appreciably effect the Al fluxes in these regions. Therefore, many of the Al fluxes in these regions exhibited negative flux values of -2.0 to $-3.0 \cdot 10^{-8}$ at.% cm/sec. The fluxes should be zero in thees regions because comparisons of concentration measurements in these regions to γ-phase concentrations in homogenized alloys shows no concentration gradients are present.

The Cr and Al fluxes at the three-phase interfaces in the couple (i.e. to the far right of the original interface) were also influenced by the smoothing parameters. The reason the Cr and Al fluxes were influenced by the smoothing parameters in these regions is because of the small concentration gradients that were present in these regions. Variations in smoothing parameter changed the smoothed concentrations in these regions very little, but these very small changes in concentration lead to measurable changes in the concentration gradients. Changing the smoothing parameters on the order of 2 lead to $\pm 2.5 \cdot 10^{-8}$ at.% cm/sec. variations in the Cr and Al fluxes in these regions.

The Cr and Al flux maxima (i.e., in regions near the original interface) were effected least by the smoothing parameters.

Changes in smoothing parameter on the order of 2 generally lead to less than a $\pm 1.5 \cdot 10^{-8}$ at.% cm/sec. variation in the Cr and Al flux maxima.

Flux Analysis

The calculated fluxes, shown in Figure 42, show many important features. The first important feature is that the flux of Al is positive in the diffusion zone of all couples, even though the gradients in the Al profiles were positive also. The fact that the Al flux is positive shows that Al is diffusing up its gradient in the γ phase from the $\beta + \gamma$ alloy to the $\gamma + \gamma'$ alloy. The positive Al flux also shows that the strong (negative) Cr gradient is causing Al to diffuse up its gradient toward the $\gamma + \gamma'$ alloy. The fact that the negative Cr gradient is causing Al to diffuse up its gradient can be seen by examining the terms in Eqn. (8):

$$J^{\gamma}_{Al} = -D_{AlAl}\frac{dC_{Al}}{dX} - D_{AlCr}\frac{dC_{Cr}}{dX} \tag{8}$$

The values of D_{AlAl}, and D_{AlCr}, for the ranges of Cr and Al concentration encountered in this study, fall in the ranges:

$$D_{AlAl}: \quad 18.1 - 24.4 \times 10^{-10}\,cm^2/sec.$$

$$D_{AlCr}: \quad 5.9 - 10.8 \times 10^{-10}\,cm^2/sec.$$

The Al gradient, dC_{Al}/dX, in all couples fell in the range 7-25 at.%/cm, while the Cr gradient, dC_{Cr}/dX, in all couples fell in the range $-70 - -350$ at.%/cm. Thus, although D_{AlAl} is approxi-
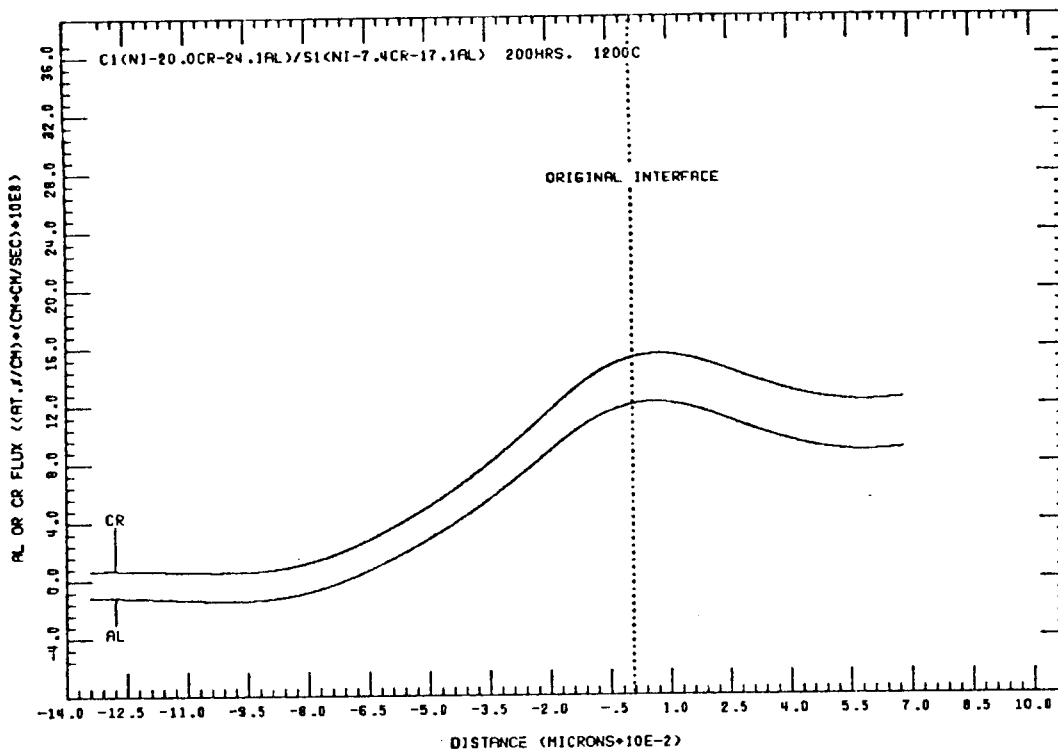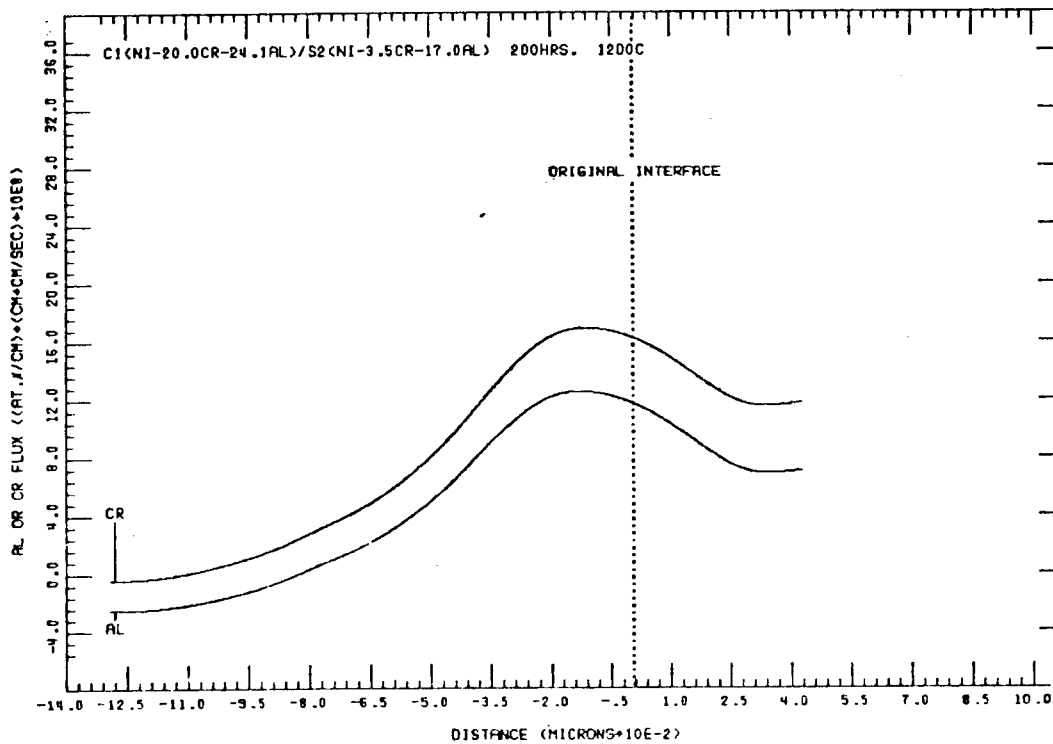
Figure 41. Calculated Cr and Al fluxes in the γ
phase.   a). C1/S1;   b). C1/S2.

97
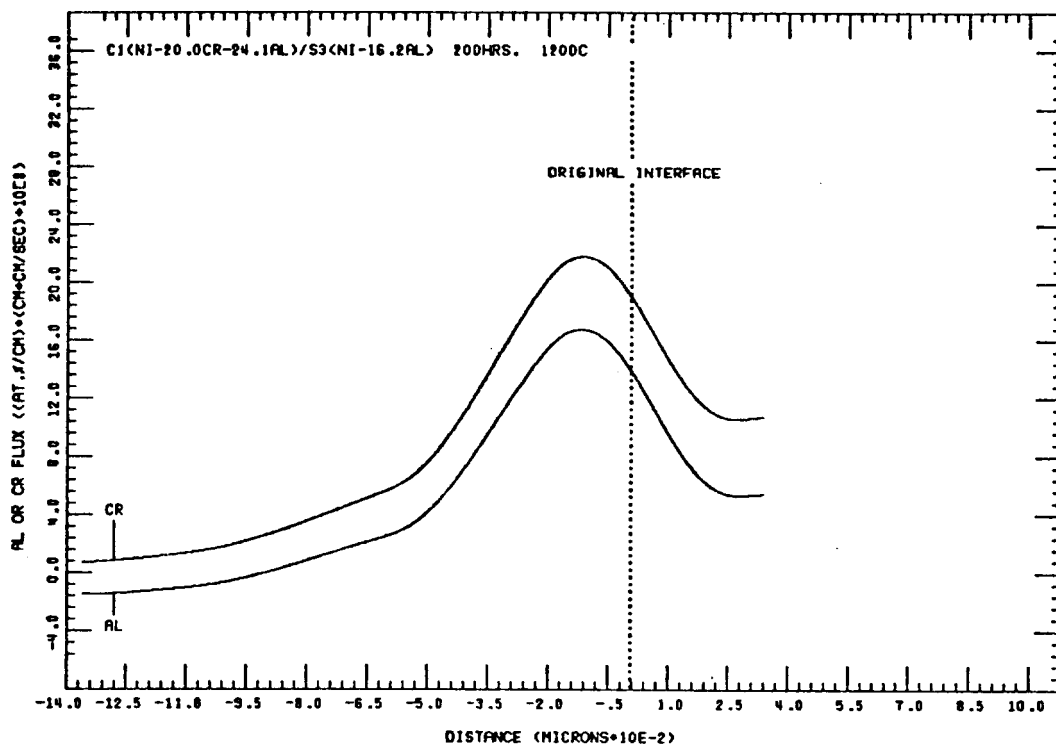
c
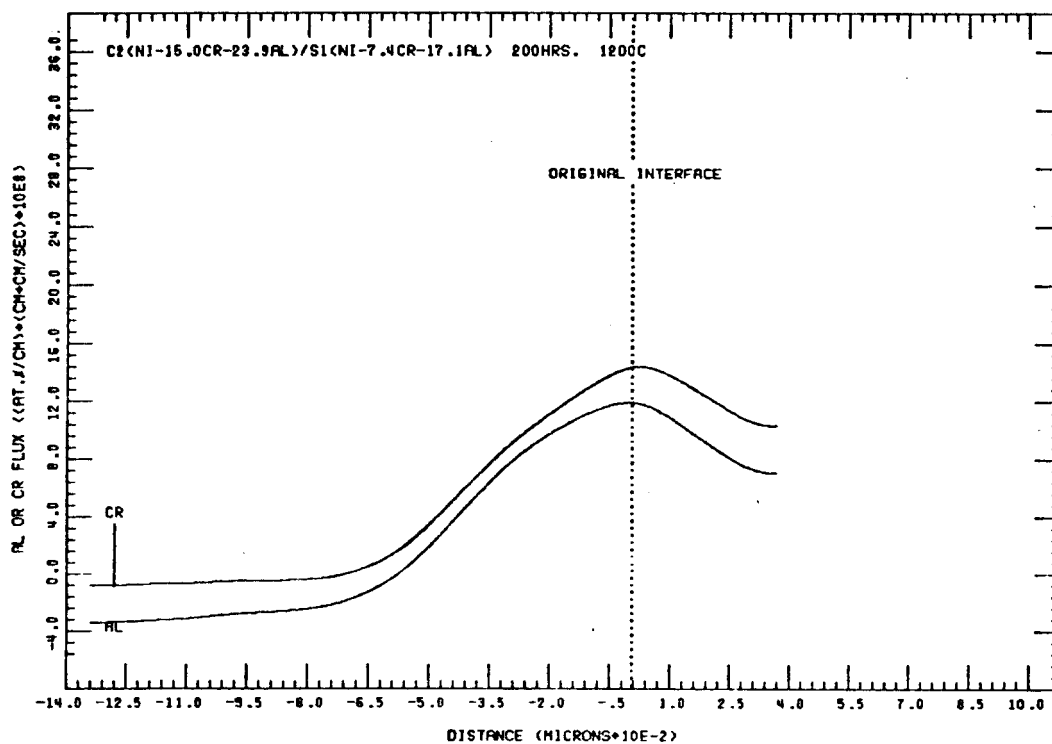
d

Figure 41 (con't.). Calculated Cr and Al fluxes in
the γ phase. c) C1/S3; d) C2/S1.

98
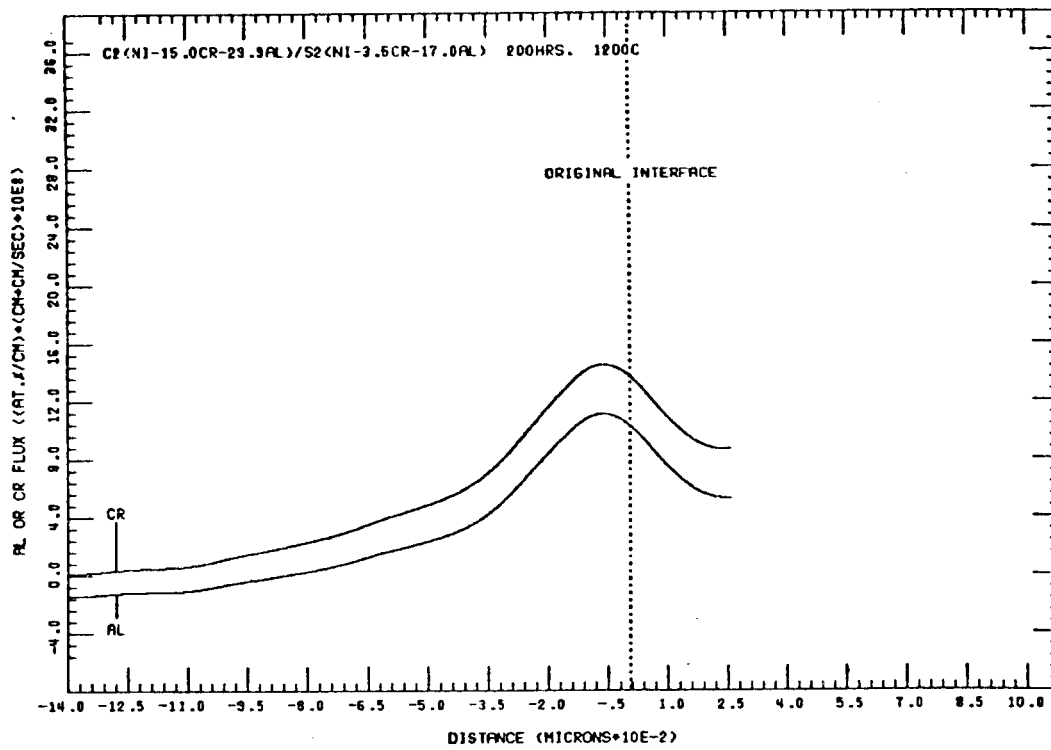
e
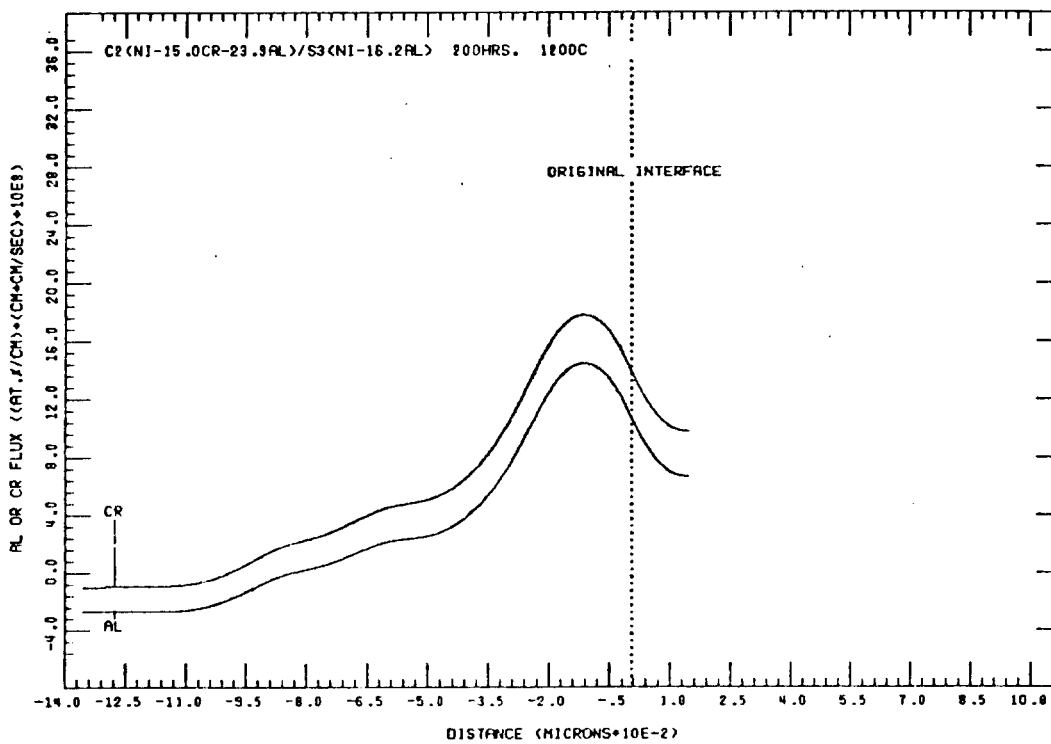
f

Figure 41 (con't.). Calculated Cr and Al fluxes in
the γ phase. e) C2/S2; f) C2/S3

99

g
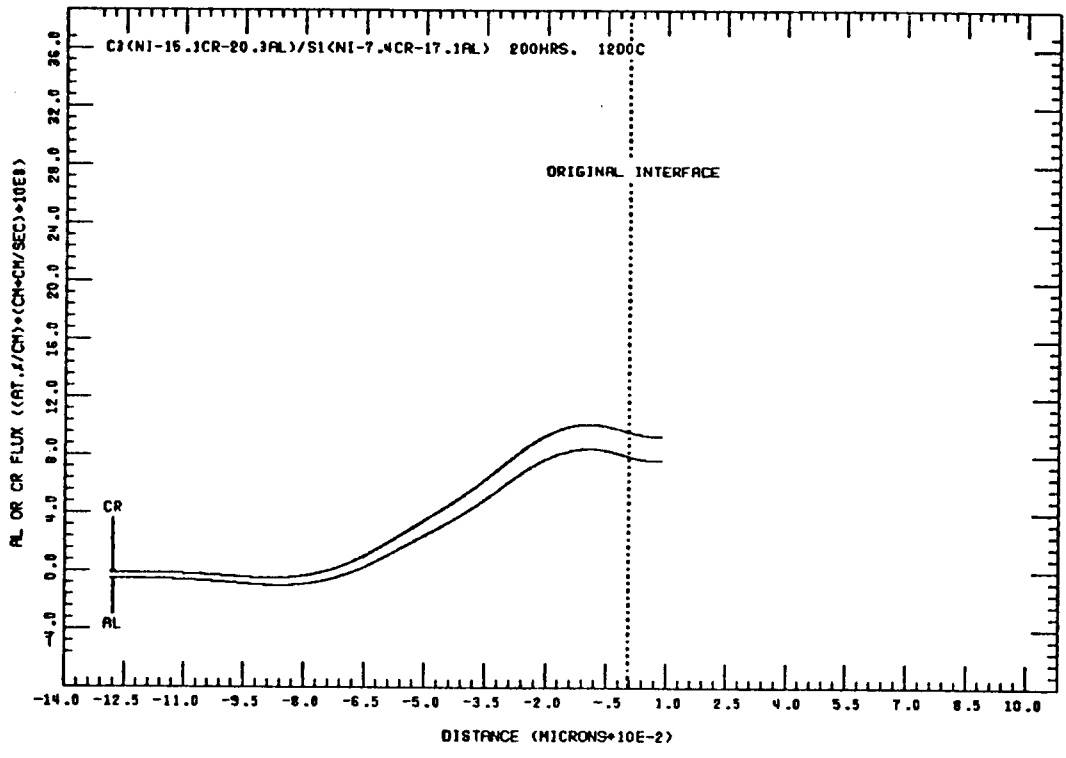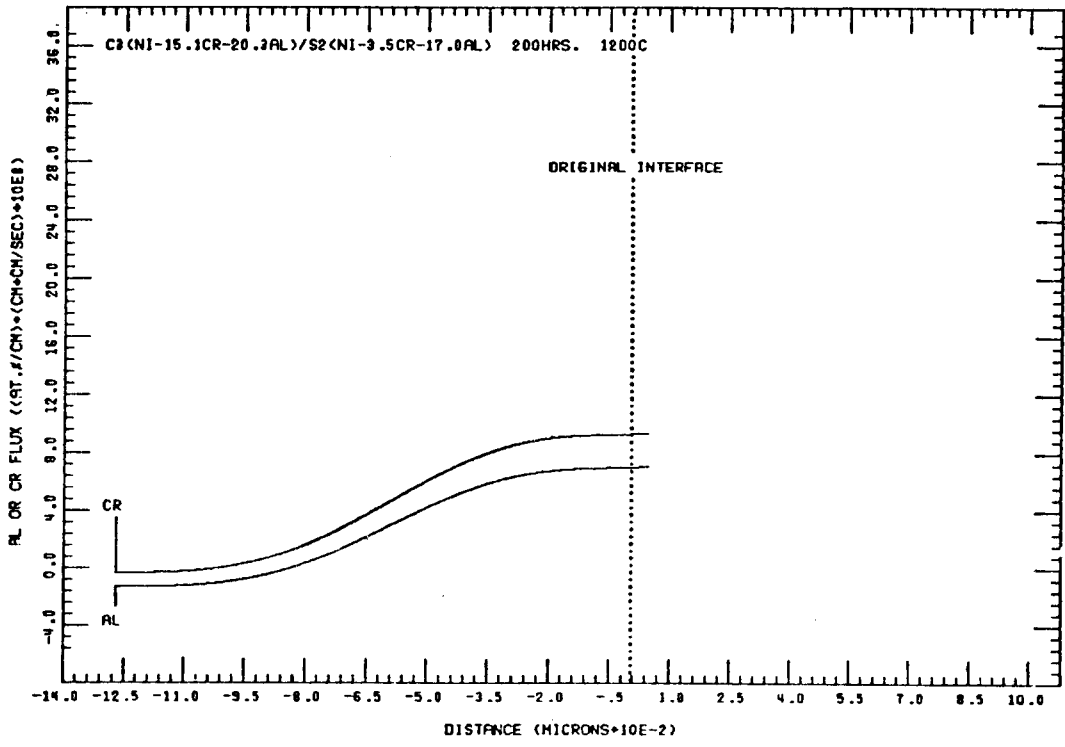
h

Figure 41 (con't.). Calculated Cr and Al fluxes in
the γ phase. g) C3/S1; h) C3/S2.

100
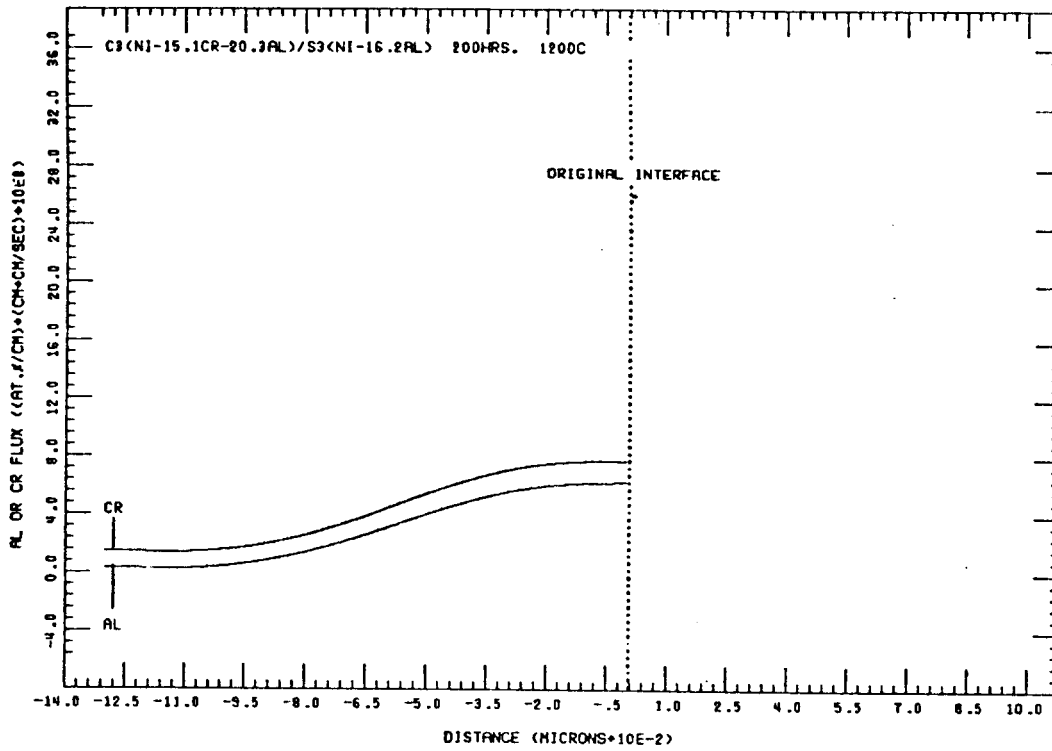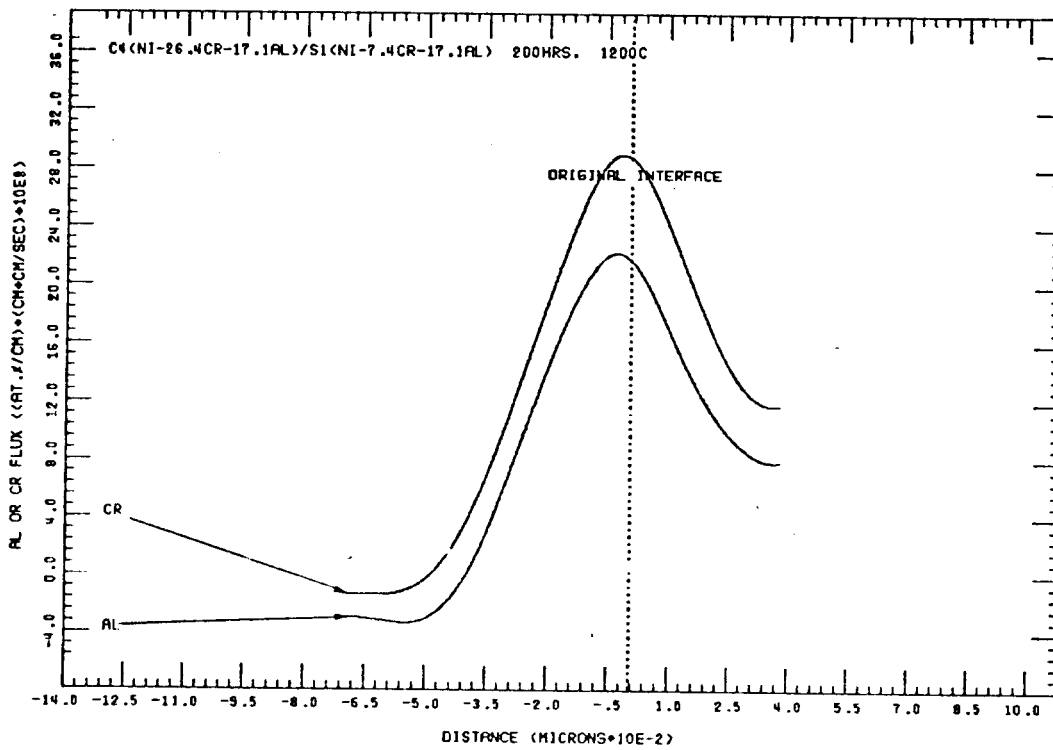
Figure 41 (con't.). Calculated Cr and Al fluxes in the γ phase. i) C3/S3; j)C4/S1

101
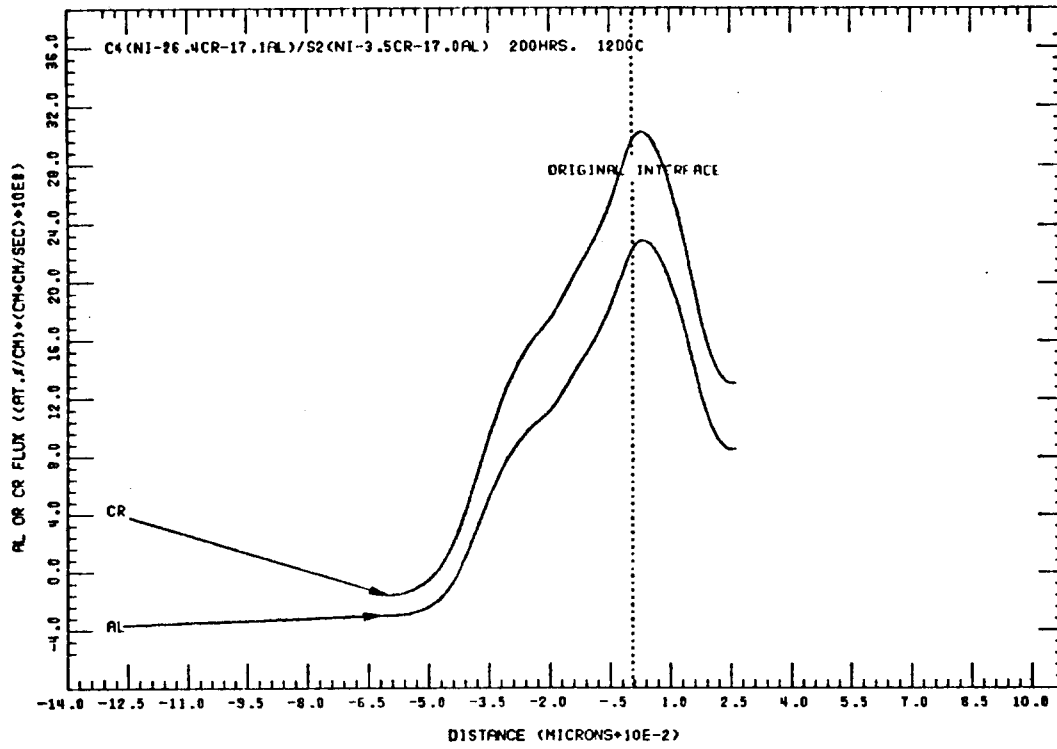
k

Figure 41 (con't.). Calculated Cr and Al fluxes in
the γ phase. k) C4/S2.

102

mately 3 times greater than D_{AlCr}, dC_{Cr}/dX is 10 times greater than dC_{Al}/dX. This large negative Cr gradient makes the absolute value of $D_{AlCr} \cdot dC_{Cr}/dX$ greater than the absolute value of $D_{AlAl} \cdot dC_{Al}/dX$. Thus, because $-D_{AlCr} \cdot dC_{Cr}/dX$ is positive, and $-D_{AlAl} \cdot dC_{Al}/dX$ is negative, the Al flux will always be positive, showing conclusively that the strong Cr gradient is causing Al to diffuse up its gradient. The effect of the Cr gradient on the Al flux can also be seen in the shape of the Al flux curves. The shape of the Al flux curves (Figure 42) was always similar to the shape of the Cr flux curves.

The second important feature of the Cr and Al fluxes in Figure 42 is that they all increase and reach a maximum at, or very near, the original interface in all couples. The maximum in the fluxes was highest for couples with C4 as common alloy, followed by couples with C1 as common alloy, C2 as common alloy, and C3 as common alloy. The maximum in the fluxes was typically higher as the bulk Cr difference between a common β+γ alloy and a given γ+γ' alloy increased.

Discussion

Interdiffusion in $\beta + \gamma / \gamma + \gamma'$ infinite diffusion couples results in the formation of complex, multi-phase diffusion zones. The results of this study allow the growth of the various layers ($\beta + \gamma$, γ, or γ') to be rationalized in terms of being controlled by either the $\beta + \gamma$ alloy composition or the $\gamma + \gamma'$ alloy composition. The causes of formation of the various layers, and the changes that occur in the layers as the $\beta - \gamma$ or $\gamma + \gamma'$ alloy composition changes will be discussed.

$\beta + \gamma$ or γ Layer Formation

Growth of a $\beta + \gamma$ or γ layer can be attributed directly to the γ-phase Cr composition in the $\beta + \gamma$ alloy. Figure 42 lists the bulk compositions of the $\beta + \gamma$ alloys, and plots the bulk Cr composition versus γ-phase Cr composition. Interdiffusion in couples with C1, C2, and C4 as common alloy resulted in $\beta + \gamma$ layer growth. Interdiffusion in couples with C3 as common alloy resulted in β pertubations at the original interface (O.I.) (couples C3/S1 and C3/S2) and γ layer growth, or no γ layer growth at all (C3/S3). The growth of the $\beta + \gamma$ layer cannot be attributed to the bulk Cr composition of the alloy because C2 and C3 had the same bulk Cr composition. The growth of the $\beta + \gamma$ layer also cannot be attributed to the bulk Al composition of the alloy because C4 had a lower bulk Al composition than C3. What the bulk compositions do control, however, is the γ-phase Cr composition. During interdiffusion, the γ-phase Cr concen-
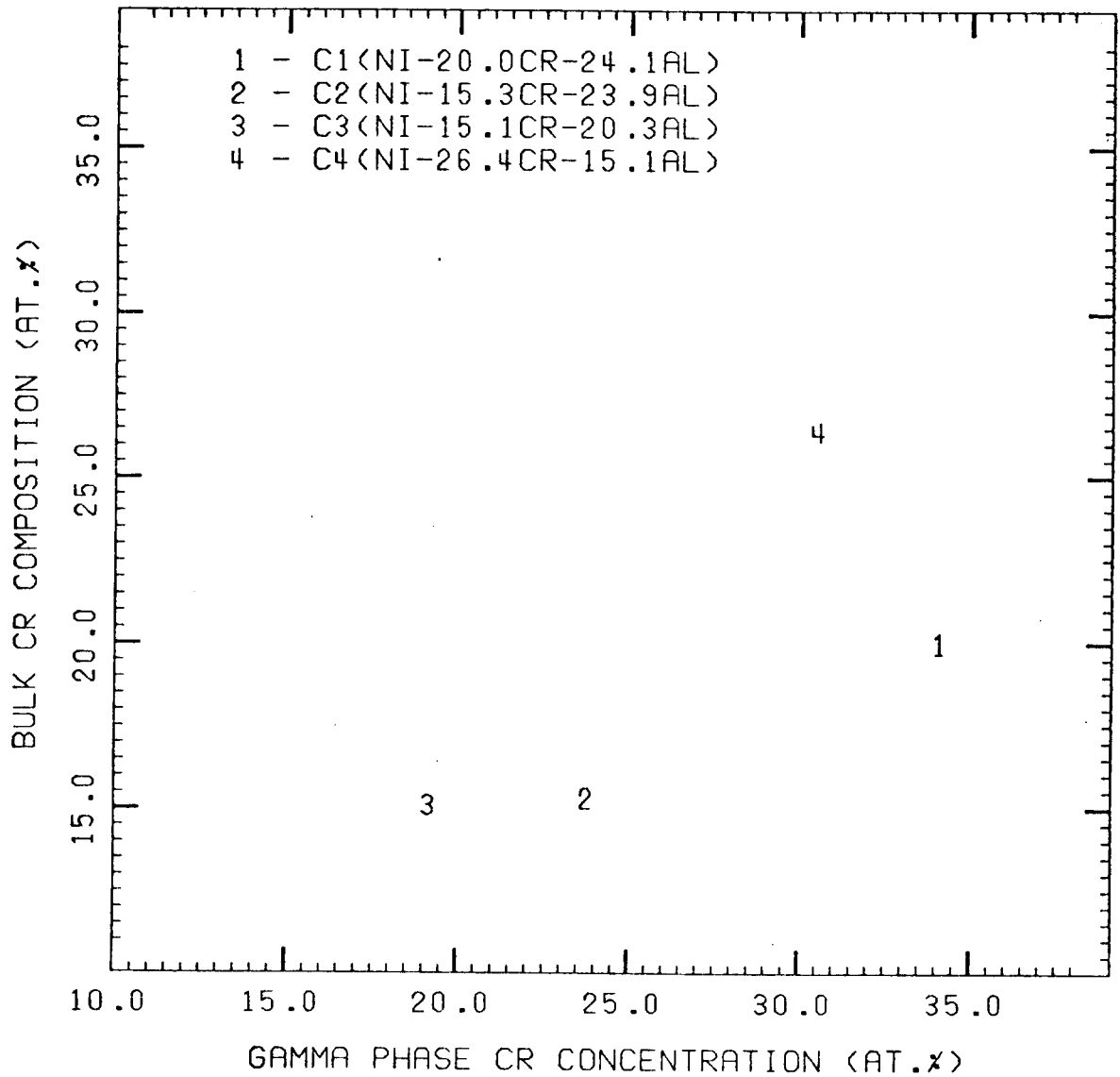
Figure 42. Bulk Cr composition of the β+γ alloys
versus γ phase Cr composition.

tration changes from its equilibrium value to approximately 14.0 at.% Cr at the γ corner of the $\beta+\gamma+\gamma'$ triangle. It is this γ-phase Cr difference (i.e., equilibrium Cr concentration in the γ-phase in the $\beta+\gamma$ alloy - Cr concentration at the γ corner of the $\beta+\gamma+\gamma'$ triangle) which is critical in determining whether a $\beta+\gamma$ or γ layer will form in the diffusion zone.

The fact that the γ-phase Cr difference is critical in detemrining whether a $\beta+\gamma$ or γ layer will form can be seen in the concentration/distance (C/D) profiles in the γ-phase and the resulting fluxes in the γ-phase. Figure 43 plots the Cr C/D profiles in the γ-phase of couples C2/S1 and C3/S1, and the Cr fluxes resulting from the C/D profiles. The maximum Cr gradient occurred near the O.I. in both couples. For couple C2/S1, the maximum Cr gradient was -140 at.%/cm, while in couple C3/S1, the maximum Cr gradient was -100 at.%/cm. The Cr concentration at the maximum gradient was 18.2 at.% Cr for C2/S1 and 16.1 at.% Cr for C3/S1. Both the larger maximum Cr gradient and higher Cr concentration at the maximum gradient in couple C2/S1 is a result of the larger Cr difference in C2/S1 compared to C3/S1. The larger Cr gradient and higher Cr concentration at the maximum gradient, which was present in all C2 couples compared to C3 couples, leads to larger Cr and Al fluxes in the γ-phase of C2 couples compared
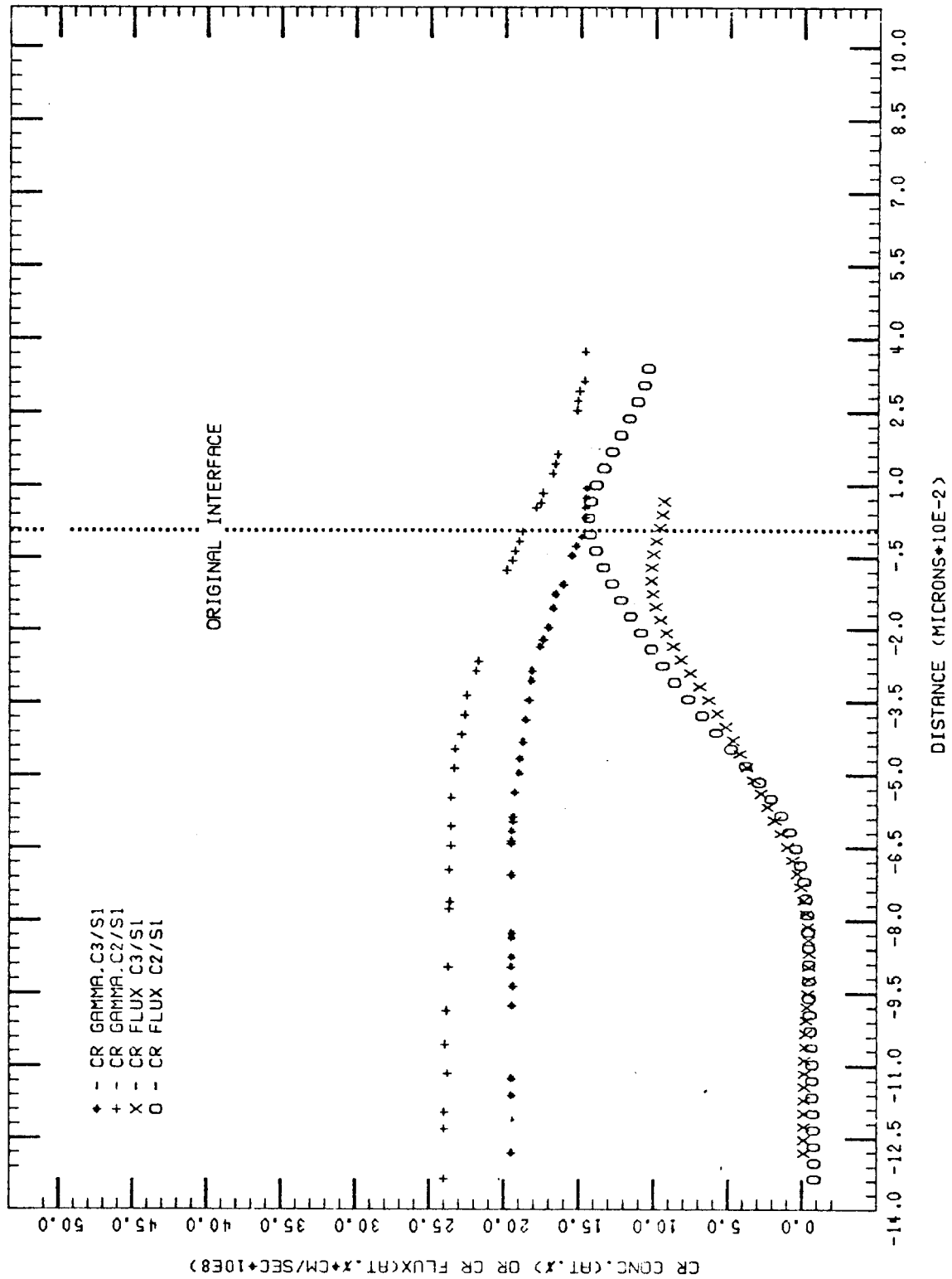
Figure 43. Cr concentration/distance profiles and Cr fluxes in the γ phase for couples C2(Ni-15.1Cr-23.9Al)/S1(Ni-7.4Cr-17.1Al) and C3(Ni-15.3Cr-20.1Al)/S1.

to C3 couples. The larger Cr and Al fluxes in the γ-phase of

C2 couples, and that β+γ growth and not γ growth occurred, points

to the correlation that the fluxes in the γ-phase and growth

of the various layers are interrelated. The β pertubations at

the O.I. (which may be though of as a very narrow β+γ layer)

in C3 couples (except C3/S3, which will be discussed later) shows

that the ability to sustain growth of a β+γ layer is dependent

on the fluxes reaching critical magnitudes in the γ-phase.

Reaching the critical flux magnitudes depends on the Cr concen-

tration gradients and the Cr concentration at the gradients,

which in turn depends on the γ-phase Cr difference.

The necessity to reach critical γ-phase flux magnitudes

before β+γ growth can occur can be supported by relating the

γ-phase fluxes to the diffusion paths and the bulk C/D profiles

in the diffusion zone. The diffusion paths for couples in which

a β+γ layer resulted from interdiffusion inflected and increased

to higher Al composition (lower Cr composition) in the β+γ phase

field. These inflections were a result of sharp decreases in

the bulk Cr C/D profiles and sharp increases in the bulk Al C/D

profiles at the O.I. in the couples. (The O.I. was where the

β+γ growth layers started in the diffusion zone.) Clearly, for

the bulk Al to flow up its gradient it must be forced to do so.

The force causing the bulk Al to flow up its gradient is the

strong negative Cr gradient. Thus, in an analogous manner to

the strong negative Cr gradient forcing Al to diffuse up its

gradient in the γ-phase, the strong negative bulk Cr gradient

forces bulk flow of Al up its gradient. However, because bulk flow, and bulk gradients, are a result of diffusion in the phases, the cause of the bulk flow and bulk gradients can be directly related to the flux maxima in the γ-phase.

At or very near, the O.I. interface in all couples, the fluxes of Cr and Al in the γ-phase reached maxima. The maximum in the fluxes corresponded exactly to the points where the bulk Cr C/D profiles began to decrease rapidly, and the bulk Al C/D profiles began to increase rapidly in the diffusion zone, as shown in Figures 44, 45, and 46 for couples with Cl as common alloy. The maxima in the fluxes indicate that at the O.I. (i.e. at the start of the $\beta + \gamma$ growth layer) the maximum amount of Cr and Al is transported per unit area from the γ-phase into the $\beta + \gamma$ growth layer. The Cr is supplied primarily by the Cr-rich γ-phase. The Al is supplied primarily by the Al-rich β phase. The fact that Al is supplied primarily by the β-phase can be supported by many reasons. First, the Al concentration in the β-phase is approximately 30.0 at.% Al compared to 9.0-14.0 at.% Al in the γ-phase. If the γ phase were to supply the necessary Al for growth of the $\beta + \gamma$ layer (which contains greater than 20.0 at.% bulk Al), it would have to dissolve preferrentially to the β-phase. This dissolution of γ is highly unlikely from considerations of the Al composition in the two phases alone, and the diffusion zone microstructures show that the γ-phase does not dissolve. The diffusion zone microstructures show that the β-phase dissolves. Therefore, dissolution of the β-phase can only be rationalized, logically, in terms of occurring to supply Al
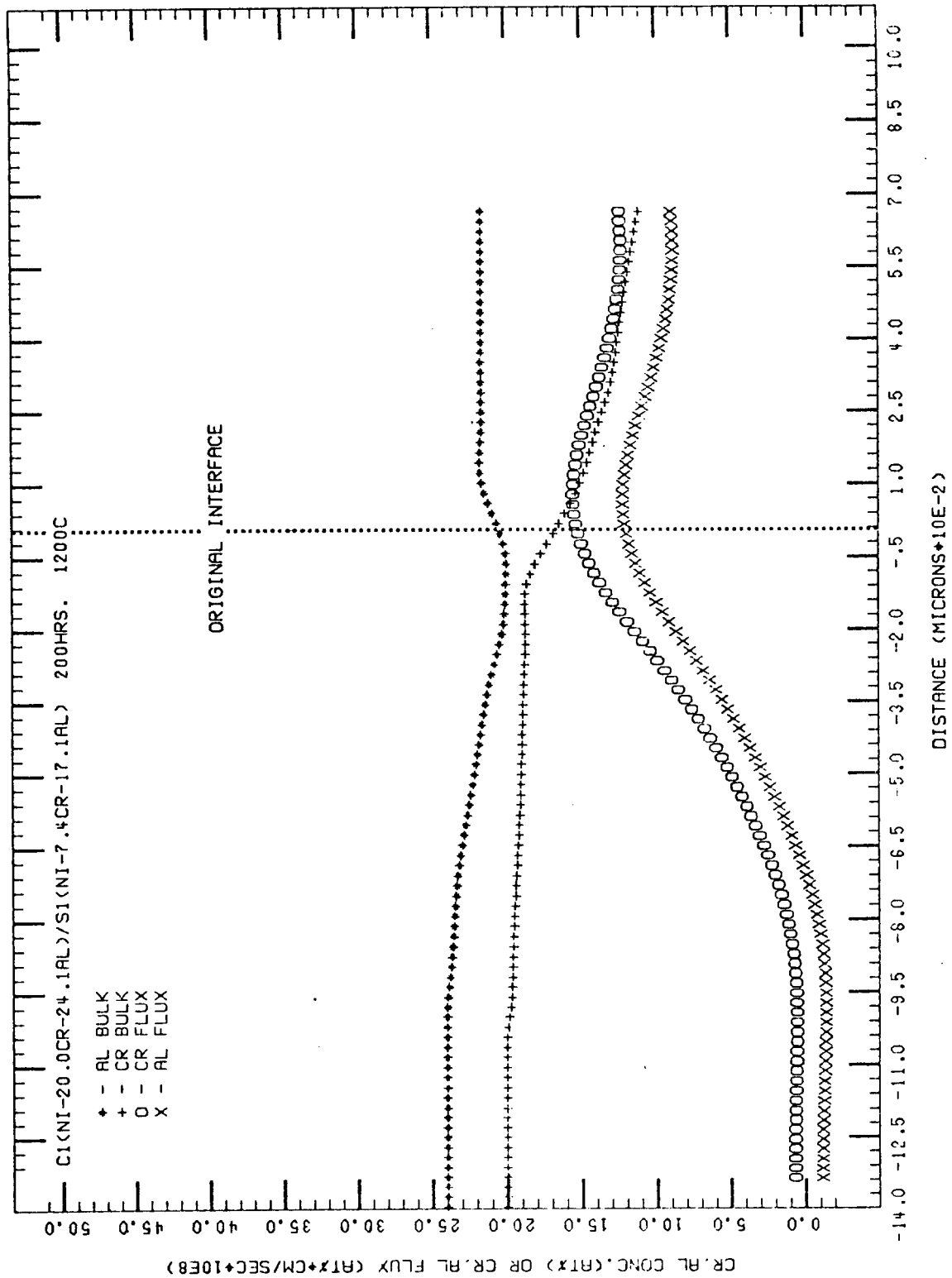
Figure 44. Bulk Cr and Al composition versus γ phase Cr and Al flux in couple
C1 (Ni-20.0Cr-24.1Al)/S1 (Ni-7.4Cr-17.1Al).

110
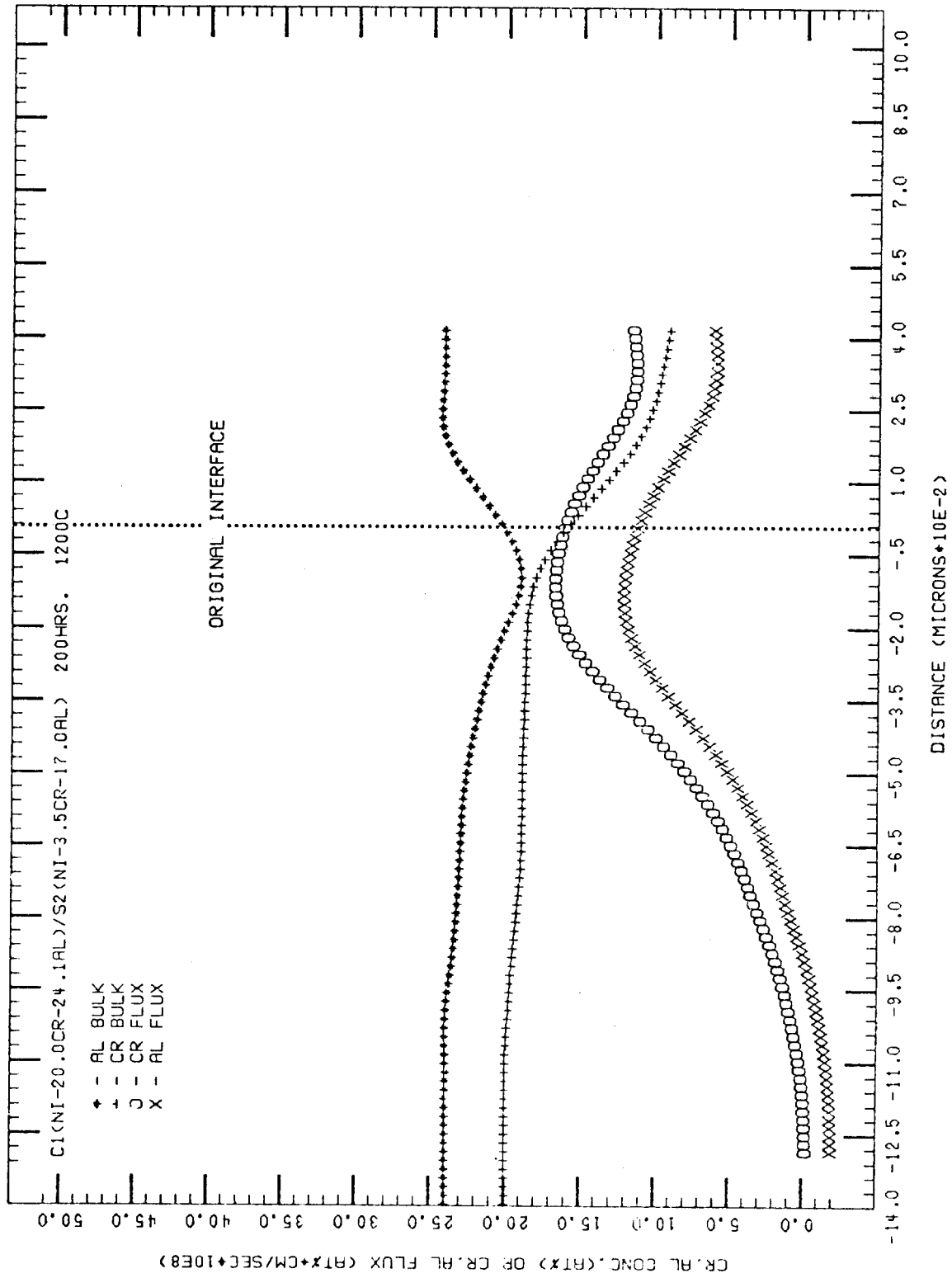
Figure 45. Bulk Cr and Al composition versus γ phase Cr and Al flux in couple
C1 (Ni-20 .0Cr-24.1Al)/S2 (Ni-3.5C4-17.0Al).
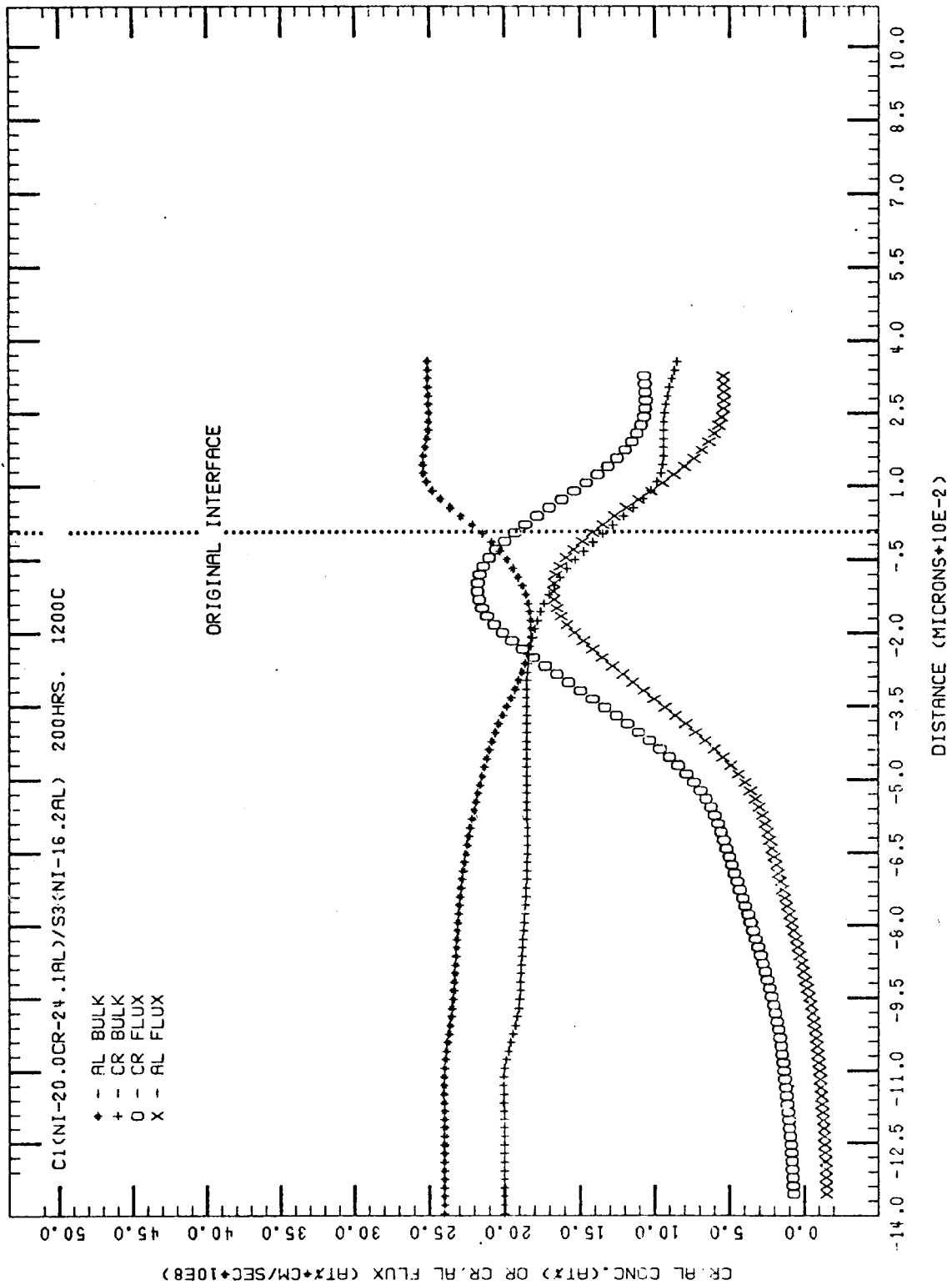
Figure 46. Bulk Cr and Al composition versus γ phase Cr and Al flux in couple C1(Ni-20.0Cr-24.1Al)/S3(Ni-16.2Al).

for growth of the β+γ layer (and the other layers in the couple). Second, the bulk flow analysis showed that the amount of Al lost from the β+γ alloy increased as the Cr composition in the β+γ alloy decreased. The diffusion zone microstructures showed that the amount of β dissolution in the β+γ alloy increased as the Cr composition in the γ+γ' alloy decreased. Third, in C4 couples, complete β dissolution occurred. Both the bulk flow analysis and γ-phase flux analysis show that Al flow occurs from the β+γ alloy to the γ+γ' alloy. The Al contained in the β phase had to go into the β+γ growth layer. The only mechanism of transport for the Al supplied by the β phase to reach the growth layer is through diffusion in the γ-phase. Furthermore, the complete β dissolution in C4 couples indicates that the γ phase is used for transport of Cr and Al to the β+γ growth layer. The β-phase simply dissolves to supply Al necessary for growth of the β+γ layer (and the other layers in the couple). Thus, the β and γ phases interact to cause growth of the β+γ layer. The maximum Cr flux in the γ-phase causes a maximum Al flux in the γ-phase. In response to the maximum Al flux in the γ-phase, and to supply Al necessary for growth of the β+γ layer, dissolution of the β phase occurs. It is these β and γ phase interactions which lead to the bulk flow and bulk gradients at the O.I. in the couple.

Thus, growth of the β+γ layer can be rationalized in terms of maximum fluxes in the γ-phase, and their ability to cause bulk gradients which lead to growth of the layers. In couple C3/S1, the pertubations of β present at the O.I. indicated that the flux

maxima in the γ-phase were large enough to cause a bulk gradient which would force bulk flow of Al up its gradient at the O.I. However, they were not large enought to sustain the bulk Cr gradient, and flow of Al up its gradient, and thus growth of the γ layer resulted. In couples that grew $\beta + \gamma$ layers, the flux maxima and the fluxes in the $\beta + \gamma$ growth layer were larger than the fluxes in C3/S1. Thus, the fluxes were large enough to sustain a negative bulk Cr gradient which would force bulk flow of Al up its gradient and result in $\beta + \gamma$ growth. In couple C3/S2, the fluxes reach no maximum, but were of the same magnitude in the γ growth layer as the fluxes in C3/S1, as shown in Figure 47. Thus, no substantial bulk Cr gradient could be generated which would force bulk Al up its gradient, and thus the bulk Al C/D profile in C3/S2 did not increase at the O.I. The fluxes were large enough, however, to grow a γ layer. In couple C3/S3, the fluxes again reached no maximum and were smaller at the O.I. than in C3/S1 and C3/S2, as shown in Figure 47. Thus, not even a γ layer resulted from interdiffusion.

In summary, the ability to grow a $\beta + \gamma$ layer depends on the ability to generate and sustain bulk Cr flow down a strong negative gradient. The strong negative Cr gradient forces bulk flow of Al up its gradient. The ability to generate and sustain these gradients is directly related to the ability to generate flux maxima in the γ phase. The ability to generate maximum fluxes in the γ phase is directly related to the Cr composition (or Cr difference) in the γ phase.
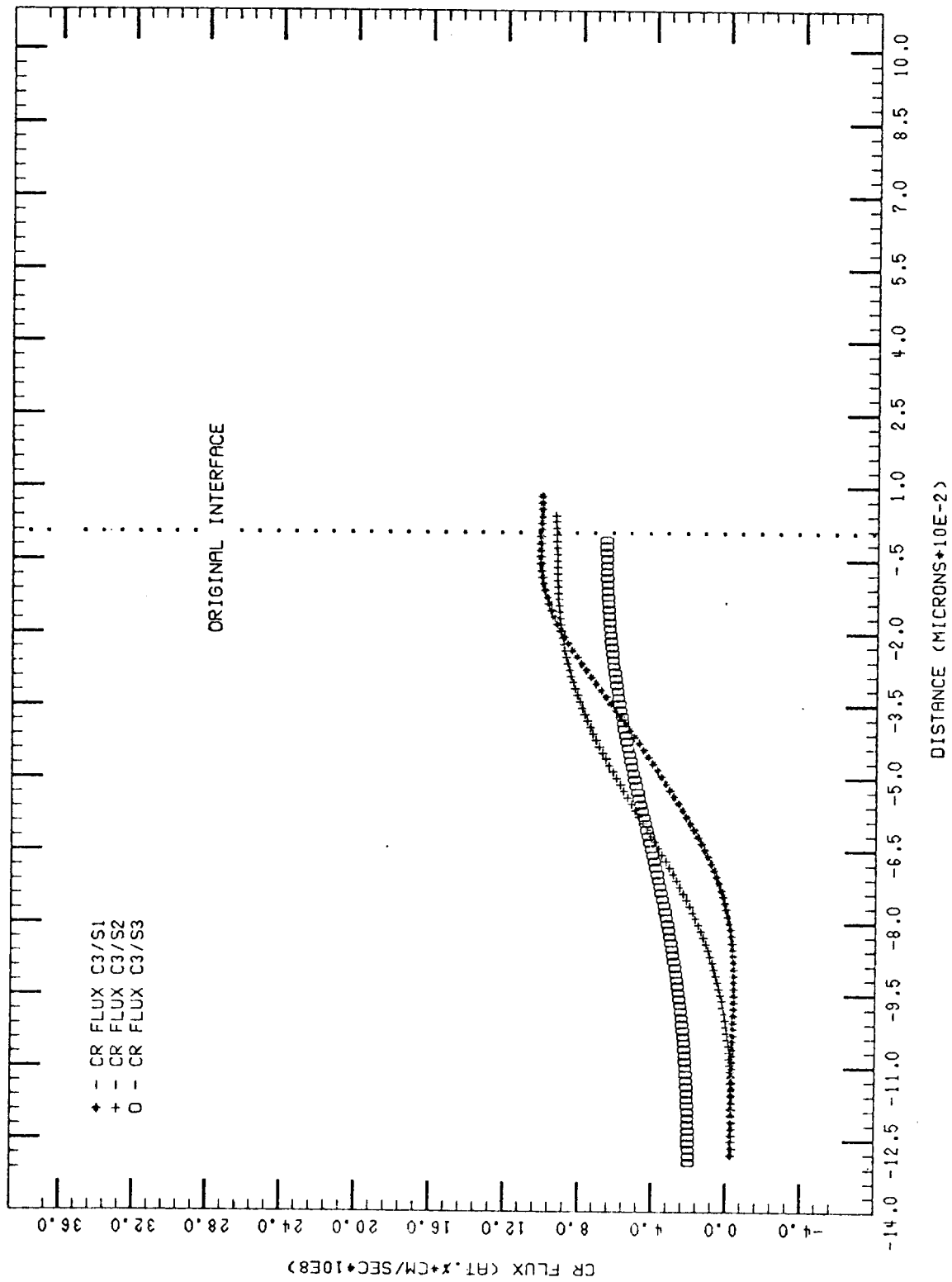
Figure 47. Cr fluxes in the γ phase for couples C3/S1, C3/S2, and C3/S3.

β Volume Fraction in the β+γ Growth Layer

When the Cr composition in the γ+γ' alloy decreased, the bulk Al composition in the β+γ growth layer increased. In the diffusion zone, the increase in the bulk Al composition was a result of increases in the volume fraction of β in the β+γ growth layer. In terms of the diffusion paths, as the Cr composition in the γ+γ' alloy decreased, the diffusion paths translated up the β+γ side of the β+γ+γ' triangle to higher Al composition. The cause of the diffusion path translation (or increase in β volume fraction) is related to the height to which the diffusion path rises in Al composition on the γ+γ' side of the triangle. For couples with S1 as common alloy, the highest Al composition point on the γ' side is where the path exits the triangle on the γ+γ' side. For couples with S2 and S3 as common alloy, the highest Al composition point on the γ' side is where the diffusion path exits the γ' phase field into the γ+γ' phase field. Thus, for γ+γ' alloys in which a γ' layer results from interdiffusion, as the Cr composition in the γ+γ' alloy decreases, the amount of diffusion path in the γ' phase field increases. As the amount of diffusion path in the γ' phase field increases, the higher it must increase in Al composition. The higher the path increases in Al composition in the γ' phase field, the higher the path increases in Al composition on the β+γ side of the triangle, or, the greater the volume fraction of β becomes in the β+γ growth layer. Thus, in order to account for the substantial increase in Al composition that occurs in the path segment in the γ' phase

116

field, a larger bulk Al discontinuity is created at the three-phase interface in the couple. This discontinuity is created by increasing the β volume fraction in the β+γ growth layer.

To account for the increase in bulk Al composition in the β+γ growth layer, as controlled by the γ+γ' alloy, the flux maxima in the γ-phase of the β+γ alloy increase. Thus, the flux maxima were higher in the γ-phase as the Cr composition in the γ+γ' alloy decreased, as shown in Figure 48 for couples with C1 as common alloy. This of course follows from what has been previously presented. The growth of the β+γ layer requires a strong negative bulk Cr gradient at the start of the β+γ growth layer. This strong negative bulk Cr gradient forces bulk flow of Al up its gradient. For the bulk Al to flow up steeper gradients (which occurs as the bulk Al composition in the β+γ growth layer, or β volume fraction, increases) the negative bulk Cr gradient must become larger. This, in fact, is observed as the γ+γ' alloy Cr composition decreases. In order to generate larger negative bulk Cr gradients, and force bulk flow of Al up steeper gradients, the flux maxima in the γ-phase increase. Again, this is observed as the γ+γ' Cr composition decreases.

γ' Layer Formation

The formation of a γ' layer in the diffusion zone can be attributed directly to the γ+γ' alloy composition. Variations in γ+γ' alloy Cr composition from 10.0 at.% Cr to 0 at.% Cr showed that the transition from a β+γ/γ+γ' interface to a β+γ/γ'

117
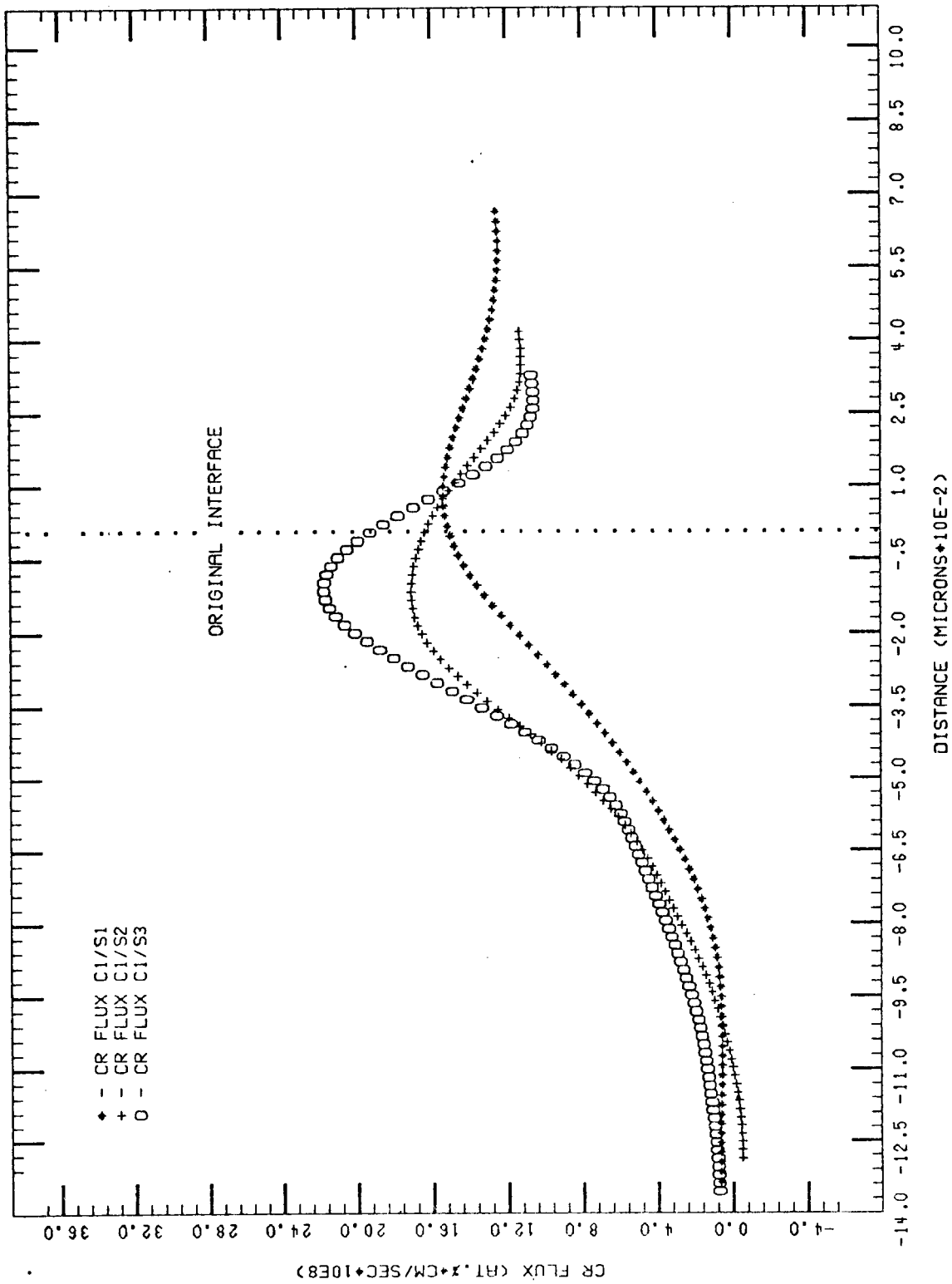
Figure 48. Cr fluxes in the γ phase for couples Cl/Sl, Cl/S2, and Cl/S3.

118

interface (where a γ' layer forms in the diffusion zone) occurs gradually as the Cr composition is decreased. In terms of the diffusion paths, the diffusion path translates up the $\gamma+\gamma'$ side of the $\beta+\gamma+\gamma'$ triangle toward the γ' corner. In the diffusion zone, the γ' volume fraction at the three-phase interface gradual increases as the $\gamma+\gamma'$ alloy Cr composition decreases until the path reaches the γ' corner. Once the path reaches the γ' corner, a γ' layer forms in the diffusion zone. The Cr composition in the $\gamma+\gamma'$ alloy at which point a γ' layer will form in the diffusion zone has been determined to be slightly less than 6.0 at.% Cr. Any further decreases in the $\gamma+\gamma'$ alloy Cr composition only leads to increased γ' growth.

$\beta+\gamma$ and γ' Growth Layer Kinetics

As the Cr composition in the $\beta+\gamma$ alloy decreased, the amount of $\beta+\gamma$ growth decreased. From the standpoint of bulk composition differences as driving forces, the decrease in the amount of $\beta+\gamma$ growth was expected. As the bulk Cr difference between $\beta+\gamma$ alloy and $\gamma+\gamma'$ alloy decreases, the driving force for $\beta+\gamma$ growth is expected to decrease and the data shows that it does. In terms of the Cr and Al fluxes in the γ-phase, this decrease in $\beta+\gamma$ growth can also be rationalized. The Cr and Al fluxes in the $\beta+\gamma$ growth layer, and at the three-phase interfaces, were typically lower as the $\beta+\gamma$ alloy Cr composition decreased. The interface velocity is related to a mass balance at the interface by:

$$\Delta C \ d\epsilon/dt = J^{\beta+\gamma}_{Cr,Al} - J^{\gamma+\gamma' \ or \ \gamma'}_{Cr,Al} \tag{1}$$

where ΔC is the Cr or Al composition difference across the interface, $d\epsilon/dt$ is the interface velocity, $J_{Cr,Al}^{\beta+\gamma}$ is the flux of Cr or Al in the β or γ phase on the $\beta+\gamma$ side of the interface and $J_{Cr,Al,}^{\beta+\gamma' \text{ or } \gamma'}$ is the flux of Cr or Al in the γ and γ' phases, if the interface is $\beta+\gamma/\gamma+\gamma'$, or the flux of Cr or Al in the γ' phase, if the interface is $\beta+\gamma/\gamma'$. If the interface is $\beta+\gamma/\gamma+\gamma'$, the similar γ' volume fractions on the $\gamma+\gamma'$ side of the interface in all couples indicates that $J_{Cr,Al}^{\gamma+\gamma'}$ is approximately constant for all couples. Likewise, if the interface is γ', the similar Cr and Al concentration gradients in the γ' phase at the interface in all couples indicates that $J_{Cr,Al}^{\gamma'}$ is approximately constant for all couples. Thus, because ΔC is fixed, as $J_{Cr,Al}^{\beta+\gamma}$ decreases, the interface velocity $d\epsilon/dt$ must decrease, and this leads to a decrease in the amount of $\beta+\gamma$ growth.

As the Cr composition in the $\gamma+\gamma'$ alloy decreased, the amount of $\beta+\gamma$ growth decreased. At first, this would seem to be a contradiction because as the bulk Cr difference between $\beta+\gamma$ alloy and $\gamma+\gamma'$ alloy increases, the driving force for $\beta+\gamma$ growth would be expected to increase. But, not only $\beta+\gamma$ growth must be considered, but also γ' growth (and $\gamma+\gamma'$ growth for γ alloy S3). As the $\gamma+\gamma'$ alloy Cr composition decreases, the amount of γ' growth increases. Thus, if the amount of growth of each layer is added for each couple (e.g. for C2/S1, $\beta+\gamma$ growth (360μm); for C2/S2, $\beta+\gamma$ and γ growth (438μm); and for C2/S3, $\beta+\gamma$, γ', and $\gamma+\gamma'$ growth (518μm)), the total amount of growth increases as the $\gamma+\gamma'$ composition decreases, in accord with an increased driv-

ing force.

From the standpoint of fluxes, the Cr and Al fluxes in the γ-phase decreased rapidly in the β+γ growth layers and to lower values as the γ+γ' Cr composition decreased. From Eqn. (1), the decrease in the flux values at the interface would lead to a decrease in the interface velocity, and therefore a decrease in the amount of β+γ growth. The amount of γ' growth increased as the γ+γ' alloy Cr composition decreased. The amount of γ' growth can also be rationalized in terms of fluxes at the interface. The Cr concentration gradient at the γ'/γ+γ' interface increased as the γ+γ' alloy Cr composition decreased. Because the Cr flux at the interface is directly proportional to the Cr concentration gradient at the interface, the Cr flux would be larger at the γ'/γ+γ' interface as the γ+γ' alloy Cr composition decreased. The larger Cr flux would lead to an increased growth velocity of the γ' layer, and thus the amount of γ' growth would increase.

The decrease in β+γ growth and increase in γ' growth as the γ+γ' alloy Cr composition decreases correlates very well with the bulk flow analysis. For couples with γ+γ' alloy S1 as common alloy, all the Cr and Al that diffused in S1 contributed to forming a β+γ layer. For couples with γ+γ' alloy S2 as common alloy, the volume fraction of β in the β+γ growth layer is higher, and a γ' layer forms. The amount of Cr and Al that diffuses into S2 must go into forming the higher bulk Al β+γ layer and the γ' layer. Although more Cr and Al is lost from the β+γ alloys with

121

S2 as common alloy, the amount of Cr and Al that diffuses into S2 cannot possibly grow a larger, higher bulk Al β+γ layer than in S1 couples, and at the same time grow a γ' layer. Thus a S2 couples result in smaller, higher bulk Al β+γ layers, and a γ' layer.

Summary

The diffusion paths for couples in Series 1, 2, and 3, are replotted in Figures 49, 50, and 51. From these Figures it can be seen that the γ+γ' alloy composition determines where the diffusion path exits the β+γ side of the β+γ+γ' triangle. Thus, the diffusion path formed between the β+γ and γ+γ' alloy must meet this fixed point. How the path procedes from the β+γ alloy to this fixed point is a function of the β+γ alloy composition, and in particular, the Cr composition in the γ-phase of the β+γ alloy. Interdiffusion with β+γ alloys of high γ-phase compositions results in β+γ growth as the mode for the path to reach the β+γ+γ' triangle. The growth of the β+γ layer is a result of strong negative bulk Cr gradients forcing bulk flow of Al up its gradient. The cause of the gradients is directly related to maximum fluxes in the γ-phase. Interdiffusion with β+γ alloys of low γ-phase Cr composition results in γ layer growth as the mode for the path to reach the β+γ+γ' triangle. The reason a γ layer, and not a β+γ layer, is grown is directly related to flux maxima in the γ-phase being insufficient to sustain a strong negative bulk Cr gradient. The inability to sustain the bulk Cr gradient leads to the inability to sustain bulk flow of Al up its gradient
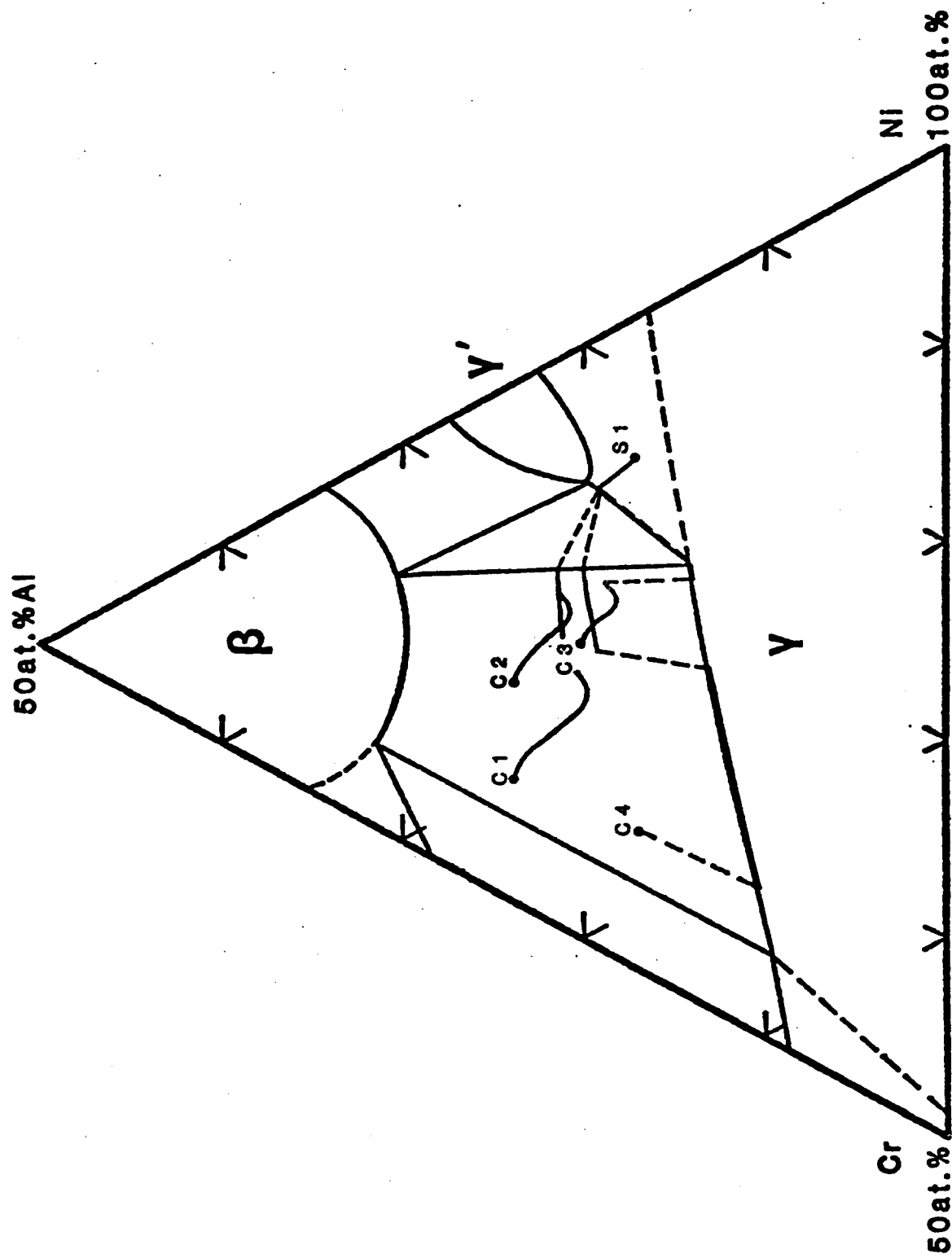
Figure 49. Diffusion paths for couples in Series 1 (C1, C2, C3, C4/S1).
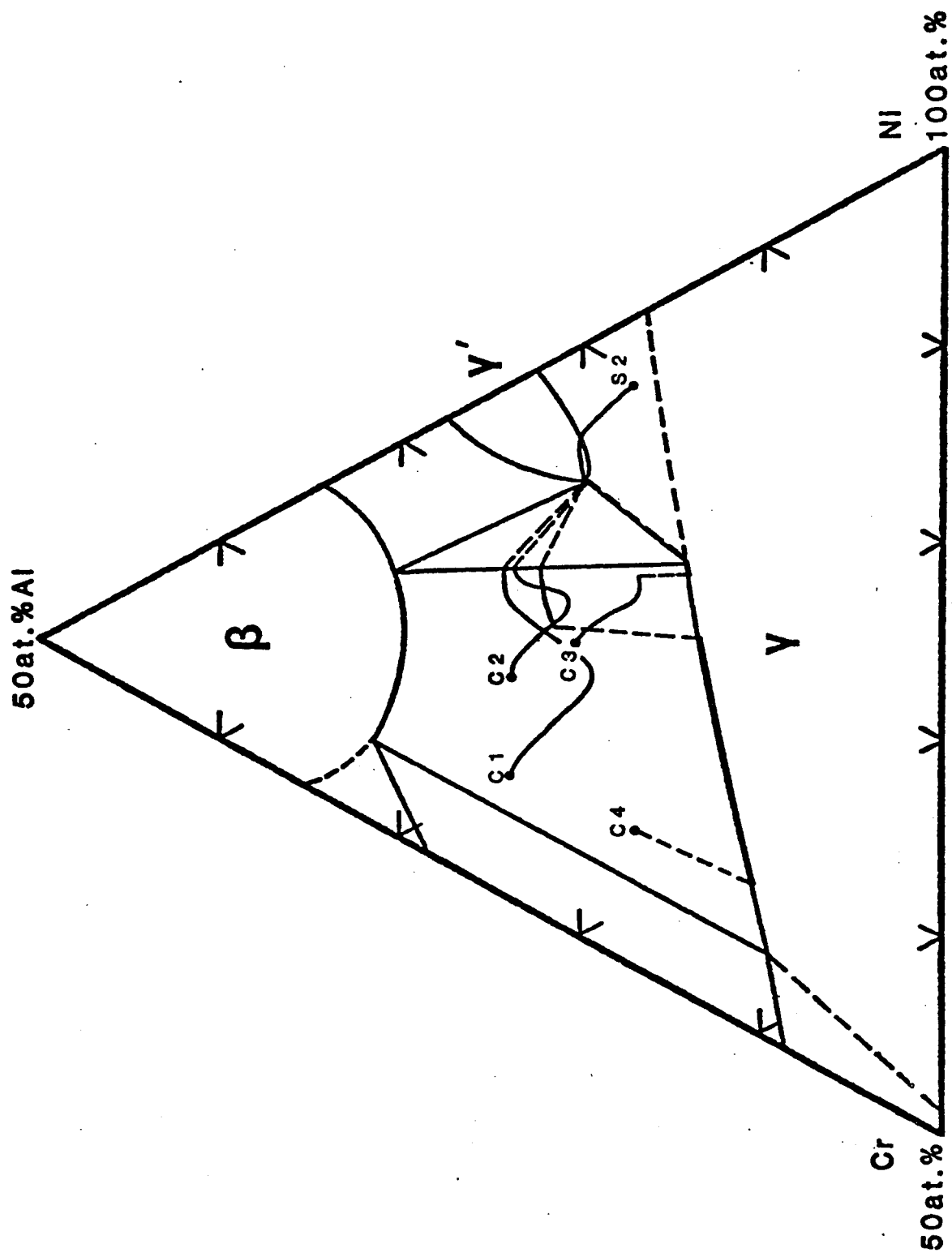
Figure 50. Diffusion paths for couples in Series 2 (C1, C2, C3, C4/S2).
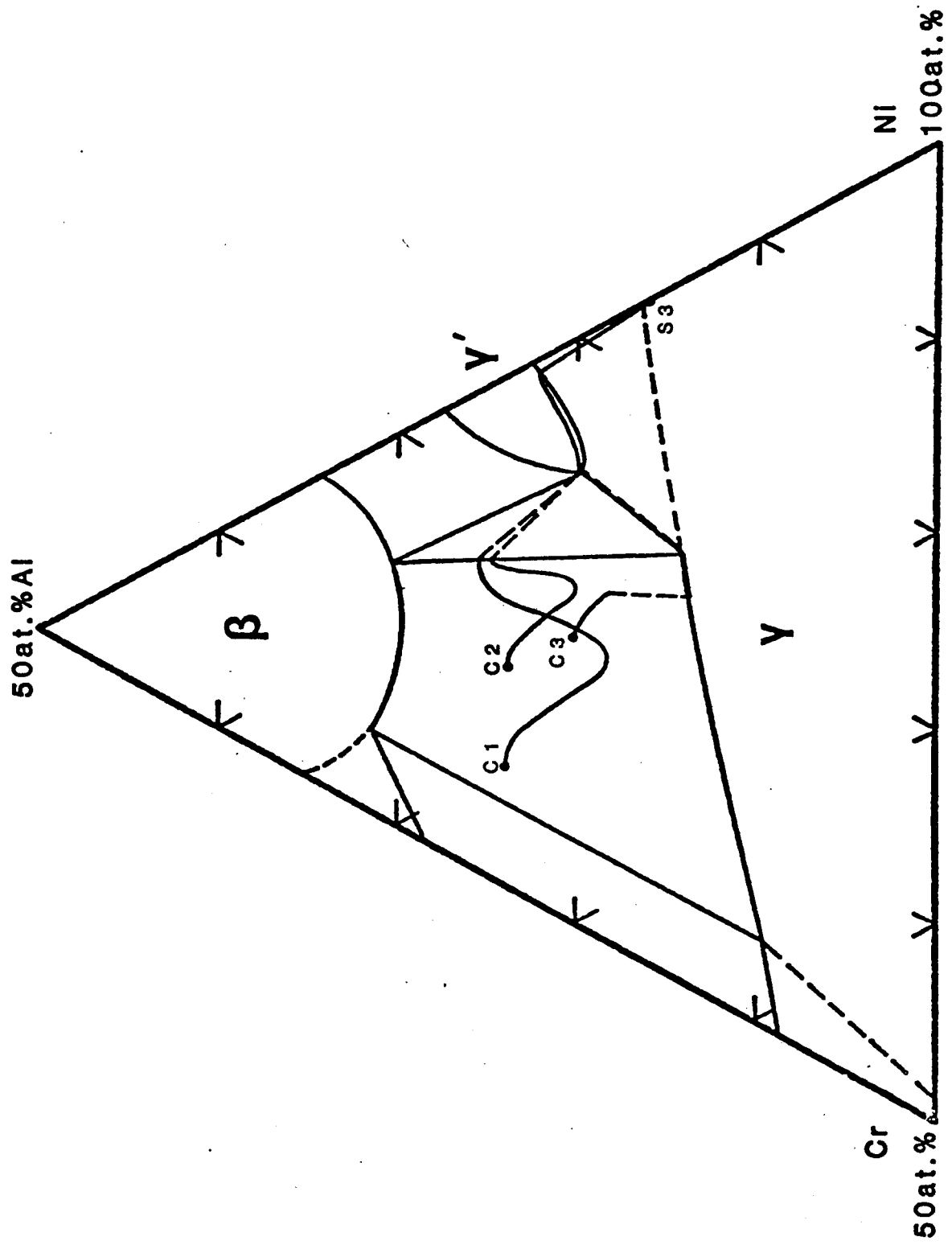
Figure 51. Diffusion paths for couples in Series 3 (C1, C2, C3/S3).

for β+γ growth to occur.

The shape of the path in the β+γ phase field is determined by volume fraction adjustments in the β and γ phases in accord with supplying Cr and Al for growth of the layers. The Cr is supplied primarily by the Cr-rich γ-phase, and the Al is supplied primarily by the Al-rich β-phase. Thus, in all couples, reductions in the volume fraction of β occurred in the β+γ alloy. These β volume fraction reductions lead to the "V" shaped paths in the β+γ phase field.

Figure 52 replots the diffusion paths for couples with Cl as common alloy. From Figure 52 it can be seen that the γ+γ' alloy composition determines the Al composition at which point the path in the β+γ phase field will enter the β+γ side of the β+γ+γ' triangle. This means the γ+γ' alloy composition determines the volume fraction of β in the β+γ growth layer. The γ+γ' alloy composition also determines whether a γ' layer will form in the diffusion zone. As the γ+γ' alloy Cr composition decreases, the amount of Cr and Al lost from the β+γ alloy increases. As the amount of Al lost from the β+γ alloy increases, greater reductions in the volume fraction of β occur, and hence the "V" section of path decreases to lower Al composition. Furthermore, as the γ+γ' alloy Cr composition decreases, the amount of β+γ growth decreases, and the amount of γ' growth increases.

Comparison to β+γ/γ Ni-Cr-Al Interdiffusion

One of the purposes of this study was to compare β+γ/γ+γ' interdiffusion to a previous study (19) of β+γ/γ interdiffusion.

126
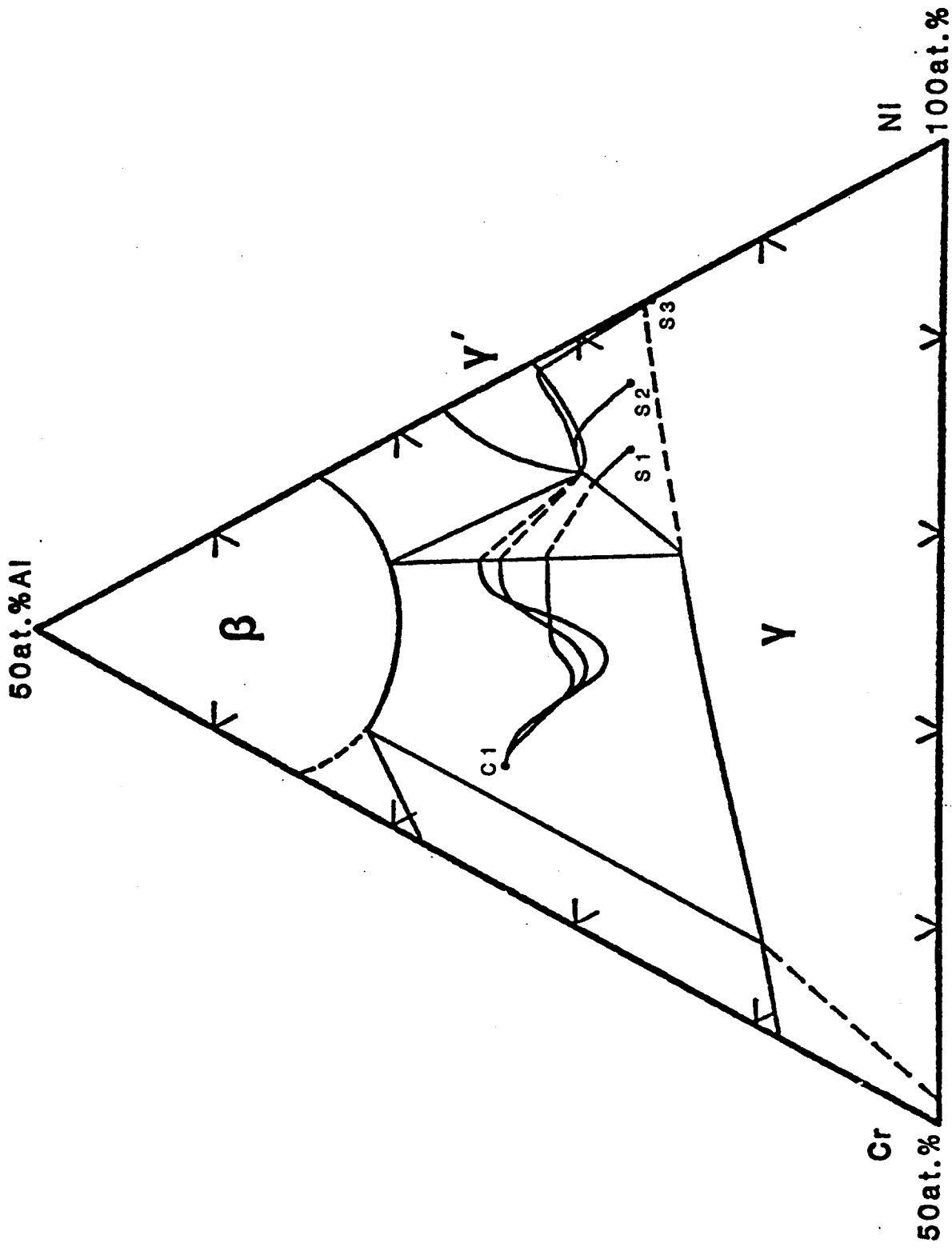
Figure 52. Diffusion paths for couples with C1 as the common alloy (C1/S1, S2, S3).

In Nesbitt's study (19), higher bulk Al gradients than Cr gradients were present   the diffusion couples. Interdiffusion of β +γ alloys with the γ Ni-Cr-Al alloys used in Nesbitt's study (19) always resulted in recession of β in the β +γ alloy. In real coating/superalloy systems, interdiffusion also results in recession of β in the coating. The γ alloys used in Nesbitt's study (19) were compositionally similar in Ni, Cr, and Al compositions to Ni-base superalloys. The γ+γ' Ni-Cr-Al alloys used in this study were structurally similar to Ni-base superalloys. The fact that Nesbitt's study (19) showed results similar to real coating/superalloy systems and this study did not leads to an important conclusion: In trying to model interdiffusion in real coating/superalloy systems using coating/Ni-Cr-Al substrates, the compositional similarity between Ni-Cr-Al alloys and superalloys is much more important than the structural similarity. The results of Nesbitt's study have since been verified by Pilsner with a real coating/superalloy system (44).

The fact that Nesbitt's (19) and Pilsner's (44) work have shown that interdiffusion in real coating/superalloy systems can be modeled with compositionally similar γ Ni-Cr-Al substrates gives this study some important implications. It logically makes sense by analogy to Nesbitt's study that, if the Al composition in superalloys was raised to the Al composition used in the γ+γ' alloys of this study, the β+γ/γ+γ' interdiffusion behavior seen in this study would occur in the real system. If this did happen, interdiffusion would not be detrimental, but

but beneficial because growth of the coating into the substrate would result. Thus the Al that diffused from the coating into the substrate would not be lost (thereby decreasing the life of the coating), but in fact would contribute to increasing the life of the coating (by growing more coating). The results of this work could then be used to understand the interdiffusion phenomena. This analogy, however, is very simplistic and could only be proven with experimentation. It does though lead to some very exciting implications, and should be pursued in greater detail.

Conclusions

1. The β+γ alloy composition, and in particular the γ-phase Cr composition in the β+γ alloy, determine whether a β+γ or γ layer will result from interdiffusion.

   a. The growth of the β+γ layer is a result of a strong negative bulk Cr gradient forcing bulk flow of Al up its gradient. The ability to generate these gradients is directly related to maximum Cr and Al fluxes in the γ-phase.

   b. Growth of the layers requires Cr and Al to be supplied by the β and γ phases. The Cr is supplied primarily by the γ-phase and the Al is supplied primarily by the β-phase. In supplying Al, the β-phase dissolves, and thus reductions in the volume fraction of β occur in the β+γ alloy.

2. The γ+γ' alloy composition determines how the diffusion path proceeds through the β+γ+γ' triangle.

   a. As the γ+γ' alloy Cr composition decreases, the diffusion path translates up the γ+γ' side toward the γ' corner. When the path reaches the γ' corner a γ' layer forms in the diffusion zone. The critical Cr composition of the γ+γ' alloy for γ' layer formation to occur has been determined to be slightly less than 6.0 at.% Cr.

   b. For β+γ alloys in which a β+γ layer resulted from interdiffusion, as the Cr composition in the γ+γ' alloy decreased, the volume fraction of β in the β+γ growth layer increased. This increase in β volume fraction caused the diffusion paths to translate up the β+γ side of the β+γ+γ' triangle to higher Al composition.

3. In general, as the Cr composition of the β+γ alloy increases (per fixed γ+γ' alloy composition) the amount of β+γ growth increases. As the Cr composition in the γ+γ' alloy decreases (per fixed β+γ alloy composition), the amount of β+γ or γ growth

decreases and the amount of γ' growth increases.

Comparing the results of this study to the results of Nesbitt's study (19) using γ Ni-Cr-Al alloys as substrates, it can be concluded that:

1. Interdiffusion in real coating/superalloy systems is accurately simulated with coating/γ Ni-Cr-Al substrates. Thus, in trying to model interdiffusion in real coating/superalloy systems using coating/Ni-Cr-Al substrates, the compositional similarity between superalloys and γ Ni-Cr-Al substrates is more important than the structural similarity between superalloys and $\gamma+\gamma'$ Ni-Cr-Al substrates.

REFERENCES

1. P. Lane, Jr. and N. M. Geyer, J. Metals, 18, 186 (1966).

2. G. W. Goward, D. H. Boone, and C. S. Giggins, Trans. ASM, 60, 228 (1967).

3. G. W. Goward, Source Book for Elevated Temperature Applications, pp. 369-386, ASM, 1979.

4. W. K. Halnan and D. Lee, High Temperature Protective Coatings, S. C. Singhal, Editor, AIME, p. 3, 1982.

5. M. Nakamori, Y. Harada, and I. Hukua, High Temperature Protective Coatings, S. C. Singhal, Editor, AIME, P. 175, 1982.

6. C. J. Spengler, S. T. Scheirer, and D. C. Barksdale, High Temperature Protective Coatings, S. C. Singhal, Editor, AIME, p. 189, 1982.

7. G. W. Goward, J. Metals, 22, 31 (1970).

8. S. R. Levine, Met. Trans., 9A, 1237 (1978).

9. F. S. Pettit and G. W. Goward, Metallurgical Treatises, J. K. Tien and J. F. Elliott, Editors, AIME, p. 603, 1981.

10. S. J. Grisaffe, The Superalloys, John Wiley and Sons, New York, p. 341, 1972.

11. J. A. Nesbitt and R. W. Heckel, High Temperature Protective Coatings, S. C. Singhal, Editor, TMS-AIME, p. 76, 1982.

12. C. A. Barrett and C. E. Lowell, Oxidation of Metals, 11, 200 (1977).

13. R. G. Ubank, Rev. Int. Htes. Temp. et Retract. 14, 21 (1977).

14. G. W. Goward, High Temperature Corrosion, R. A. Rapp, Editor, NACE, p. 556, 1983.

15. R. F. Decker, "Strengthening Mechanisms in Nickel-base Superalloys," Climax Molybdenum Company Symposium, Zurich, Switzerland, p. 3, (1969).

16. R. F. Decker and C. T. Sims, The Superalloys, John Wiley and Sons, New York, p. 36, 1972.

17. P. Kofstad, High Temperature Oxidation of Metals, John Wiley and Sons, New York, pp. 112-146, 1966.

18. J. A. Nesbitt, "Solute Transport During Cyclic Oxidation of Ni-Cr-Al Alloys," M.S. Thesis, Michigan Technological University, Houghton, MI, 1981, (also available as NASA Contractor Report No. 165544, May 1982).

19. J. A. Nesbitt, "Overlay Coating Degradation by Simultaneous Oxidation and Coating/Substrate Interdiffusion," Ph.D. Dissertation, Michigan Technological University, Houghton, MI, 1983.

20. R. A. Mulford and D. P. Pope, Acta. Metall., 21, p. 1375, (1973).

21 P. K. Footnear and B. P. Richards, J. Materials Science, 17, p. 2141, (1982).

22. R. A. Ricks, A. J. Porter, and R. C. Ecob, Acta. Metall., 31, p. 43, (1983).

23. R. W. Guard, J. H. Westbrook, Trans. AIME, 215, p. 807, (1959).

24. C. Lall, S. Chin, and D. P. Pope, Met. Trans., 10A, p. 1323, (1979).

25. S. Chakravortz, D.R.F. West, Metals Tech., p. 414, (Oct. 1980).

26. A. Baldan, D.R.F. West, J. Materials Science, 16, p. 24, (1981).

27. B. Reppich, Acta. Metall., 30, p. 87, (1982).

28. D. H. Maxwell, J. F. Baldwin, and J. F. Radavich. Metallurgia and Metal Forming, p. 333, (Oct. 1975).

29. A. D. Smigelskas and E. O. Kirkendall, Trans. AIME, 171, p. 130, (1974).

30. B. D. Cullity, Elements of X-Ray Diffraction, Addison-Wesley Publishing Co., pp. 506-507, 1978.

31. <u>Metals Handbook</u>, ASM, 8th Edition, 8, p. 288, 1973.

32. <u>Metals Handbook</u>, ASM, 8th Edition, 1, p. 342, 1972.

33. A. Smigelskas and E. Kirkendall, Trans. AIME, <u>171</u>, 130 (1947).

34. L. Onsager, Phys. Rev., <u>37</u>, 405, (1931).

35. L. Onsager, Phys. Rev., <u>38</u>, 2265, (1931).

36. L. Onsager, Ann. N.Y. Acd. Sci., <u>46</u>, 241, (1945-6).

37. J. S. Kirkaldy, Can. J. Phys. <u>35</u>, 435, (1957)

38. A. S. Norkiewicz and J. I. Goldstein, Met. Trans., <u>6A</u>, 891, (1975).

39. D. Tu, "Diffusion and Pack Aluminizing Study in the Ni-Cr-Al System," Ph.D. Dissertation, SUNY, Stoney Brook, NY, 1982.

40. M.M.P. Janssen, Met. Trans., <u>4</u>, 1623, (1973).

41 A. J. Hickl and R. W. Heckel, Met. Trans., <u>6A</u>, 431, (1975).

42. IMSL Library Reference Manual, Chapter I, Vol. 2, 9th Edition, IMSL, Inc., 1982.

43. M L. James, G. M. Smith, and J. C. Wolford, <u>Analog and Digital Computer Methods</u>, International Textbook Co., Scranton, pp. 323-7, 1964.

44. B. H. Pilsner, "The Effects of Substrate Composition (MAR-M247) on Coating Oxidation and Coating/Substrate Interdiffusion," M.S. Thesis, Michigan Technological University, Houghton, MI, 1984.

APPENDIX A

Bulk Composition Analysis

The Ni, Cr, and Al bulk compositions in all the alloys used in this study were determined by use of a scanning electron microscope (SEM), an energy dispersive X-ray spectrometer (EDS), and a ZAF numerical correction scheme. The SEM was a JEOL model 35C operated at an accelerating voltage of 20 KeV and a beam current of approximately $1 \cdot 10^{-9}$ amperes. The EDS system consisted of an EDAX Si(Li) counting system coupled to a 711 series multichannel analyzer. The EDS system was connected to a Texas Instrument 733 ASR high speed data terminal interfaced to a Data General NOVA2 mini-computer. The mini-computer contained both stripping routines and various correctional schemes.

The correction scheme used in this study to obtain quantative bulk compositions was the well established ZAF method (1). The ZAF method corrects measured realitive X-ray intensity data for three primary sources of interference between elements in the alloy. These three sources of interference are:

1. An atomic number effect (Z), which occurs because an element scatters and retards incident electrons differently in an alloy as opposed to the pure state.

2. Absorption (A) of characteristic X-rays of one element by the other elements in the alloy.

3. Fluorescence (F) of X-rays generated by an element as it absorbs primary X-rays generated by other elements.

Equations for these interference phenomena are well developed (1-2). In general, the composition of element i can be represented by:

$$C_i = (ZAF)_i K_i \qquad (1)$$

where:

C_i = composition of element i in the alloy

Z = atomic number correction

A = absorption correction

F = Fluorescence correction

K_i = Ratio of the measured X-ray intensity of element i in the alloy to the measured X-ray intensity of pure element i (often referred to as "K-ratio").

Considering the Ni-rich portion of the Ni-Cr-Al system used in this study, the interference effects and the corresponding corrections will be larger for Al concentration predictions then for Cr and Ni concentration predictions. This can be seen by examining the critical parameters in each correction term.

The atomic number correction (Z) is critically dependent upon the average atomic number of the alloy. If there is a difference between average atomic number of the alloy and that of the pure element, than a correction is required. In this study, the average atomic numbers of the alloys ranged from 23.58 to 25.6. Comparing these numbers to the atomic numbers of Al(Z=13), Cr(Z=24), and Ni(Z=28) shows that Al has the largest difference. Thus, Al will have the largest Z

correction, with Cr having a Z correction of almost 1.

The three major variables affecting the absorption correction (A) are the operating voltage, the take off angle (angle at which X-rays emerge from the sample), and the mass absorption coefficient. Absorption is minimized as the operating voltage is decreased, the take off angle is increased, or the mass absorption coefficient is decreased. Because the operating voltage and take off angle are fixed, the magnitude of the absorption correction can be determined from the mass absorption coefficients. In this study, the mass absorption coefficients ranged from 2370-2718 cm^2/g for Al, 0-141 cm^2/g for Cr, and 61-113 cm^2/g for Ni. By far, Al has the largest mass absorption coefficients, and thus will have the largest absorption correction.

Fluorescence occurs when the energy of a characteristic X-ray peak from one element in the alloy is greater than the critical excitation energy for emission of a characteristic X-ray from another element in the alloy. A fluorescence correction (F) is necessary because more X-rays are generated from the fluoresced element than would have been produced by electron excitation alone. The critical excitation voltages for K_α X-ray generation for Ni, Cr, and Al are 8.33, 5.99, and 1.56 KV respectively. Thus, Al will be fluoresced by Cr and Ni, and will have the largest fluorescence correction.

In this study it was found that the Z, A, and F corrections for Cr and Ni were small, or very near 1. The Z and F

corrections for Al were small, but the A correction was quite large - many times double the Z and F correction.

Each correction term, Z, A, and F, is a function of the composition of the element i in the alloy (i.e., Z, A, F = $f(C_i)$). Thus, compositions obtained from Eqn. (1) involve iteration. The general sequence of events involved in obtaining compositions with the ZAF method are as follows:

1. Use the K-ratio to estimate a composition for the Z, A, and F correction terms.

2. Calculate the composition using Eqn. (1).

3. Repeat until convergence is achieved.

Many modifications of the basic ZAF correction scheme have been incorporated into computer programs and are commercially available. The ZAF correction scheme used to obtain bulk compositions in this study was a modified version of the computer program designated FRAME (3-4). Input into the program consisted of the K ratios for each element in the alloy, the characteristic X-ray line measured (K_α in this study), the operating voltage, and the angles between the incident electron beam, sample surface, and EDS collector.

To obtain bulk compositions the SEM was operated in a scan mode. Using unetched samples, a magnification of 500X was found to be sufficient to obtain a representative area of the microstructure. The spectrum generated by a given sample was measured through

400,000 counts. The spectrum was then entered into the mini-computer where the characteristics peaks of Ni, Cr, and Al were stripped from the continuous spectrum. The stripped K_α peaks were converted into K-ratios which were then used as input into the ZAF correction program as previously described. Output of the program consisted of a listing of the weight fractions for each element. In all cases, the sum of the weight fractions of Ni, Cr, and Al was in the range 0.95-1.00.

REFERENCES

1. J. I. Goldstein, D. E. Newbury, P. Echlin, D. C. Joy,
    C. Fiori, E. Lifshin, <u>Scanning Electron Microscopy
    and X-Ray Microanalysis</u>, Plenum Press, N.Y.,
    Chapter 7, 1981.

2. K.F.J. Heinrich, <u>Electron Beam X-Ray Microanalysis</u>,
    Van Nostrand and Reinhold Co., N.Y., 1981.

3. EDIT/EP Operators Manual, EDAX International, Inc.,
    Manual #80-00503-00, 1975.

4. J. I. Goldstein, H. Yakowitz, <u>Practical Scanning Elec-
    tron Microscopy</u>, Plenum Press, N.Y., Chapter 10,
    1975.

APPENDIX B

Phase Concentration Measurements

All β, γ, and γ' phase compositions and all concentration/distance profiles were determined by use of an electron microprobe (EM) and a subsequent ZAF correction scheme (ZAF). The electron microprobe was a Materials Analysis Co. model MAC400, operated at 15KV and 150 microamperes. The electron probe spot size was estimated (1) to be approximately 4-5μm. Two wavelength spectrometers were utilized to measure Cr and Al X-rays. The Cr X-rays were measured in a sealed detector with a LiF crystal while the Al X-rays were measured in a flowing P-N (90% Ar, 10% CH_4) gas detector with a TAP crystal. Cr and Al concentrations on γ, γ' and β alloys of known composition were measured to assess the accuracy of the EM/ZAF procedure.

Measurement Procedure

Measurements of standard compositions, phase compositions, and concentration/distance profiles involved collecting X-ray intensities for Cr and Al. The X-rays were counted for six ten second periods at each spot were a measurement was taken. At the start, finish, and at various intervals during the measurement procedure, the pure element (Cr and Al) X-ray intensities were measured. Again, six ten second counts were made. The sample current was measured at each time the pure

elements were measured using a Faraday cup on the sample
holder. The starting and finishing time, and the time at
which each spot was measured was also recorded. The aver-
aged pure element intensities at the start and finish, the
averaged measured intensities of the sample, and the time of
each, were input into a computer program (2) to correct for
background, instrument drift, and dead time. The corrected
intensities for the sample were divided by the corrected
pure element intensities to produce K ratios for Cr and Al.
The K ratios were then input into the ZAF correction program.

The ZAF correction program MULTI8 (3) was used to calcu-
late Cr and Al atomic fractions from the K ratios, giving
the Ni atomic fraction by difference. As previously dis-
cussed,[1] the MULTI8 program corrects for three primary sources
of interference between elements in the alloy. In addition
to the K ratios, parameters input into MULTI8 included: the
X-ray emergence angle, the atomic numbers and atomic weight
of the elements being measured, the operating KV, the exci-
tation potential and fluorescence yield of each element, and
the appropriate mass absorption coefficients (i.e. mass ab-
sorption coefficients for Al K_α X-rays in pure Al, pure Cr,
and pure Ni, etc.). The values of the fluorescence yield
of each element and the appropriate mass absorption coeffi-
cients used in the program are given elsewhere (2). Each
iteration of the MULTI8 program normalized the Ni, Cr, and

[1]See Appendix A - Bulk Composition Analysis.

Al concentrations to 100%, thereby including the effect of Ni on the ZAF correction of Cr and Al. Output of the MULTI8 program consisted of a listing of the weight and atomic fractions of Ni, Cr, and Al, and the position (distance) at which the measurement was taken.

The accuracy of the concentration measurements made in this study with the EM/ZAF procedure was determined by measuring Cr and Al concentrations on standards of known composition. The standards used, and the accuracy of the measurements is discussed below.

γ-Phase Standards

Seven high bulk Cr, low bulk Al (HCR-LAL) γ phase alloys used in an earlier study (2), and five low bulk Cr, high bulk Al (LCR-HAL) γ phase alloys prepared in this study, were used as γ phase standards. The alloys were prepared by repeated arc melting of pressed elemental powders, followed by an anneal of approximately 150 hours at 1250°C. The HCR-LAL alloy concentrations were determined by atomic absorption. The LCR-HAL alloy concentrations were determined by wet chemical analysis. Numerous microprobe measurements were taken on each standard. The measurements were averaged and compared to those obtained by atomic absorption and wet chemistry. Table B-1 compares the concentration measurements taken on the HCR-LAL γ standards to the concentrations obtained by atomic absorption. Table B-2 compares the concen-

TABLE B-1

Comparison of the Concentrations[1] of the γ-Phase Standards as Measured by Atomic Absorption and the EM/ZAF Procedure

Standard[2]	Atomic Absorption	EM/ZAF[3]	ΔC
S1	57.90 (+0.26)Ni		
	35.88 (+0.10)Cr	36.49 (+0.38)Cr	0.61
	6.22 (+0.36)Al	6.59 (+0.44)Al	0.37
S2	61.30 (+0.14)Ni		
	30.71 (+0.03)Cr	31.04 (+0.52)Cr	0.33
	7.94 (+0.24)Al	7.41 (+0.27)Al	0.53
S3	64.44 (+0.07)Ni		
	25.62 (+0.00)Cr	25.88 (+0.14)Cr	0.26
	9.94 (+0.14)Al	10.34 (+0.29)Al	0.40
S4	70.13 (+0.10)Ni		
	18.60 (+0.02)Cr	18.72 (+0.16)Cr	0.12
	11.26 (+0.26)Al	10.98 (+0.20)Al	0.28
S5	69.19 (+0.15)Ni		
	25.82 (+0.05)Cr	26.22 (+0.24)Cr	0.40
	4.98 (+0.25)Al	5.48 (+0.32)Al	0.50
S6	76.03 (+0.03)Ni		
	19.23 (+0.00)Cr	19.66 (+0.27)Cr	0.43
	4.75 (+0.06)Al	5.08 (+0.30)Al	0.33
S7	86.93 (+0.13)Ni		
	7.71 (+0.02)Cr	8.10 (+0.17)Cr	0.36
	5.36 (+0.25)Al	5.23 (+0.19)Al	0.13

1. All concentrations in atomic percent

2. Standard designation used in Ref. (2)

3. Ni concentrations were determined by difference

TABLE B-2

Comparisons of the Concentrations[1] of the γ-Phase Standards
as Measured by Wet Chemistry and
the EM/ZAF Procedure

Standard	Wet Chemistry[2]	EM/ZAF	ΔC
G1	77.20 Ni		
	9.09 Cr	9.56 (+0.36)Cr	0.47
	13.71 Al	13.42 (+0.34)Al	0.29
G2	80.03 Ni		
	6.69 Cr	7.24 (+0.38)Cr	0.55
	13.29 Al	12.98 (+0.38)Al	0.31
G3	82.78 Ni		
	4.35 Cr	4.65 (+0.25)Cr	0.30
	12.87 Al	13.48 (+0.86)Al	0.61
G4	83.14 Ni		
	2.21 Cr	2.42 (+0.14)Cr	0.21
	14.65 Al	14.82 (+0.37)Al	0.17
G5	85.90 Ni		
	0.05 Cr	0.00 (+0.00)Cr	0.05
	14.05 Al	13.59 (+0.40)Al	0.46

1. All concentrations in atomic percent

2. No standard deviations were given

tration measurements taken on the LCR-HAL γ standards to the concentrations obtained by wet chemistry. As shown, the agreement between the EM/ZAF concentration measurements and the atomic absorption or wet chemistry measurements is good. For the HCR-LAL γ-phase standards, the maximum difference between the two measurements (i.e., ΔC) is approximately 0.5 at.% Al and 0.6 at.% Cr. For the LCR-HAL γ-phase standards, the maximum difference between the measurements is approximately 0.6 at.% Al and 0.5 at.% Cr. Considering the measurements made on both sets of γ-phase standards, the accuracy of the EM/ZAF procedure for the γ phase is estimated as being ±0.6 at.% Al and ±0.6 at.% Cr. These accuracies are near those found in a previous study (2) for the same EM/ZAF procedure and γ-phase standards.

γ'-Phase Standards

Three γ'-phase alloys were used as standards in this study. The alloys were prepared from pressed elemental powders followed by an anneal of greater than 400 hours at 1200°C. The alloy concentrations were analyzed by wet chemical analysis. Table B-3 compares the concentration measurements taken on the γ'-phase standards to the concentration measurements obtained by wet chemistry. As shown, the agreement between the EM/ZAF procedure and the wet chemical analysis is good. The maximum difference between the measurements is approximately 0.30 at.% Al and 0.5 at.% Cr. Thus, the accuracy of the γ'-phase measurements made in this study can be estimated as ±0.3 at.% Al and ±0.5 at.% Cr.

TABLE B-3

Comparisons of the Concentrations[1] of γ'-Phase and β-Phase Standards as Measured by Wet Chemistry and the EM/ZAF Procedure

γ' Standard	Wet Chemistry[2]	EM/ZAF	ΔC
GP1	75.34 Ni		
	4.19 Cr	4.71 (±0.21) Cr	0.52
	20.46 Al	20.17 (±0.41) Al	0.29
GP2	77.20 Ni		
	2.10 Cr	2.52 (±0.21) Cr	0.46
	20.70 Al	20.57 (±0.21) Al	0.13
GP3	78.08 Ni		
	0.05 Cr	0.00 (+0.00) Cr	0.05
	21.87 Al	21.55 (±0.26) Al	0.32

β Standard			
B1	50.20 Ni		
	0.00 Cr	0.00 (+0.00) Cr	0.00
	49.80 Al	48.98 (±1.8) Al	0.82

1. All concentrations in atomic percent

2. No standard deviations were given

β-Phase Standard

One NiAl β phase alloy was used as a standard in this study. An attempt was made to make β phase alloys containing Cr but success was limited. The alloys that were made suffered oxidation down cracks in the sample buttons during annealing. The cracks formed in the hard, brittle phase during cooling in the arc melter. Many of the alloys (even <2 at.% Cr) contained Cr segregations that could not be eliminated by a high temperature anneal. In view of these problems, and the problems encountered with β-phase alloys in an earlier study (2), only the NiAl alloy was used as a standard. The NiAl alloy was supplied in the as-cast condition (4) and had to be encapsulated in quartz tubing, evacuated, and annealed at 1200°C for 6 hours. The short annealing time was used to avoid excessive oxidation of the extremely small sample. Table B-3 compares the concentration measurement obtained by wet chemistry. As shown, the difference between the measurements is only 0.82 at.% Al but this is somewhat misleading. The standard deviation of the EM/ZAF measurements was approximately 2 at.% Al. This large standard deviation may be attributed to inhomogeniety of the β-phase standard. Considering the possible inhomogeniety of the β-phase standard, the accuracy of the β-phase Al concentration measurements made in this study is estimated as being ±1.0-2.0 at.% Al. Because no β-phase standards could be made that contained Cr, the accuracy of the β-phase Cr concentration measurements could not be assessed quantitatively. However, considering the accuracy of the γ and

γ' Cr concentration measurements, the Cr concentration measure-
ments in the β phase are probably of similar accuracy. Thus,
the β-phase Cr concentration measurements are estimated as being
within ± 0.6 at.% Cr.

REFERENCES

1. D. C. Joy, Scanning Electron Microscopy and X-Ray Micro-
    analysis Short Course, Lehigh University, Bethlehem,
    PA, June 13-17, 1983.

2. J. A. Nesbitt, "Overlay Coating Degradation by Simul-
    taneous Oxidation and Coating/Substrate Interdiffu-
    sion," Ph.D. Dissertation, Michigan Technological
    Unviersity, Houghton, MI, Appendix A, 1983.

3. K. E. Heinrich, R. L. Myklebust, H. Yakowitz, and S. D.
    Rasberry, "A Simple Correction Procedure for Quanti-
    tative Electron Probe Microanalysis," NBS Technical
    Note. 719, 1972.

4. Supplied by S. M. Merchant, Department of Metallurgy and
    Materials Eng., Lehigh University, Bethlehem, PA, 1983.

APPENDIX C

Partial NiCrAl Phase Diagram at 1200°C

In order to gain insight into the diffusional interaction between $\beta+\gamma/\gamma+\gamma'$ alloys, and to plot quantitative diffusion paths, the Ni-rich (50-100 at.% Ni) portion of the NiCrAl phase diagram at 1200°C was determined. The $\beta+\gamma+\alpha$, $\beta+\gamma$, $\beta+\gamma+\gamma'$, and $\beta+\gamma'$ phase fields were quantitatively determined by electron microprobe analysis using homogenized alloys and diffusion couples. Table C-1 lists the alloys used to determine the phase fields. Figure C-1 shows the partial NiCrAl phase diagram (1200°C) determined from these alloys. The method used to determine each phase field (i.e., homogenized alloy and/or diffusion couple) will be discussed later. The accuracy of the measurements was discussed in Appendix B.

All alloys used in this study were prepared from pressed elemental powders, followed by argon arc melting on a water-cooled copper hearth.[1] After melting, the alloys were annealed at temperatures at or greater than, 1200°C for times greater than 300 hours to obtain homogeneous microstructures. Determination of homogeneity was made using the electron microprobe and is discussed below.

Determination of Homogeneity

The production of X-rays from a section of alloy inci-

---

[1]See Experimental Procedure for more information.

TABLE C-1

Alloys Used to Determine the Partial NiCrAl
Phase Diagram at 1200°C

Alloy Designation	Alloy Composition[1]		Phases Present[3,4]
	Nominal	Bulk EDAX[2]	
β+γ+α Phase Field			
1	Ni-30.0Cr-21.25Al	Ni-30.0Cr-20.8Al	β+γ+α
β+γ Phase Field			
4	Ni-14.4Cr-26.4Al	Ni-14.8Cr-25.2Al	β+γ
5	Ni-9.6Cr-26.9Al	Ni-10.8Cr-25.7Al	β+γ
C1	Ni-19.8Cr-24.7Al	Ni-20.0Cr-24.1Al	β+γ
C2	Ni-14.9Cr-24.7Al	Ni-15.3Cr-23.9Al	β+γ
C3	Ni-14.9Cr-20.8Al	Ni-15.1Cr-20.3Al	β+γ
C4	Ni-26.0Cr-16.9Al	Ni-26.4Cr-17.1Al	β+γ
β+γ+γ' Phase Field			
14	Ni-7.5Cr-24.1Al	Ni-8.2Cr-22.9Al	β+γ+γ'
β+γ' Phase Field			
6	Ni-4.8Cr-29.0Al	Ni-5.0Cr-27.3Al	β+γ'
7	Ni-2.4Cr-30.7Al	Ni-2.7Cr-29.0Al	β+γ'
8	Ni-0.91Cr-32.4Al	Ni-0.85Cr-31.8Al	β+γ'
9	Ni-33.5Al	Ni-31.8Al	β+γ'
γ' Phase Field			
GP1	Ni-4.7Cr-22.1Al	Ni-4.9Cr-19.4Al	γ'
GP2	Ni-2.4Cr-22.5Al	Ni-2.2Cr-20.8Al	γ'
GP3	Ni-23.7Al	Ni-21.4Al	γ'

TABLE C-1 (Continued)

Alloy Designation	Alloy Composition		Phases Present
	Nominal	Bulk EDAX	
$\gamma+\gamma'$ Phase Field			
S1	Ni-2.4Cr-18.1Al	Ni-7.4Cr-17.1Al	$\gamma+\gamma'$
S2	Ni-3.7Cr-18.1Al	Ni-3.5Cr-17.0Al	$\gamma+\gamma'$
S3	Ni-18.1Al	Ni-16.5Al	γ
S4	Ni-10.0Cr-16.3Al	--[5]	γ
S5	Ni-6.0Cr-17.8Al	--	$\gamma+\gamma'$

1. All compositions in atomic percent

2. See Appendix A - Bulk Composition Analysis for details

3. At 1200°C

4. All alloys containing β except 8 and 9 contained Cr segregations in the β of not greater than 3.0 vol %

5. EDAX system not available

NiCrAl Phase Diagram 1200C

Figure C-1. Partial NiCrAl phase diagram at 1200°C.

dent to an electron beam is statistical in nature (1). The number of X-rays which interact with X-ray detectors is completely random in time, but has a fixed mean value. The distribution of the number of determinations of X-ray counts from one spot on an alloy vs. the number of X-ray counts for a fixed time interval may be approximated by a normal (Guassian) probability distribution (1-3). The normal probability distribution for X-ray emission, shown in Figure C-2, is described by the normal density function (4, 5):

$$f(X,\mu,\sigma) = \frac{1}{\sigma\sqrt{2\pi}} e^{-\frac{1}{2}(\frac{X-\mu}{\sigma})^2} \qquad -\infty \leq X \leq \infty \qquad (1)$$

where X is a measureable random variable (in this case, X-ray counts), μ is the true mean of random variable X, and σ is the error associated with measuring random variable X (standard deviation). Figure C-2 shows that for an infinite number of determinations of X-ray counts from one spot on an alloy, the most frequent (probable) X-ray count measured will have a value equal to μ. The ideal standard deviation ($\sigma=\mu^{\frac{1}{2}}$) results from fluctuations that cannot be eliminated as long as quanta are counted (1).

Considering a homogeneous alloy or phase, assuming ideal conditions (e.g. no drift of electronic components, exact refocusing at each spot, etc.) and an infinite number of X-ray count determinations per spot, a set of X-ray counts measured at a given spot should have a mean value equal to μ. Thus, in assessing whether an alloy is homogeneous or not, all that
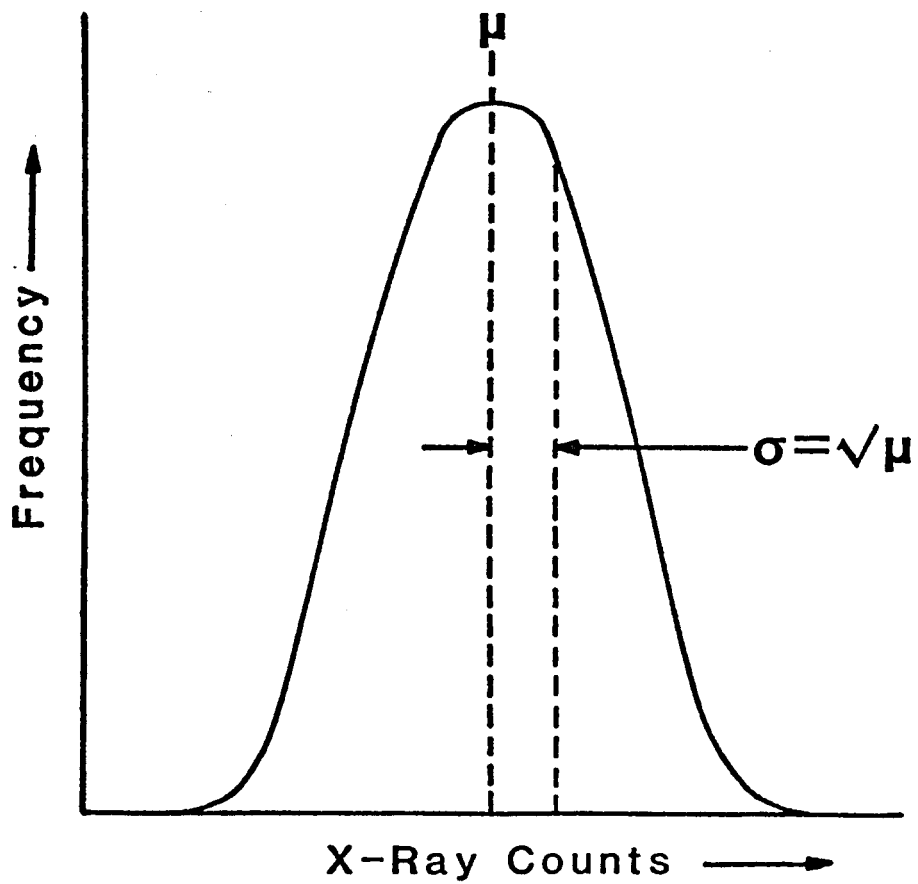
Figure C-2. Frequency of obtaining a X-ray count vs. X-ray counts.

need be done is determine if the average value of X-ray counts

per spot, is the same for each spot (i.e. every spot measured

should have an average of X-ray counts equal to μ). This

task would be simple if conditions were ideal and an infinite

number of determinations of X-ray counts per spot could be

made. In reality, however, conditions are not ideal and only

finite determinations of X-ray counts per spot can be made.

Each set of X-ray counts measured at a given spot will have

a different mean value because of the finite nature of the

sample (4). To determine if the mean values are representa-

tive of the true mean of the alloy, μ, assuming it is homo-

geneous, statistics must be used. Using null hypothesis tests

(4, 5), it can be determined for all spots measured if the

mean values of X-ray counts are significantly like or signifi-

cantly different from μ, even though μ is not known. If the

mean values do not meet these specific tests, the alloy or

phase can be rejected as not being homogeneous. Therefore,

in estimating homogeneity, it must be determined if the mean

value of X-ray counts per spot, for all spots, fall within

specific limits, or confidence levels.

To obtain estimates of the level of homogeneity (%), cer-

tain limits or confidence levels must be established. A sim-

plified criterion that has been used to estimate homogeneity

(1) utilizes two parameters: 1. The mean value of the X-ray

counts measured at a given spot j, $\overline{X}_j$, given by:

$$\overline{X}_j = (\sum_{i=1}^{n} X_i)/n \tag{2}$$

and 2. The mean value of the $\bar{X}_j$'s, $\bar{X}$, given by:

$$\bar{X} = (\sum_{j=1}^{N} \bar{X}_j)/N \tag{3}$$

where X_i = the number of X-ray counts taken at spot j.

n = the total number of determinations of X-ray counts taken at spot j.

N = the total number of spots measured.

The criterion states that all the $\bar{X}_j$'s must fall within $\bar{X} \pm 3\bar{X}^{\frac{1}{2}}$ limits for an alloy or phase to be considered homogeneous (1). This limit is derived from the fact that 99.7% of the area under a normal distribution is contained in $\bar{X} \pm 3\bar{X}^{\frac{1}{2}}$ limits. Therefore, if an $\bar{X}_j$ does not fall within this limit, it is safe to assume it is significantly different from the true mean of the alloy μ, had the alloy been homogeneous. Using this criterion the variation of the element of interest in the alloy or phase, or the level of homogeneity, is given by (1):

$$(\pm 3\bar{X}^{\frac{1}{2}}/\bar{X}) \; 100 \qquad (\%) \tag{4}$$

A more rigorous determination of the level of homogeneity involves the use of the standard deviation, S, of the $\bar{X}_j$'s, given by:

$$S = \left[\sum_{j=1}^{N} \frac{(\bar{X}_j - \bar{X})^2}{N=1} \right]^{\frac{1}{2}} \tag{5}$$

and the degree of statistical confidence used in the determi-

nation of $\overline{X}$ (1). By utilizing the standard deviation, S, possible errors arising from instrument drift, X-ray focusing errors, and X-ray production variability is included in the analysis. The degree of confidence in the determination of $\overline{X}$ simply reflects an attempt to avoid a risk, α, of rejecting a good result (i.e. a $\overline{X}_j$ representative of μ) a large percentage (say 95-100%) of the time. The degree of confidence is given by $1-\alpha$ and high degrees of confidence have typical values 0.95-0.995. The use of a degree of confidence allow a range of homogeneity to be defined in which it can be expected that only a small number of measurements will be outside this range (1). The level of homogeneity for a confidence level of $1-\alpha$, is given by (1):

$$\pm \frac{W_{1-\alpha}}{C} = \pm \frac{(t_{N-1}^{1-\alpha})\ S(100)}{N^{\frac{1}{2}},\ \overline{X}} \quad (\%) \tag{6}$$

where $W_{1-\alpha}$ is the range of homogeneity (wt.%), C is the true weight fraction of the element of interest, and $t_{N-1}^{1-\alpha}$ is the Student t Statistic (4, 5) for a $1-\alpha$ confidence level and N-1 degrees of freedom. Student t values for various levels of confidence and degrees of freedom can be found in tabulated form in many probability books (4, 5).

Calculations of the level of homogeneity (L.H.) for Cr and Al in each phase were performed on the alloys used for phase diagram determination and diffusion couples. Before L.H. was calculated, the X-ray count averages, $\overline{X}_j$'s, were checked to be within the limits $\overline{X} \pm 3\overline{X}^{\frac{1}{2}}$. If all the $\overline{X}_j$'s were

within these limits, Eqn. (6) was used to calculate L.H.
The highest tabulated degree of confidence, $1-\alpha = 0.995$, was
used for finding the Student t statistic in Eqn. (6). A L.H.
of $\leq \pm 1.0\%$ was set as being the maximum deviation for which
the alloys would be considered homogeneous (1). Counts were
measured at 10-25 different areas (random selection) of the
same phase, with 1-5 spots determined per phase area. Calcu-
lated L.H. for Cr and Al in the phases present in the alloy,
and the time and temperature at which the alloys were annealed,
is shown in Table C-2. As shown, almost all the L.H. were
below $\pm 1.0\%$. The L.H. for Al in the γ phase for most of the
alloys containing β was slightly greater than 1.0%. This oc-
curs because the concentration of Al in the γ phase is low
(~9-14 at.%). The low concentration leads to low X-ray count
averages. It is more difficult to measure the same L.H. as
the concentration present in the alloy decreases (1). The
value of $S/\overline{X}$ in Eqn. (6) will increase as C and the number of
X-ray counts per spot $(\overline{X}_j)$ decreases. To obtain the same num-
ber of X-ray counts per spot, the time of analysis must be
increased. The analysis time per spot in this study was fixed.
Therefore, more spots should have been taken on the elements
with low concentrations to obtain a lower L.H. However, to
obtain a L.H. of 0.5 for Al in the γ phase of the alloys con-
taining β, N must be greater than 160 (i.e. 160 separate spots
in the γ phase must be analyzed). The length of time to do
this would have been phenomenal, and therefore, the same

TABLE C-2

Calculated Levels of Homogeneity for Alloys Used to Determine the Partial NiCrAl Phase Diagram at 1200°C

Alloy Designation	Time (hr)/ Temperature (°C)	Phase	$L.H.^1 = \pm \dfrac{(t_{N-1}^{0.995})S(100)}{N^{\frac{1}{2}}\bar{X}}$ (%)	
			Cr	Al
1	350/1200	β	0.68	0.30
		γ	0.13	1.10
		α	0.33	3.90
4	350/1200	β	0.44	0.29
		γ	0.22	0.99
5	350/1200	β	0.72	0.51
		γ	0.45	1.08
C1	150/1250	β	0.72	0.52
	200/1200	γ	0.25	1.10
C2	150/1250	β	0.86	0.58
	200/1200	γ	0.24	1.18
C3	150/1250	β	0.72	0.43
	200/1200	γ	0.33	0.73
C4	150/1250	β	0.44	0.55
	200/1200	γ	0.47	0.68
6	400/1200	β	0.63	0.38
		γ	0.56	0.59
7	400/1200	β	1.03	0.41
		γ'	1.04	0.71
8	400/1200	β	1.41	0.51
		γ'	1.80	0.44
9	400/1200	β	--[2]	0.53
		γ'	--	0.74
14[3]	400/1200	β	0.75	0.47

TABLE C-2 (Continued)

Alloy Designation	Time (hr)/ Temperature (°C)	Phase	$L.H.=\pm\dfrac{(t_{N-1}^{0.995})S(100)}{N^{\frac{1}{2}}\bar{X}}$ (%)	
			Cr	Al
GP1	450/1200	γ'	0.61	0.52
GP2	450/1200	γ'	1.06	0.48
GP3	450/1200	γ'	--	0.54
S3	50/1250 100/1200	γ	--	0.69

1. L.H. = Level of Homogeneity

2. All dashes indicate Ni-Al alloys, therefore, no L.H. was calculated for Cr

3. γ and γ' could not be distinguished with unetched sample

number of spots per phase was measured. Typically, as the ......

L.H. for an element goes above ±1.0%, the concentration in

the phase drops below 10 at.%. The L.H. of 3.9 for Al in the

α phase of alloy 1 simply reflects the fact that approximately

1-2 at.% Al is contained in that phase. Likewise, some of the

high L.H. for Cr in the γ' phase of the β+γ' and γ' alloys

reflects a Cr concentration below 5 at.% Cr. When the L.H.

was above 1.0% for one element, the other element L.H. was

sufficiently below 1.0% to indicate the phase was homogeneous.

Although calculations of L.H. revealed the alloys were

homogeneous, other independent checks of homogeneity were

performed. Concentration scans were run between phases to

determine if any concentration gradients existed between

phases. In all cases, the scans revealed a step-like concen-

tration profile, signifying no concentration gradients be-

tween phases. L.H. were recalculated for β+γ alloys used in

diffusion couples. Spots were measured after 200 hours at

1200°C in the bulk section of the alloy, well removed from

the diffusion zone. In all cases, the L.H. did not signifi-

cantly change from the value listed in Table C-2. In view

of the L.H. calcualtions and the checks, it was concluded

that the alloys were indeed homogeneous under the analytical

measuring sensitivity of the electron microprobe.

Cr Segregations

All alloys containing β, listed in Table C-1, except

alloys 8 and 9 were found to contain segregations of Cr in, or

adjacent to, the β phase. A survey of the available litera-
ture on studies involving the Ni-Cr-Al system showed, in each
case, similar occurrences of Cr segregation in the β (6-12).
In these studies, the Cr segregations were identified as being
the α(Cr) phase because they had high concentrations of Cr
and low concentrations of Ni and Al. No work has been done
to quantitatively determine if these segregations are indeed
α(Cr).

The identification of the Cr segregations (also referred
to as "particles") as α(Cr) creates a series of anomalies
that cannot be explained by the phase diagram. Observations
of the Cr segregations in the alloys used in this study, and
the anomalies associated with their presence are presented
below:

1. As cast, no Cr segregations could be detected opti-
    cally or under high magnification (1000X-2000X) with
    a scanning electron microscope for all alloys in
    which β crystallized from the melt except the three
    phase alloy $\beta + \gamma + \alpha$ (alloy 1). If the Cr segre-
    gations are present as cast, they must be sub-micron
    in size, and would only be detected by transmission
    electron microscopy.

2. After heat treatment at high temperature (T$\geq$1200°C)
    all alloys containing β (except alloys 8 and 9) con-
    tained Cr segregations. The segregations could be
    seen after very short annealing times (t<24 hours
    at temperature). Even after prolonged anneals
    (t>600 hrs.) at 1200°C, the Cr segregations per-
    sisted in the alloys. The segregations were mor-
    phologically similar in all alloys, with a blocky,
    faceted appearance. The size of the particles
    varied throughout a given alloy and were in the
    range of 1-10 μm. The volume fraction of the par-
    ticles varied from alloy to alloy and were in the
    range of 1-3 vol.%.

3. After long annealing times (t>300 hrs.), the Cr segrega-
    tions appeared to be in equilibrium with the surrounding
    matrix. Concentration/distance profiles measured from
    the middle of large particles to the middle of adjacent
    equilibrium phases (i.e. β, γ, γ', etc.) showed step-
    like concentration profiles - indicating negligible
    concentration gradients between particles and phases.
    The segregations did coarsen with time during the ini-
    tial heat treatments (i.e., at times less than 300 hrs.),
    but in all cases, the composition of the particles
    did not change.

4. Both three phase alloys, alloy 1 (β+γ+α) and alloy 14
    (β+γ+γ'), contained Cr segregations. The segregations
    in alloy 1, in the form of finely distributed particles
    in the β, were morphologically different from the α
    phase. The Cr segregations were blocky and faceted
    while the α phase was globular and of much larger size.
    The existence of 4 phases - β, γ, α and Cr segregations
    or β, γ, γ' and Cr segregations is a definite viola-
    tion of the Gibbs phase rule for a three component
    system.

5. The composition of Cr in the α phase in alloy 1 was
    different from the composition of Cr in the particles.
    The composition of the α phase was determined by elec-
    tron microprobe analysis to be approximately 84.0-86.0
    at.% Cr. The particles contained between 94.0-97.0
    at.% Cr.

6. The Cr segregations found in β+γ and β+γ' alloys is in
    violation of the Gibbs phase rule for a three compon-
    ent system. The alloys cannot be equilibrium three-
    phase alloys because the compositions of β and γ or β
    and γ' change as the bulk composition changes. Fur-
    thermore, the compositions of the γ phase in all
    equilibrated alloys was found to correspond exactly
    to the γ/γ+β phase boundary determined by Nesbitt
    (12, 13) using diffusion couples and β+γ alloys oxi-
    dized at 1200°C. Thus, independent methods of bound-
    ary determination, with and without Cr segregations,
    have yielded the same phase boundary. This means the
    Cr segregations do not appear to effect the equilibrium
    between phases in the two-phase fields.

7. Cr segregations were found in larger volume fraction
    in some of the lower bulk Cr β+γ alloys than in larger
    bulk Cr β+γ alloys. If the segregations were α(Cr),
    this observation makes no sense because the high bulk

Cr alloys would be expected to have more α than the low bulk Cr alloys.

In view of these observations, and the anomalies associated with them, it appears that the identification of the Cr segregations as α(Cr) has been spurious. A possible alternate explanation of the Cr segregations is that they are a Cr carbide. The Ni powder used in making the alloys contained approximately 0.1 wt.% graphite which originated from the Ni powder fabrication process (14). Chemical analysis of three alloys (one β+γ alloy, one γ alloy, and one γ' alloy) showed carbon contents of 0.085, 0.034, and 0.035 wt.%. The higehst carbon content was found in the β+γ alloy. In comparison, the carbon contents found in cast Ni-base superalloys are normally in the range of 0.1 wt.% (15, 16), and lead to the formation of several types of carbides (15-20). No carbides were found to be present in a low carbon (0.01 wt.%) Ni-base superalloy (15). The typical carbides that have been observed in normal carbon (0.1%) containing superalloys are of four types: MC, $M_{23}C_6$, Cr_7C_3, and M_6C, where M represents a carbide forming element (e.g. Ta, Ti, W, Nb, Cr) or some combinaticn of these elements (15). Out of these carbide types, $M_{23}C_6$ is usually Cr rich (15, 17-20).

The fact that the alloys used in this study contained appreciable levels of carbon (comparable to the carbon levels in normal carbon containing Ni-base superalloys), along with the fact that Cr is a carbide former, does suggest the Cr

segregations may be carbides. An estimate of the driving force for Cr carbide formation can be made with thermodynamic data supplied by Worrell in an analysis of the Cr-C-O system (21). Table C-3 lists the Gibbs free energy of formation as a function of temperature for the compounds: Cr_2O_3 (s), $C_{23}C_6$ (s), Cr_8C_3 (s), and Cr_3C_2 (s). The free energy function for Cr_2O_3 was included so that the free energy values of the carbides could be compared to it. At 1200°C (1473 K) the free energies of formation for Cr_2O_3, $Cr_{23}C_6$, Cr_7C_3, and Cr_3C_2 are -180842, -164394, -67468, and -31645 cal/mole, respectively. As can be seen, the free energy of formation for $Cr_{23}C_6$ is very near that of Cr_2O_3. The other Cr carbides have appreciably lower free energies of formation. Although the free energy of formation calculated for each carbide gives no idea how favorable the kinetics of formation are, it does show there is a driving force for formation - especially $Cr_{23}C_6$.

If the Cr segregations are Cr carbide, many of the observations and anomalies previously presented can be explained. The fact that the segregations appear to precipitate only during high temperature heat treatments correlates with the finding that $M_{23}C_6$ carbides in Ni-base superalloys are products of solid-state precipitation (15, 18). The fact that the segregations appear to be in equilibrium with the surrounding matrix also supports carbide formation. The carbide, once formed, could exist in equilibrium with the sur-

TABLE C-3

Thermodynamic Data for Stable Compounds Occurring
in the Cr-C-O System[1]

Compound	Gibbs Free of Formation, cal per mole
Cr_2O_3 (S)	$-270,400 + 60.8T$
$Cr_{23}C_6$ (S)	$-139,500 - 16.9T$
Cr_7C_6 (S)	$-54,800 - 8.6T$
Cr_3C_2 (S)	$-29,500 - 3.9T$

1. Taken from Reference 21.

rounding phases, without upsetting the equilibrium between phases if the carbide were not present (i.e. the phase boundaries could be the same with, or without, the carbide present). If the segregations were a carbide, their appearance in three phase alloys would not be a violation of the Gibb's phase rule because the system would be 4 component (Ni-Cr-Al-C) and not 3 component (Ni-Cr-Al). Being a carbide would also explain why the segregations have a different Cr concentration than the equilibrium α(Cr) phase in the $\beta+\gamma+\alpha$ alloy. It would also explain why some of the low bulk Cr $\beta+\gamma$ alloys have larger volume fractions of Cr segregations than the high bulk Cr $\beta+\gamma$ alloys. The carbide formation would be a stronger function of the carbon concentration in the alloy than the Cr concentration, and thus the low bulk Cr alloys probably have higher carbon contents than the high bulk Cr alloys. The only observation that does not support the segregations being a carbide (or α(Cr)) is that they are found only in alloys containing the β phase. The $\gamma+\gamma'$ and γ alloys did not contain Cr segregations.

Effort was made in this study to try and identify whether the Cr segregations were α(Cr) or Cr carbide. Transmission electron microscopy was utilized in an effort to obtain a diffraction pattern of the particles. The effort was unsuccessful because no particles could be located. The difficulty in locating the particles stems from their small size, small volume fraction, and random orientation in the matrix.

Standard phase extraction techniques (15) were also employed
in an effort to dissolve away the matrix, leaving the par-
ticles (assuming they were carbides) as a residue. Diffrac-
tion patterns of the residue from phase extractions did not
yield any results. Time did not permit further analyses of
the Cr segregations. Studies should be initiated to specifi-
cally identify these particles.

Finally, because the $\gamma/\beta+\gamma$ phase boundary determined in
this study corresponds exactly to the $\gamma/\beta+\gamma$ phase boundary
determined by Nesbitt (12, 13) using alloys without Cr seg-
regations, it appears the segregations are not effecting the
equilibrium between phases (e.g. $\beta+\gamma$, $\beta+\gamma'$, etc.). In fur-
ther support of this, the boundaries determined in this study
correlate very well with the boundaries determined by Nesbitt
(12) and Taylor and Floyd (6) at 1150°C. In view of these
facts, it is concluded that the phase diagram determined in
this study is an accurate representation of the phase equili-
brium that exists in the Ni-Cr-Al system at 1200°C.

Phase Field Determination

Two standard techniques were used to determine the phase
fields of the partial NiCrAl phase diagram (Figure C-1) deter-
mined in this study: homogenized alloys and diffusion
couples (22). In most cases, homogenized alloys were util-
ized to obtain equilibrium tie lines. Diffusion couples were
used to determine some portions of the phase fields, and also

to check the boundaries determined by the homogenized alloys.
The alloys used to determine each phase field are listed in
Table C-1. The method used to determine each phase field is
discussed below.

1. $\beta+\gamma+\alpha$. Alloy 1 was used to determine the $\beta+\gamma+\alpha$ tri-
   angle. All phases were of sufficient size to allow
   accurate electron microprobe measurements. The com-
   position of the α phase, not shown in Figure C-1,
   was determined to be approximately 86.0 at.% Cr,
   1.5 at.% Al. The low solubility of Al in α is in
   accord with the findings of Taylor and Floyd (6) at
   1150°C and Tu (11) at 1025°C. The solubility of Ni
   in α correlated very well with the solubility of Ni
   in α at 1200°C in the binary Ni-Cr system (23).

2. $\beta+\gamma$. Six homogenized alloys (Table C-1) were
   used to determine the $\beta+\gamma$ phase field. The equi-
   librium tie lines shown in Figure C-1 correspond
   to the four alloys used in diffusion couples, namely:
   C1, C2, C3, and C4. The concentration/distance pro-
   file obtained from diffusion couples were also plotted
   on the phase diagram to check the boundaries deter-
   mined by the homogenized alloys. In all cases, the
   points fell along the boundaries determined by the
   homogenized alloys.

3. $\beta+\gamma+\gamma'$. Alloy 14 was used only to determine the β
   corner of the triangle. The γ and γ' phases in the
   alloy could not be distinguished unetched. Thus,
   the γ and γ' corners of the triangle had to be
   determined at three phase interfaces ($\beta+\gamma/\gamma+\gamma'$
   or $\beta+\gamma/\gamma'$) present in the diffusion couples. The
   β corner, determined with alloy 14, was found to be
   in excellent agreement with β phase measurements
   at three phase interphases. In view of this, it was
   concluded that the γ and γ' measurements made at
   three phase interfaces were also representative of
   the $\beta+\gamma+\gamma'$ equilibrium.

4. $\beta+\gamma'$. Four homogenized alloys (Table C-1) were used
   to determine the $\beta+\gamma'$ phase field. The tie lines
   corresponding to these alloys are shown in Figure C-1.
   The measured phase compositions of alloy 9 (Ni-31.8Al)
   corresponded exactly to those found in the $\beta+\gamma'$ phase
   field at 1200°C in the Ni-Al system.

5. $\gamma+\gamma'$. Microprobe measurements on homogenized $\gamma+\gamma'$ alloys could not be obtained because the γ and γ' phases could not be distinguished unetched, and the γ' was on the order of the probe spot size. The $\gamma'/\gamma+\gamma'$ boundary was determined with $\gamma'/\gamma+\gamma'$ interfaces present in diffusion couples, and binary Ni-Al data at 1200°C. The $\gamma/\gamma+\gamma'$ boundary was only estimated using the γ corner of the $\beta+\gamma+\gamma'$ triangle, binary Ni-Al data, the γ and $\gamma+\gamma'$ alloys listed in Table C-1, and the data of Taylor and Floyd (6) and Nesbitt (12) at 1150°C. It is therefore represented by a dashed line in Figure C-1.

REFERENCES

1. J. I. Goldstein, D. E. Newbury, P. Echlin, D. C. Joy, C. Fiori, E. Lifshin, _Scanning Electron Microscopy and X-Ray Microanalysis_, Plenum Press, N.Y., pp. 430-433, 1981.

2. H. A. Liebhafsky, H. G. Pfeiffer, and P. D. Zemany, Anal. Chem., 27, 1257, (1955).

3. H. A. Liebhafsky, H. G. Pfeiffer, E. H. Winslow, P. D. Zemany, and S. S. Liebhafsky, _X-Rays, Electrons and Analytical Chemistry_, Wiley Interscience, N.Y., 1972.

4. I. Miller, J. E. Freund, _Probability and Statistics for Engineers_, Prentice-Hall, Inc., New Jersey, 2nd Edition, 1977.

5. M. M. Eisen, C. A. Eisen, _Probability and its Applications_, Quantum Publishers, Inc., N.Y., 1975.

6. A. Taylor and R. W. Floyd, J. Inst. Metals, 81, 462, (1952).

7. G. W. Goward, D. H. Boone and C. S. Giggins, Trans. ASM, 60, 238, (1967).

8. H. W. Lavendel, J. Metals, 27, 4, (1975).

9. C. A. Barret and C. E. Lowell, Oxi. Metals, 11, 203, (1977).

10. S. R. Levine, Met. Trans., 9A, 1242, (1978).

11. D. Tu, "Diffusion and Pack Aluminizing Study in the Ni-Cr-Al System," Ph.D. Dissertation, SUNY, Stoney Brook, N.Y., 1982.

12. J. A. Nesbitt, "Overlay Coating Degradation by Simultaneous Oxidation and Coating/Substrate Interdiffusion," Ph.D. Dissertation, Michigan Technological University, Houghton, MI, 1983.

13. J. A. Nesbitt, "Solute Transport During Cyclic Oxidation of Ni-Cr-Al Alloys," M.S. Thesis, Michigan Technological University, Houghton, MI, 1981.

14. The International Nickel Company, Inc., INCO Nickel Powder Type 123, One New York Plaza, N.Y., N.Y., 10004.

15. H. C. Nguyen, "The Effect of Tantulum and Carbon on the Structure/Properties of a Single Crystal Nickel-Base Superalloy," M.S. Thesis, Michigan Technological University, Houghton, MI, 1984.

16. R. F. Decker, "Strengthening Mechanisms in Nickel-Base Superalloys," Climax Molybdenum company Symposium, Zurich, Switzerland, (1969).

17. M. A. Burke, J. Greggi, Jr., G. A. Whitlow, Scripta. Met., 18, 91, (1984).

18. B. J. Pearcey, and R. W. Smashey, Trans. AIME, 239, 451, (1967).

19. R. T. Holt and W. Wallace, In. Metals. Rev., Review 203, March 1976.

20. W. V. Youdelis and O. Kwon, Met. Sci., 17, 385, (1983).

21. W. L. Worrell, Trans. AIME, 233, 1173, (1965).

22. A. D. Romig and J. I. Goldstein, Applications of Phase Diagrams in Metallurgy and Ceramics, G. C. Carter, Editor, NBS Sp-496, p. 463, 1977.

23. Metals Handbook, ASM, 8th Edition, 8, p. 291, 1973.

APPENDIX D

Diffusion Paths and Diffusion Path Determination

Interdiffusion between two ternary alloys of the same system results in changes in concentration of the two solute elements, 1 and 2 and the solvent element, 3, with distance into each alloy. Following Onsager's initial formalism (1-3), Kirkaldy solved the differential equations describing semi-infinite single phase/single phase ternary interdiffusion (4-8). The analytical solutions were able to determine the concentrations of 1 and 2, C_1 and C_2, as a function of the parameter $\lambda = \text{distance}/(\text{time})^{\frac{1}{2}}$. Through these solutions, and borne out by experiment, it was found that the functions $C_1(\lambda)$ and $C_2(\lambda)$ have unique values for a given value of λ (4, 5). This means the diffusion profile, once established (i.e. after a finite time), does not change but merely varies dimensionally with time (9). Elimination of λ between the functions $C_1(\lambda)$ and $C_2(\lambda)$ yields a relationship in the form $C_1 = C_1(C_2)$ (10-11). This expression is a function of the concentrations C_1 and C_2 only (i.e. distance and time have been eliminated), and therefore defines an invariant line on the appropriate ternary isotherm (11). This invariant line is referred to as a diffusion path (10, 12).

A diffusion path represents how the bulk composition changes in the diffusion zone of a diffusion couple. Consider first a diffusion path between two single phase alloys, each of the same phase, as shown in Figure D-1. The
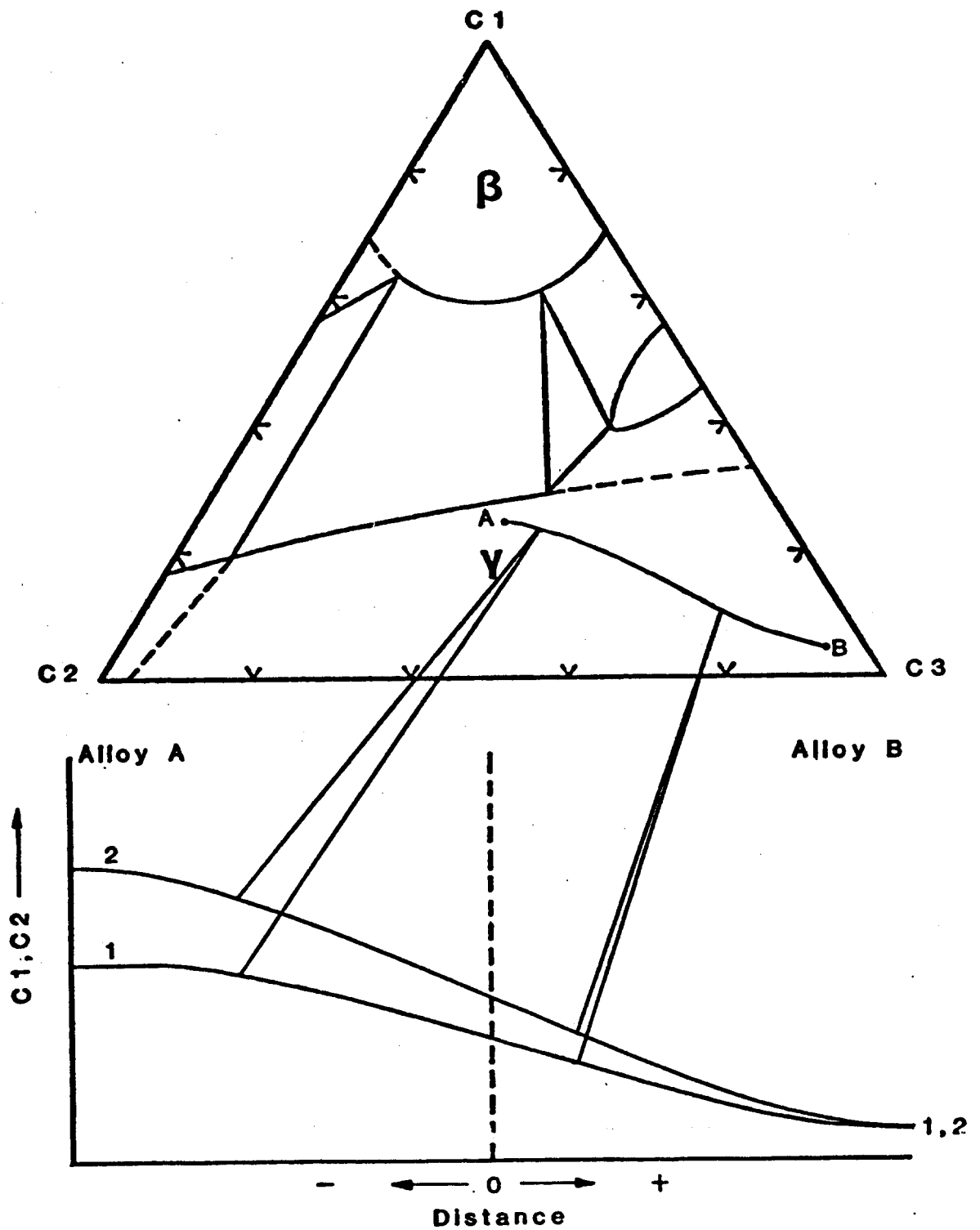
Figure D-1. Hypothetical diffusion path constructed from the concentration/distance profiles of solute elements 1 and 2 in a γ/γ diffusion couple.

diffusion path can easily be constructed from a measured concentration/distance (here after referred to as C/D) profile. The C/D profile measures how the bulk composition of 1 and 2 change with distance because all diffusion has occurred in a single phase. Therefore, each C_1 and C_2 at a given distance represent the bulk compositions at that distance, and translate to a unique point on the ternary diagram. Translating each C_1, C_2 combination over the entire length of the diffusion zone to the ternary diagram will yield the diffusion path.

Consider second, a diffusion path between two single phase alloys, each a different phase. The diffusion path must now cross a two-phase field between the two terminal alloys. If, after diffusion, the interface between the alloys is planar, the diffusion path simply cuts across the two-phase field via an equilibrium tie line (12), as shown in Figure D-2. The C/D profile in this situation would show a discontinuity in C_1 and C_2 at the two-phase interface. The diffusion path would be constructed the same as for a path between two single phase alloys of the same phase, with the discontinuity in C_1 and C_2 at the interface translating to an equilibrium tie line on the ternary diagram. Following the convention of Clark (13), a dashed line crossing the two-phase field parallel to the tie lines (shown in Figure D-2) is used to represent the interface between the two phases with interfacial compositions designated by the ends of the tie line. The
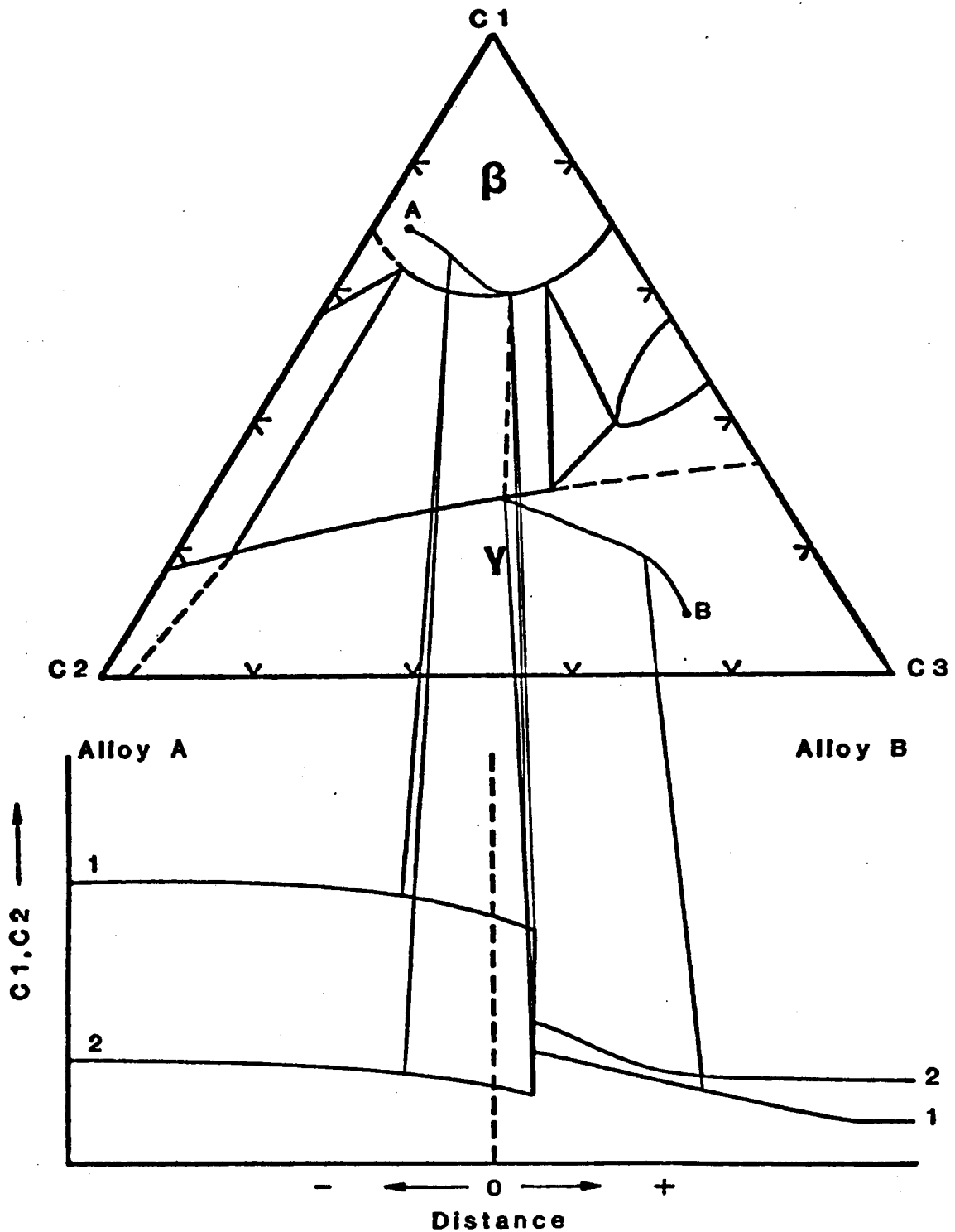
Figure D-2. Hypothetical diffusion path constructed from the concentration/distance profiles of solute elements 1 and 2 in a γ/β diffusion couple. The interface between the alloys remains planar.

line represents no spatial extent.

The situation depicted above changes, however, if a two-phase layer appears in the diffusion zone. The appearance of the two-phase layer indicates the diffusion path cuts across tie lines in the two-phase field (12), as shown in Figure D-3. In the two-phase layer, C/D profiles must be measured in each phase and do not correspond to the bulk composition. In order to plot a diffusion path cutting tie lines in a two-phase field, C/D profiles in each phase must be known, and also the volume fraction of one of the phases with distance (9). Only with this information can bulk compositions be calculated via the lever rule and plotted as a diffusion path through the two-phase field. The C/D profile for the entire couple (shown in Figure D-3) will contain three regions - two single-phase regions and one two-phase region. The profiles of C_1 and C_2 in the one phase regions will translate directly to diffusion paths in the respective one phase fields on the ternary diagram. In the two-phase region, the profiles of C_1 and C_2 in each phase will determine which tie lines are cut by the diffusion path (9). Measured volume fractions of one of the phases with distance will define the position at which the diffusion path cuts the tie lines (9). Using the lever rule, bulk compositoins can be calculated at each distance in the two phase layer. The calculated bulk compositions can be translated to the ternary diagram and a diffusion path can be constructed through the two-phase field.
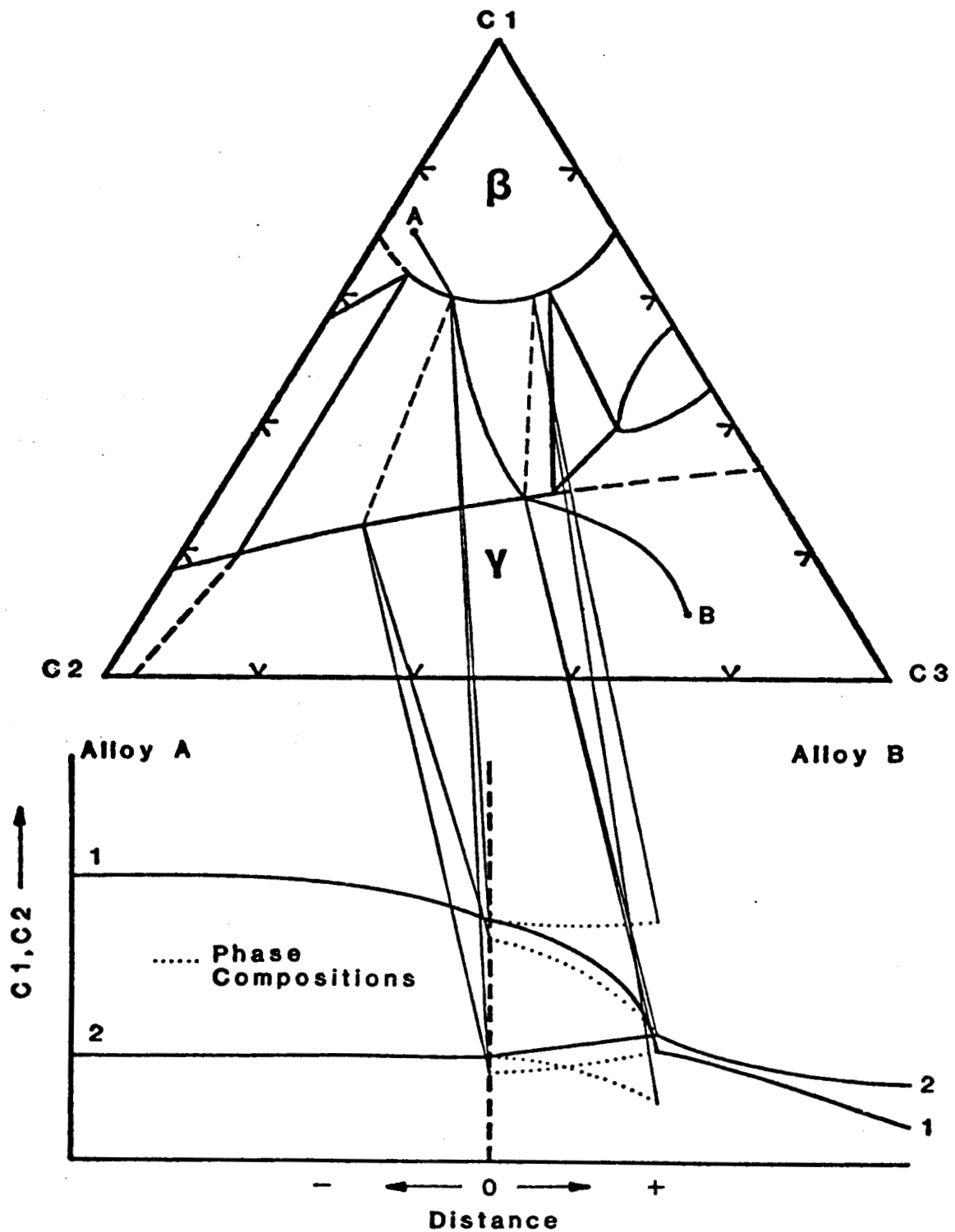
Figure D-3. Hypothetical diffusion path constructed from the concentration/distance profiles of solute elements 1 and 2 in a γ/β diffusion couple. A two-phase layer forms in the diffusion zone.

In a similar manner, if a diffusion path enters a three-phase field from a side, and exits along another side, concentrations in the phases as well as the volume fraction of one of the phases must be known to determine how the diffusion path passes through the three-phase field. It should be noted, following the convention of Clark (13), that a diffusion path through a three-phase field is represented by a dashed line. This is because the equilibrium between the three phases (e.g. a two-phase layer adjacent to a single phase layer of a different phase, or adjacent two-phase layers with a common phase) must be an interface only (i.e. a three layer cannot form in the diffusion zone). The line represents no spatial extent.

In summary, construction of a quantitative complex, multiphase diffusion path can only be done from a measured C/D profile. The path through a one-phase field is determined from a C/D profile in the one phase layer of the diffusion zone. The path through a two-phase field (assuming tie lines are cut) is determined from C/D profiles in the phases in the two-phase layer and the volume fraction of one of the phases with distance through the two-phase layer. The path through a three-phase field is determined in the same manner as for a path through a two-phase field.

Clark and Rhines (12) were forerunners in plotting complex multiphase diffusion paths. Since then, only a small number of workers (10-11, 14-19) have studied the development

of complex, multiphase diffusion paths. Clark and Rhines (12) and Kirkaldy and Brown (10) have summarized theorems pertaining to plotting diffusion paths on the ternary diagram. In response to a discussion of the work by Kirkaldy and Brown (10), Clark (13) put forth rules concerning how diffusion paths should be plotted on the ternary diagram. All paths constructed in this study conformed to the theorems of Kirkaldy and Brown (10). The diffusion path plotting convention proposed by Clark (13) was also followed.

In this study, the terminal alloys were composed of two-phase/two-phase ($\beta+\gamma/\gamma+\gamma'$) alloys and two-phase / one-phase ($\beta+\gamma/\gamma$) alloys. Interdiffusion resulted in complex multiphase diffusion paths. All diffusion path segments in the $\beta+\gamma$ regions were determined following the suggestion of Clark (9). C/D profiles of Cr and Al in the β and γ phases were measured with the electron microprobe analyzer. The volume fraction of the γ phase at specific distances was also measured using lineal analysis (20). The β and γ phase concentrations and the volume fraction of γ, all at a given distance, were input into a computer program which calculated the bulk Cr and Al compositions at that distance. The procedure was repeated throughout the diffusion zone. After the bulk Cr and Al compositions were obtained throughout the diffussion zone, they were plotted versus distance to yield the variation of the bulk compositions in the diffusion zone. Typically, the calculated bulk Cr and Al compositions did not fall along smooth curves, and thus smooth curves had to be drawn through

the data points. In doing this, the volume fraction of γ at any given distance measured from the bulk Cr curve usually did not equal the volume fraction of γ measured at the same distance from the bulk Al curve. Typically, the volume fractions of γ calculated from the bulk Cr curve and bulk Al curve were off by less than 10.0 vol.%, which was within the standard deviation of the volume fraction measurements made by lineal analysis. Using the bulk Cr and Al curves, Cr and Al compositions at given distances in the diffusion zone were extracted and plotted on the NiCrAl phase diagram. The points on the NiCrAl phase diagram were connected to yield the diffusion path through the $\beta+\gamma$ phase field.

One adherent assumption in calculating diffusion paths through two-phase fields is that each parallel layer of the couple (parallel to the original interface) is in equilibrium across the whole couple, with no lateral diffusion. This assumption allows the measured phase concentrations at a given distance to define which tie lines are cut, and the measured volume fraction at a given distance to determine at what points the tie lines are cut. This assumption is quite valid for the section of diffusion path that resulted from diffusion in the $\beta+\gamma$ alloy. Lateral microprobe traces (at a given distance) over at least two to three β and γ phases showed, within experimental error, that local equilibrium existed. In the $\beta+\gamma$ growth layer, however, the very nature of the columnar layers suggested that some lateral diffusion must occur (10,21). If lateral diffusion occurs extensively, deviations from equilibrium tie line compositions

can occur. This fact was found to occur in non-planar interfaces in a study of multi-phase diffusion in the Fe-Ni-Al system (19). Lateral microprobe traces were performed at given distances in the $\beta+\gamma$ growth region. The results showed that some lateral diffusion was occurring. The extent of lateral diffusion was very small - signified by very small concentration gradients (i.e. each measurement was almost within the standard deviation of the previous measurement) - and insignificant compared to the change in concentration that occurred along the long axis of the columns. It was therefore assumed that local equilibrium existed everywhere, and thus the diffusion path was represented by a stationary line connecting a continuous series of local equilibria.

Segments of the diffusion paths that entered the three-phase $\beta+\gamma+\gamma'$ triangle from the $\beta+\gamma$ side were calculated in the same manner as for the path segments in the $\beta+\gamma$ phase field. Path segments that exited the triangle on the $\gamma+\gamma'$ side were determined by measuring the volume fraction of γ' at the growth layer $(\beta+\gamma$ or $\gamma)/\gamma+\gamma'$ interfaces in the couples. Diffusion path segments through the $\gamma+\gamma'$ phase field were obtained by connecting the point where the path entered the $\gamma+\gamma'$ phase field to the $\gamma+\gamma'$ alloy composition. Therefore, these segments are estimated. All other diffusion path segments (i.e., segments in the γ phase, and segments in the γ' phase) were determined from C/D profiles in the respective phase layers in the diffusion zone.

Estimations of the accuracy of the calculated diffusion path segments in the $\beta+\gamma$ phase field were made using the standard

deviations of the volume fraction measurements made by lineal analysis (20). On average, a standard deviation of approximately ±5.0 vol.% γ was found. Inputting the limits (i.e., measured value ± standard deviation) into the computer program along with the measured phase concentrations gave variations in bulk Cr and Al composition of 2.0 at.% or less. Thus, the accuracy of the diffusion path segments in the $\beta+\gamma$ phase field is estimated as being approximately ±2.0 at.% (Cr or Al). This accuracy was confirmed by measuring bulk compositions at given distances in the diffusion zone with a scanning electron microscope line scan, KEVEX 8000 series energy-dispersive X-ray analyzer and subsequent Magic V ZAF correction routine. The measurements were always within 1.5 at.% (Cr or Al) of the calculated values.

Finally, it should be noted that diffusion paths are the most concise analytical representation of the structure that results from diffusion (9). They show on the ternary isotherm the final steady state sequence of phases that appear in the diffusion couple (9). Kirkaldy et.al. (10) has argued that in plotting diffusion paths on the ternary isotherm, time and distance have been eliminated, and hence most of the kinetic information contained in the C/D profile is lost. In view of this, efforts have been made in this study to present both forms of information - diffusion paths and the C/D profiles from which the paths originated.

REFERENCES

1. L. Onsager, Phys. Rev., $\underline{37}$, 405, (1931).

2. L. Onsager, Phys. Rev., $\underline{38}$, 2265, (1931).

3. L. Onsager, Ann. N.Y. Acad. Sci., $\underline{46}$, 241, (1945-6).

4. J. S. Kirkaldy, Can. J. Phys., $\underline{35}$, 435, (1957).

5. J. S. Kirkaldy, Can. J. Phys., $\underline{36}$, 899, (1958).

6. J. S. Kirkaldy, Can. J. Phys., $\underline{36}$, 907, (1958).

7. J. S. Kirkaldy, Can. J. Phys., $\underline{36}$, 917, (1958).

8. J. S. Kirkaldy, Can. J. Phys., $\underline{37}$, 30, (1959).

9. J. B. Clark, Discussion to Reference 10.

10. J. S. Kirkaldy and L. C. Brown, Can. Met. Quart., $\underline{2}$, 89, (1963).

11. D. E. Coates and J. S. Kirkaldy, Met. Trans., $\underline{2}$, 3467, (1971).

12. J. B. Clark and F. N. Rhines, ASM Trans., $\underline{51}$, 199, (1959).

13. J. B. Clark, Trans. AIME, $\underline{227}$, 1250, (1963).

14. A. G. Guy, H. Fechtig, and R. H. Buck, Trans. AIME, $\underline{233}$, 1178, (1965).

15. J. S. Kirkaldy and D. G. Fedak, Trans. AIME, $\underline{224}$, 490, (1962).

16. C. W. Taylor, Jr., M. A. Dyaananda, and R. E. Grace, Met. Trans., $\underline{1}$, 127, (1970).

17. R. D. Sisson, Jr. and M. A. Dayananda, Met. Trans., $\underline{3}$, 647, (1972).

18. L. E. Wirtz and M. A. Dayananda, Met. Trans., $\underline{8A}$, 567, (1977).

19. G. H. Cheng and M. A. Dayananda, Met. Trans., $\underline{10A}$, 1407, (1979).

20. J. E. Hilliard, J. W. Cahn, Trans. AIME, $\underline{221}$, 344, (1961).

21. J. S. Kirkaldy, Discussion to Reference 12.

1. Report No. NASA CR-174852	2. Government Accession No.	3. Recipient's Catalog No.
4. Title and Subtitle A Study of Interdiffusion in β + γ/γ + γ' Ni-Cr-Al Alloys at 1200 °C		5. Report Date February 1985
		6. Performing Organization Code
7. Author(s) Lawrence A. Carol		8. Performing Organization Report No. None
		10. Work Unit No.
9. Performing Organization Name and Address Michigan Technological University Houghton, Michigan		11. Contract or Grant No. NAG 3-244
		13. Type of Report and Period Covered Contractor Report
12. Sponsoring Agency Name and Address National Aeronautics and Space Administration Washington, D.C. 20546		14. Sponsoring Agency Code 505-33-62

15. Supplementary Notes

16. Abstract

Ternary diffusion in the NiCrAl system at 1200 °C has been studied with β + γ/γ + γ' infinite diffusion couples. Interdiffusion resulted in the formation of complex, multiphase diffusion zones. Concentration/distance profiles for Cr and Al in the phases present in the diffusion zone were measured after 200 hr. The Ni-rich portion of the NiCrAl phase diagram (1200 °C) was also determined. From these data, bulk Cr and Al profiles were calculated and translated to diffusion paths on the ternary isotherm. Growth layer kinetics of the layers present in the diffusion zone were also measured. Results of this work showed that the diffusion paths proceeded from the β + γ alloy composition to the γ + γ' alloy composition as a result of Cr and Al transport from the β + γ alloy to the γ + γ' alloy. The paths stayed in the β + γ phase field, or along the γ/β + γ phase boundary and usually proceeded through the β + γ + γ' triangle to the γ + γ' alloy composition. Progression of the path from the β + γ alloy composition to the triangle occurred by growth of β + γ or γ layers. Which layer was grown depended on the β + γ alloy composition, and in particular, the Cr concentration in the γ-phase. Calculated bulk concentration/distance profiles showed that strong negative bulk Cr gradients were largely responsible for formation and growth of the β + γ layers. Development of the strong bulk Cr gradients was related to maximum Cr fluxes in the γ-phase. The ability to develop maximum Cr fluxes in the γ-phase was a function of the γ-phase Cr concentration. The γ + γ' alloy composition was found to determine where the diffusion paths proceeded through the β + γ + γ' triangle. As the γ + γ' alloy Cr composition decreased, the diffusion paths translation up the β + γ and γ + γ' side of the triangle to higher Al composition. The path translated up the β + γ side of the triangle resulted in increased volume fractions of β in the β + γ growth layers. Translation of the path up the γ + γ' side resulted in increased volume fractions of γ' at the β + γ/γ + γ' interfaces. At γ + γ' alloy compositions less than 6.0 at % Cr, the paths move into the γ' phase field and a γ' growth layer forms in the diffusion zone.

17. Key Words (Suggested by Author(s)) NiCrAl alloy Overlay coatings Interdiffusion	18. Distribution Statement Unclassified - unlimited STAR Category 26		
19. Security Classif. (of this report) Unclassified	20. Security Classif. (of this page) Unclassified	21. No. of pages 189	22. Price* A09